University of KwaZulu Natal

Multiscaling Analysis and Modelling of Bursty Impulsive Noise in Broadband Power Line Communication Channels

Author:
Mike Omondi Asiyo

Supervisor:
Prof Thomas J. O. Afullo

This thesis submitted in fulfillment of the requirements for the degree of Doctor of Philosophy: Electronic Engineering

in the

College of Agriculture, Engineering & Science

February 2017

Multiscaling Analysis and Modelling of Bursty Impulsive Noise in Broadband Power Line Communication Channels

Author:
Mike Omondi Asiyo

Supervisor:
Prof Thomas J. O. Afullo

This thesis submitted in fulfillment of the requirements for the degree of Doctor of Philosophy: Electronic Engineering

in the

College of Agriculture, Engineering & Science

As the candidate's supervisor, I have approved this thesis for submission.

Signed ..... Date .....

Name: Prof Thomas J. O. Afullo

Declaration 1 - Plagiarism

I, **Mike Omondi Asiyo**, declare that this thesis titled, **"Multiscaling Analysis and Modelling of Bursty Impulsive Noise in Broadband Power Line Communication Channels"** and the work presented in it are my own. I confirm that:

1. The research reported in this thesis, except where otherwise indicated, is my original research.
2. This thesis has not been submitted for any degree or examination at any other university.
3. This thesis does not contain other persons' data, pictures, graphs or other information, unless specifically acknowledged as being sourced from other persons.
4. This thesis does not contain other persons' writing, unless specifically acknowledged as being sourced from other researchers. Where other written sources have been quoted, then:
   (a) Their words have been re-written but the general information attributed to them has been referenced
   (b) Where their exact words have been used, then their writing has been placed in italics and inside quotation marks, and referenced.
5. This thesis does not contain text, graphics or tables copied and pasted from the Internet, unless specifically acknowledged, and the source being detailed in the thesis and in the References sections.

Signed .....Date .....

Declaration 2 - Publications

The following papers have been published/submitted for publication, and parts of their materials are included in the thesis:

1. Mike O. Asiyo and Thomas J.O. Afullo, "Analysis of Bursty Impulsive Noise in Low-Voltage Indoor Power Line Channels: Local Scaling Behaviour," *SAIEE Africa Research Journal (ARJ 2016-683) - Accepted for publication*.

2. Mike O. Asiyo and Thomas J.O. Afullo, "Multifractal Analysis of Bursty Impulsive Noise in Low-Voltage Indoor Power Line Channels," in *Southern Africa Telecommunication Networks and Applications Conference (SATNAC)*, Fancourt, George, Western Cape, South Africa, 4-7 Sept 2016, 86-90.

3. Mike O. Asiyo and Thomas J.O. Afullo, "Prediction of Long-Range Dependence in Cyclostationary Noise in Low-Voltage PLC Networks," in *Progress of Electromagnetics Research Symposium* , Shanghai, China, 8-11 Aug 2016, 4954-4958.

4. Mike O. Asiyo and Thomas J.O. Afullo, "Power Line Communications Channel Multipath Phenomena and RMS Delay Spread," in *Southern Africa Telecommunication Networks and Applications Conference (SATNAC)*, Arabella, Hermanus, Western Cape, South Africa, 6-9 Sept 2015, 93-97.

Signed .....Date .....

Abstract

Doctor of Philosophy: Electronic Engineering

Multiscaling Analysis and Modelling of Bursty Impulsive Noise in Broadband Power Line Communication Channels

by Mike Omondi Asiyo

Power line communication (PLC) networks have the potential to offer broadband application services to homes and small offices cheaply since no additional wiring is required for it implementation. However, like other communication systems, it has its own challenges and the understanding of its channel characteristics is key to its optimal performance evaluation and deployment. Multipath propagation due to impedance mismatch and bursty impulsive noise are the important challenges that must be understood and their effects minimized for optimal system performance. Noise in power line communication networks is non-Gaussian and as such cannot be modelled as the convenient additive white Gaussian noise. The noise is known to be impulsive and in most cases, occurs in bursts. Therefore, it can be referred as bursty impulsive noise. Due to unique nature of this noise in power line channels, modulation and decoding schemes optimized for Gaussian channels may not necessarily work well in PLC systems. Recently developed noise models though take into consideration memory inherent in PLC noise, models capturing both long range correlations and multiscaling behaviour are not yet available in the literature. Furthermore, even though it is known that PLC noise has memory (i.e., it is correlated), the statistical properties of it is not well documented in the literature and will be the focus of this thesis.

In this thesis, multiscaling behaviour of PLC noise is investigated. Both fractal and multifractal analysis methods are employed on noise data collected in three different scenarios (small offices, stand-alone apartment and University electronic laboratory) and their characteristics analysed. Multifractal analysis is employed since it is able to characterize both the strengths and frequency of occurrence of bursts in power line noise. Specifically, the contributions in this thesis are as follows: Firstly, empirical evidence is provided that PLC noise clearly manifests long range correlations behaviour. This is achieved by calculating the Hurst parameter (which is a measure of self similarity) in data from the above scenarios. Various methods employed to estimate this Hurst parameter reveal that in all the scenarios, long range dependence is evidenced.

Secondly, multifractal detrended fluctuation analysis (MDFA) and multifractal detrending moving average (MDMA) analysis have been used to investigate the temporal correlations and scaling behaviour of power line channel noise measured from the three different scenarios mentioned earlier. Empirical results show that power line noise clearly manifests both long-range correlation and multifractal scaling behaviour with different strengths depending on the environments where they

were captured. From the estimated singularity spectrum which is left truncated, it is evident from the two methods used that power line noise is sensitive to small fluctuations and is characterized by large scaling exponents. Multifractal analysis of the reshuffled time series noise reveal that the multifractal nature of PLC noise is as a result of long range correlation inherent in the noise and not from the heavy tailed distributions in it.

Thirdly, we propose a multiplicative cascade model for PLC noise that is able to reproduce the empirical findings concerning the PLC noise time series: its local scaling behaviour and long range correlations. Model parameters are derived from the shape of multifractal spectrum of the PLC time series noise collected from measurement campaigns. Since in the recent past, the main challenge in PLC systems has been on how to model bursty impulsive PLC noise, the proposed model will be very useful in evaluating system performance of PLC networks in the presence of the bursty impulsive noise inherent in PLC networks. Moreover, bursts of different frequencies and strengths can be modelled by this proposed model and hence their effects on system performance evaluated. This will also open up investigations into designing modulation and decoding schemes that are optimal in systems prone to bursty impulsive noise.

Acknowledgements

Firstly, I would like to express my wholehearted gratitude to my doctoral advisor Prof. Thomas Afullo for his continuous support and encouragement during the research period even when things looked impossible. His deep insight and invaluable suggestions not only helped me overcome obstacles during my Ph.D. studies but also during my Master's program. I have been privileged to have worked with him and I have learned a lot from him.

Secondly, I am greatly indebted to my family for the sacrifice they endured during my absence because of the studies. Your encouragement and piece of mind I got because of your love and standing by me, words can not express. May you be blessed as I look forward to joining you again to enjoy the fruits of our sweat.

Lastly, it would be impossible to acknowledge people individually who in one way or another contributed to the success of this study. I highly appreciate, and may our good Lord reward you in abundance with a good life as He fulfils the desires of your hearts.

Dedicated to:

my beloved wife Suzie and our children (Devin, Ivana & Darien).
Love you all!

Contents

List of Figures

List of Tables

List of Abbreviations

2PN two-port networks

ACF Autocorrelation function

AWGN additive white Gaussian noise

CB coherence bandwidth

CGM cyclostationary Gaussian model

DFA detrended fluaction analysis

DMA detrending moving average

DSO Digital Storage Oscilloscope

FIR finite impulse response

HMM hidden Markov model

ISI Inter-symbol Interference

KL Kullback-Leibler

LRD long-range dependence

LPTV linear periodically time-varying

LTI linear time-invariant

MDFA multifractal detrended fluctuation analysis

MDMA detrending moving average algorithm

OFDM Orthogonal frequency division multiplexing

PLC Power line communication

PSD power spectral density

PDF probability density function

PDP Power Delay Profile

RMS Root Mean Square

WTMM wavelet transform modulus maxima

CHAPTER 1

Introduction

1.1 Introduction

Power line communications (PLC) is becoming popular for broadband applications, multimedia sharing and is part of smart grid systems due to its ubiquitous nature and it is economically viable since no extra wiring is required for communication purposes. With the vision of smart cities and smart homes, communication and remote control will be key to successful deployments of these technologies. This will increase more pressure on the already scarce spectrum resource. Therefore, communication via the already available power networks will be on the increase for obvious reasons. Moreover, power networks are available even in the very remote areas in most parts of the world and broadband internet access can be implemented even in these remote areas. PLC systems are plug and play which again reduces further the cost of installation and usage.

However, like any other communication channel, PLC has challenges of multipath (due to impedance mismatch), path loss and impulsive noise [1, 2]. This is because power networks were not originally designed and optimized for data transmission in mind but rather for low-frequency high voltage power transmission. Data transmission entails mostly high-frequency low-voltage signal. These extreme cases of transmission requirements make it even more challenging, however, there are technologies already in place for the transmission of both of these signals via the power networks. As such high-speed data transmission is still a daunting task. The most difficult challenge is characterising and modelling the PLC noise.

PLC noise generators are from both within the network and also by induction and radiation from without the network [3]. The noise generators (which are mainly electrical loads) randomly come on and off at different times of the day. This may imply that the noise in PLC networks may seem to be independent and identically distributed random variables and thus may seem to be uncorrelated. However, contrary to this, empirical analysis shown that PLC noise is both deterministic, stochastic and correlated, and hence very difficult to understand and model [4]. This has resulted in an increased research on investigating and characterising noise found in power line networks.

1.2 Motivation

Power line communication channels are prone to multipath propagation due to impedance mismatch, and impulsive noise whose characteristics are still not well established in the literature. Moreover, measurements show that this impulsive noise appears in bursts, non-Gaussian and cyclostationary and as such cannot be modelled as the convenient additive white Gaussian noise (AWGN). Transceivers optimised for AWGN may not necessarily perform well for the PLC noise. Therefore, investigating the characteristics of PLC noise is very important for accurate modelling of the same. Some authors have proposed models with memory that capture correlation/memory inherent in PLC noise, see for example [5, 6]. These two models are based on Markov chains to provide the dependence required. However, it is known that Markov or Poisson models (classical models) rely heavily on the independence assumption or rather weak dependence. Even classical limit theorems like Law of Large numbers do also rely on independence and states that at large scales, Poisson processes can be approximated by their mean arrival rate. All these assumptions are in most cases for convenience in modelling. However, in real world situations, we encounter data traces which are bursty or spiky even at large scales. In other words, they exhibit strong dependence. Can this strong dependence be analysed and modelled in the real world scenario? The answer to this question is affirmative, thanks to multifractal analysis techniques already available in the literature.

Strong dependence due to spiky or bursty arrivals has been found in river flows and high-speed communication networks and it has been shown to have high effects on reservoir and buffer designs, and in bandwidth allocation among others. Moreover, scaling behaviour brings about non-classical properties affecting the estimation of all parameters, not necessarily those describing scaling. This has an influence on the predictive capabilities of performance models and hence their usefulness in practical implementation. It is, therefore, important that the scaling behaviours of a signal be detected so that the best statistical tools for analysis be chosen well that suits their accurate analysis.

In estimating the strong dependence/correlation, the Hurst parameter, which indicates long-range dependence (LRD) intensity, is normally used. It addresses both long-range correlations and high variability even on large scales or aggregation levels. It can be seen as a global measure of self-similarity. It is the first parameter to be estimated in characterising fractal/multifractal properties of a signal or measure. However, when the data is spiky or bursty, like PLC noise, LRD measure is not enough to give full information of the signal. The strengths and frequency of occurrence of these bursts are better quantified by local scaling parameter. Local scaling analysis not only gives a feel of the general behaviour of a signal, but also captures rare events present in the signal. For this reason, in this thesis, apart from estimating long-range dependence in PLC noise, we perform multifractal/multiscaling analysis of the noise to capture all these important characteristics present in the signal. Multifractal spectrum, working on the assumption of large deviation principle, provides both the strength of bursts, say α, and the frequency of occurrence of this α will be encountered, that is $f(\alpha)$. The larger the value of $f(\alpha)$, the more often one will see α.

With empirical evidence that PLC noise is bursty, analysis and modelling the frequency of these bursts will go a long way in attaining more accurate PLC noise models and will take into consideration multiscaling behaviour inherent in it. This will again call for new methods of designing error correction schemes in PLC systems that will be able to incorporate more accurately bursts of errors due to impulsive noise in the networks. That is to say that impulsive noise mitigation schemes should be able to consider the strengths and frequency of occurrence of these bursts. Though mitigation schemes are not the focus of this thesis, it will form an interesting topic for our future work.

1.3 Objectives

The main specific objectives of the thesis can be deduced from the ongoing discussion and can be summarised as follows:

(i.) To characterize and provide insight to PLC noise long-range dependence through analysis of power line noise captured in different environments.

(ii.) To characterize noise in power line networks through multifractal analysis, providing insight into the measures of strength and frequency of occurrence of the bursty impulsive component of the noise.

(iii.) To investigate the source of local multiscaling behaviour of the bursty impulsive noise in PLC networks.

(iv.) To develop a noise model that is able to capture the multiscaling properties of bursty impulsive noise inherent in PLC networks.

1.4 Contributions

The main contributions of this thesis are as follows.

- Firstly, to understand the multipath phenomenon present in PLC channels, we used simulations to investigate the effects of various physical variables (number of branches in a network, branch length, and terminal impedance variations) of power networks on the transfer function of the channel in the frequency domain.

- Secondly, the study was able to establish that PLC noise shows strong dependence, that is, it exhibits long-range correlation. This we were able to ascertain in all the locations which noise measurements were done (Laboratory, Small Office and stand-alone Apartment). Since PLC noise has also been found to be cyclostationary, we were able to remove the nonstationarity by deseasonalization of the signal before using known methods of Hurst parameter estimation. The Hurst parameter gives an indication of presence of long-range correlation.

- Thirdly, the study was also able to characterise PLC noise though multifractal analysis. In the multifractal analysis, the time series signal was first decomposed into a scale-dependent measure (both in time and scale domain) before computing the multifractal spectrum indirectly by the q-order statistics of the measure. We were also able to show that the multifractal nature of PLC noise is mainly as a result of contributions from low-frequency components of the noise.

- Finally, a five-parameter generalised binomial multiplicative cascade model has been proposed to be adopted in PLC noise modelling in an attempt to capture the scaling behaviour of the noise present in power networks.

1.5 Thesis Structure

The rest of this thesis is structured as follows. Chapter 2 gives a detailed review of the two main challenges of PLC systems. The first one being multipath propagation due to impedance mismatch at the terminations and at joints. Power network is a branched network and understanding how these branches affect the propagation of signals in the communication channel is a first step in coming up with a reliable system. The second one, which is the main focus of this thesis is noise models in the PLC systems. We give a detailed review of the already noise models and their focus as far as PLC noise characteristics are concerned.

In chapter 3, we perform simulations of the PLC channel with the aim of understanding the multipath propagation phenomenon in PLC networks. The focus is mainly on the effects of a number of branches, branch lengths and load/terminal

impedance on the transfer function of the network in the frequency domain. Again, the effects of these variables on the root mean square delay spread which is a measure of the multipath richness of a channel. The work in this chapter contributed to one conference paper [7] published.

Chapter 4 focuses on estimating long-range dependence/correlation of PLC noise. Here deseasonalization of the noise is first performed to remove non-stationarities and periodicities which affect the estimators of long-range dependence parameter. We then employ three known methods of calculating the estimate of Hurst parameter which is an indicative of the intensity of long-range correlation. The work in this chapter contributed to one conference paper [8] published.

Multifractal analysis using two methods: multifractal detrended fluctuation analysis (MDFA) and detrending moving average algorithm (MDMA) are employed to characterise PLC noise is the focus of chapter 5. The work in this chapter contributed to one conference paper [9] published and one journal paper under review [10].

In chapter 6, a generalised binomial cascade model is proposed to be adopted in modelling the multifractal characteristics inherent in PLC noise. The model parameters are derived from the multifractal analysis presented in chapter 5. Chapter 7 concludes the thesis and outlines recommendations for future work.

CHAPTER 2

Literature Review

In this chapter, the challenges specific to power line communication channels are reviewed and we highlight how these challenges have been tackled in the literature. The missing gaps, which form the basis of study in this thesis are also highlighted.

2.1 Introduction

Power line communication has recently gained a lot of research interest because of its low cost which can be comparable to wireless communications. No new wire installation is required for communications over power lines. However, this channel is normally very hostile to communication applications since power networks were optimized for low frequency high voltage signal transmission. For meaningful communication system design, channel modelling is of great importance so as to match the system to specific channel characteristics. The PLC channel exhibits both frequency-selective and time-varying behaviour. The former is a result of reflections and transmissions at discontinuities due to impedance mismatch, while the latter is due to change in topology, cable parameters and load impedance.

The PLC channel also shows strong low-pass and high attenuation behaviour which restricts network coverage and applicable frequency bands [11],[12]. The channel model should be able to capture all these characteristics with high accuracy to aid in choosing transmission techniques and system performance analysis. Moreover, power grid wiring standards also vary from country to country, hence, predicting the PLC channel becomes very challenging. Recent development on multipath channel characterization and modelling can be found in [1],[13],[14],[15],[16],[17],[18] and the references therein. In addition to all these, the

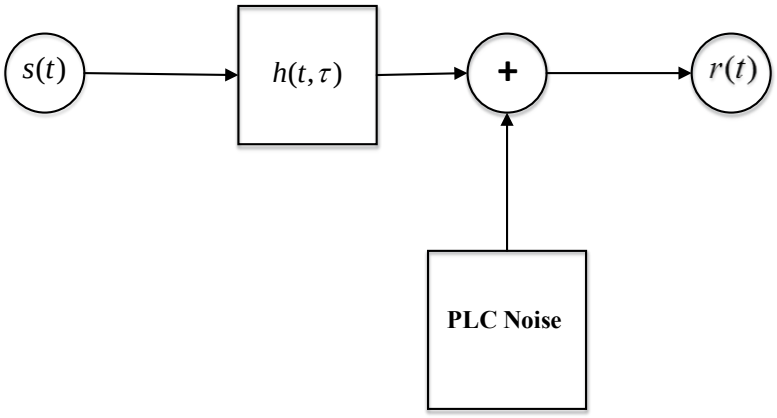

FIGURE 2.1: Graphical illustration of PLC channel with additive noise

noise experienced in PLC is not additive white Gaussian noise, but can be grouped as coloured background noise, narrowband interference and impulsive noise [3].

The PLC channel characteristic is very difficult to predict due to its random nature. Impedance mismatch, which makes the signals in PLC to undergo multipath propagation, can be seen as a random parameter. This is due to the fact that electrical loads are being switched on and off randomly by different users in the power network. Again, even when these loads are on, their impedances vary depending on their nature and operational characteristics. These electrical loads are also a source of some components of PLC noise. The effect is that their contributions to channel impairments are twofold. Figure 2.1 shows a simple power line communication system model. The transmitted signals $s(t)$ undergoes multipath propagation and is also affected by the additive channel noise. Hence, for proper reception at the receiver, both the channel and noise characteristics need to be known and their effects mitigated.

The PLC network was not designed for data transmission in mind but for electrical power delivery to various loads at low frequencies, typically 50/60 Hz. On the other hand, transmission of data happens at very low voltages but high frequencies, typically $1 - 30$ MHz and even beyond for next generation broadband PLC. These extremes necessitate a coupling circuit that will reject the 50 Hz signal and allow measurements of the high-frequency signal in addition to providing protection to the PLC measurement equipment. Again, the loads in power networks are switched on and off randomly and this causes further impedance mismatch and even the coupling circuit should be adapted to these changes. This phenomenon makes even the design of the coupling unit a challenging one for the measurements made to be trusted for modelling the PLC channel and/or noise.

2.2 Multipath Propagation in PLC Networks

Mainly, there are two approaches that have been followed in PLC channel modelling: top-down and bottom-up approaches [18]. The details of these approaches, their strengths and shortcomings are discussed in the following sections.

2.2.1 Top-Down Approach

In the top-down approach, the PLC channel is treated as a 'black box' and numerous measurements are collected by exciting the channel with a reference signal either in frequency or time domain. The transfer characteristics of the channel can then be described either in frequency or time domain using a few relevant parameters. The measurement data is used to fit a model, and the model parameters are derived from measurements. The model should accurately capture properties of the signal propagating in the channel and the multipath effects on the signal [1],[19]. In essence, there are two factors considered in describing channel transfer function, the model parameters and modelling algorithms. These two factors determine the accuracy and reliability of the model [18].

The main advantage of this approach is that the statistical results derived from measurements can be used to generate channels to analytically study the PLC channel and system performance. It also has a share of its challenges. The model parameters are network and frequency band specific. Currently, there are global campaigns for measurements in as many areas as possible to validate or redesign the available models. The top-down modelling also lacks the physical connection with reality and as such it is difficult to describe the spatial correlation present in power networks. Power networks are bus systems hence the received signal may have high correlation [11]. Since this approach is based on measurements, it is prone to measurement errors. A few of accepted models are discussed in the next sections.

2.2.1.1 Echo Model

Transmission behaviour of power line channels can suitably be described by multipath propagation approach. The first multipath model was proposed in [20] and represents the PLC channel as a sum of N Dirac pulses representing signals from N different paths. These Dirac pulses are multiplied by complex attenuation factor ρ_v and are delayed by τ_v and it can be represented as eqn. (2.1)

$$h(t) = \sum_{v=1}^{N} |\rho_v| . e^{j\varphi_v} . \delta(t - \tau_v) \tag{2.1}$$

where $\rho_v = |\rho_v| . e^{j\varphi_v}$, $e^{j\varphi_v}$ is the phase shift component, $\varphi_v = \arctan \frac{\mathrm{Im}(\rho_v)}{\mathrm{Re}(\rho_v)}$. Taking Fourier Transform of eqn. (2.1), the transfer function characteristics of the model

as a function of frequency can be represented as eqn. (2.2)

$$H(f) = \sum_{v=1}^{N} |\rho_v| . e^{j\varphi_v} . e^{-j2\pi f \tau_v}. \tag{2.2}$$

The echo model is a sum of the product of attenuation factor and delayed Dirac delta pulses. The attenuation factor is a product of reflection and transmission factors along each echo path. Even though this model captures the notches of the channel transfer function of the PLC channel, it is not able to show the low-pass behaviour of the channel. Hence, it is applicable in areas where low-pass behaviour is not relevant [12]. The model parameters are then fitted to measurements. It was shown that $N = 5$ gives a fairly good fit. However, the number of paths can be optimised by minimising the root mean square error and the maximising correlation between measurements and model simulations [20].

2.2.1.2 Multipath Signal Propagation Model

Multipath signal propagation model, also known as *Zimmermann Model*, is an adaptation of the *Echo Model* discussed in the previous subsection. In [1], the authors demonstrated that even a simple network with a direct path and only one branch can have infinitely many additional paths (echoes) between the transmitter and the receiver. These echoes must be considered in a model representing channel characteristics. When the joints/branches are not matched to the transceiver, then reflections and transmissions will occur at the discontinuities. Each of the paths followed by a signal will have a weighting factor that is a product of reflection and transmission factors along the path. The weighting factors depend on the frequency of occurrence of the reflections and transmissions along a given path. The higher the frequency of occurrence, the smaller the weighting factor. Again, longer paths exhibit higher attenuation and so have negligible influence on the overall signal. This makes it reasonable to approximate the infinitely many paths by only a few definite dominant paths.

The reasoning so far is similar to the one in echo model. The modification of this model comes from including an attenuation factor due to cable losses in the individual paths. This attenuation is a function of both cable length (d_i) and transmission frequency (f). The attenuation due to cable loss is given by eqn. (2.3)

$$A(f, d_i) = e^{-\alpha(f).d_i} = e^{-(a_0 + a_1 . f^k).d_i} \tag{2.3}$$

where the parameters a_0, a_1 and k can be found from previously known cable parameters. These parameter values can also be derived from measured transfer functions [20]. The modified transfer function in the frequency domain is then

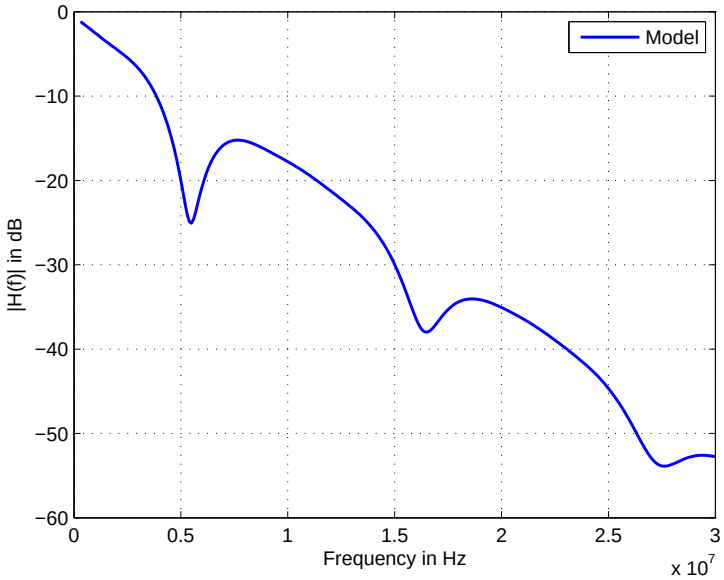

FIGURE 2.2: Amplitude response for reference model (2.4) with 4 paths

given by eqn. (2.4)

$$H(f) = \sum_{i=1}^{N} g_i . e^{-(a_0 + a_1 . f^k) . d_i} . e^{-j2\pi f \tau_i} \tag{2.4}$$

where g_i is the weighting factor and is generally complex and is frequency dependent but is normally assumed to be real-valued. The delay τ_i in each path is given by eqn. (2.5)

$$\tau_i = \frac{d_i \sqrt{\varepsilon_r}}{c_0} = \frac{d_i}{v_p} \tag{2.5}$$

where ε_r and c_0 are respectively the dielectric constant of the insulating material and the speed of light. Again, same as in echo model, the fitting of this model to measurements can be refined by controlling the number of paths. For simple networks, a four-path model can sufficiently represent the impulse response of the channel [1]. Figure 2.2 and Figure 2.3 show simulation results of both four (4) path and fifteen (15) path models respectively. Different shapes for the transfer functions and position of the notches are evident from the figures which has been influenced by the number of propagation paths in the network. As the number of paths increases so is the complexity of the transfer function.

2.2.2 Bottom-Up Approach

The bottom-up approach is based on transmission line theory. Unlike in the top-down approach where model parameters are derived from measurements, here the approach starts from a theoretical derivation of model parameters. It describes

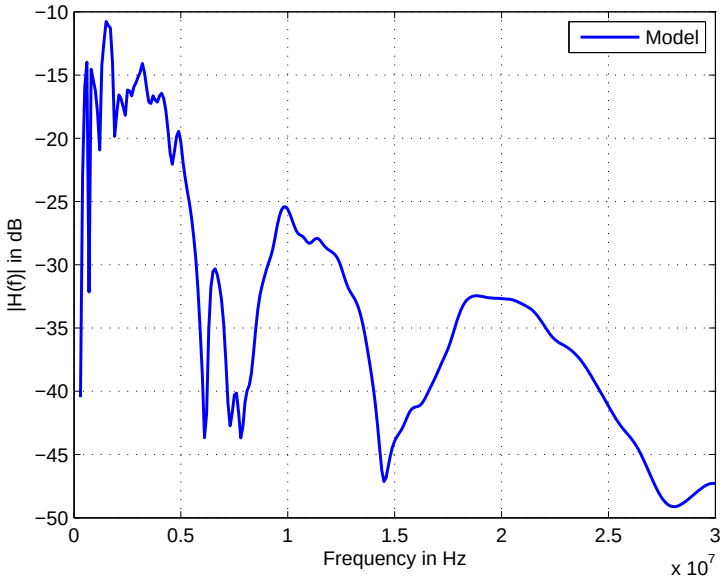

FIGURE 2.3: Amplitude response for reference model (2.4) with 15 paths

clearly the relationship between the network behaviour and the model parameters and as such necessitates complete information about of the power network (topology,cable parameters, the load impedance of the terminals). This makes it computationally very complex and the complexity grows with the complexity of the network. Moreover, full knowledge of the power network is a serious challenge and is very difficult to predict. Again, wiring practices vary from country to country and coming up with a universally acceptable model that can be applicable anywhere is still a dream for the future [11], [18].

Power line networks are known to be heavily branched with terminations. A popular approach in analysis and synthesis of PLC systems is to 'see' it as a cascade of two-port networks (2PN). From this analysis can be done using either Transmission parameters T (also known as ABCD parameters) or Scattering parameters (S-parameters). A representation of PLC network as a 2PN is given in Figure 2.4. The transmitter is represented by a voltage source with source impedance Z_s, the PLC transmission line as 2PN and the receiver is represented as a load of Z_L [21, 22].

The transmission parameters of the network can be determined from eqn. (2.6)

$$\begin{bmatrix} V_1 \\ I_1 \end{bmatrix} = \begin{bmatrix} A & B \\ C & D \end{bmatrix} \begin{bmatrix} V_2 \\ I_2 \end{bmatrix} \tag{2.6}$$

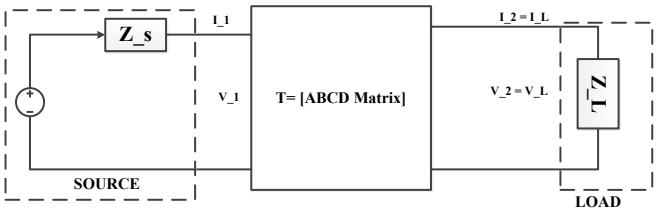

FIGURE 2.4: A PLC System represented as a two-port network connected to a voltage source and a load

Similarly, when the PLC network is considered as a cascade of two 2PN, the ABCD parameters become eqn. (2.7)

$$\begin{bmatrix} A & B \\ C & D \end{bmatrix} = \begin{bmatrix} A_1 & B_1 \\ C_1 & D_1 \end{bmatrix} \begin{bmatrix} A_2 & B_2 \\ C_2 & D_2 \end{bmatrix} \tag{2.7}$$

Seeing a PLC network as a cascade simplifies its analysis by decomposing the complicated network to simpler circuits and then multiplying their corresponding ABCD parameters to determine the transmission parameters of the whole network. From the ABCD parameters, the PLC channel transfer function and input impedance can be estimated respectively by eqns. (2.8) and (2.9) [23]

$$H(f) = \frac{V_L}{V_s} = \frac{Z_L}{AZ_L + B + CZ_LZ_s + DZ_s} \tag{2.8}$$

$$Z_1(f) = \frac{V_1}{I_1} = \frac{AZ_L + B}{CZ_L + D} \tag{2.9}$$

The transfer function and the impedances are frequency dependent, though this has been omitted in the equations for simplicity purposes. Transmission line cable characteristics are equally important in understanding the PLC channel response. Equivalent circuit representation of a transmission cable is as shown in Figure 2.5 and when the cable parameters are known, then the characteristic impedance Z_c eqn. (2.10) and propagation constant λ eqn. (2.11) can be calculated, respectively, as [21, 22]

$$Z_c = \sqrt{\frac{R + j\omega L}{G + j\omega C}} \tag{2.10}$$

$$\lambda = \sqrt{(R + j\omega L)(G + j\omega C)} = \alpha + j\beta \tag{2.11}$$

where, R, G, L, and C are cable per unit length resistance, admittance, inductance and capacitance respectively.

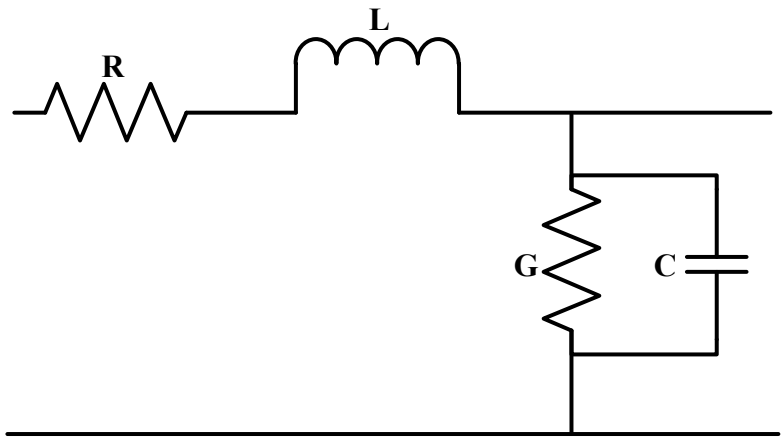

FIGURE 2.5: Equivalent circuit for PLC Transmission Line

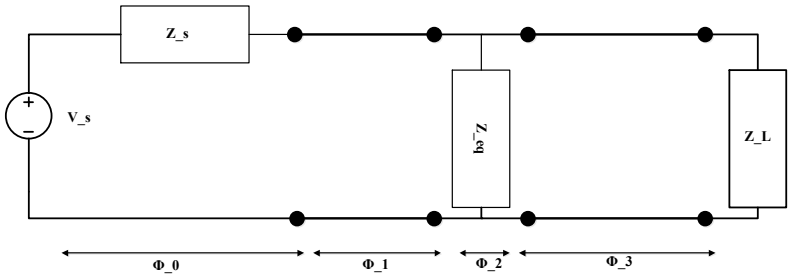

FIGURE 2.6: Equivalent circuit for PLC with one tap bridge topology

The ABCD matrix for transmission line with Z_c being the characteristic impedance, propagation constant of λ and a length of l can be calculated as eqn. (2.12)

$$\begin{bmatrix} A & B \\ C & D \end{bmatrix} = \begin{bmatrix} \cosh(\lambda l) & Z_c \cdot \sinh(\lambda l) \\ \frac{1}{Z_c} \cdot \sinh(\lambda l) & \cosh(\lambda l) \end{bmatrix} \tag{2.12}$$

From these parameters, the transfer function of a transmission line can be calculated from eqn. (2.8) with the help of eqn. (2.12).

When we consider a transmission line with one bridge tap as shown in Figure 2.6, we can partition the line into various sections and determine the ABCD matrix of each section. The corresponding transmission matrix of the network can be computed as eqn. (2.13)

$$\Phi = \prod_{i=0}^{N_s} \Phi_i \tag{2.13}$$

The source matrix is computed as eqn. (2.14)

$$\Phi_0 = \begin{bmatrix} 1 & Z_s \\ 0 & 1 \end{bmatrix} \tag{2.14}$$

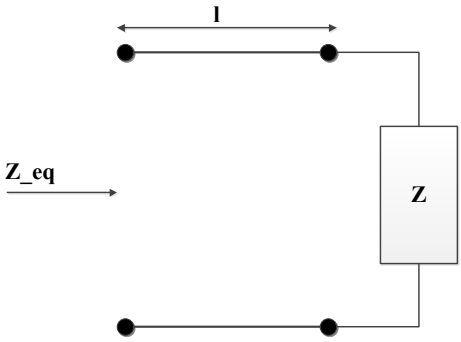

FIGURE 2.7: Equivalent circuit of a tap bridge

where, Z_s is the source impedance and the second section transmission matrix is given by eqn. (2.15)

$$\Phi_1 = \begin{bmatrix} \cosh(\lambda_1 l_1) & Z_1 \cdot \sinh(\lambda_1 l_1) \\ \frac{1}{Z_1} \cdot \sinh(\lambda_1 l_1) & \cosh(\lambda_1 l_1) \end{bmatrix} \tag{2.15}$$

Transmission matrices of all the taps can be calculated individually by first representing the bridges with an equivalent circuit and then computing its equivalent impedance Z_{eq}. The bridge circuit representation is as shown in Figure 2.7 from which Z_{eq} is given by eqn. (2.16);

$$Z_{eq} = Z_c \cdot \frac{Z + Z_c \cdot \tanh(\lambda l)}{Z_c + Z \cdot \tanh(\lambda l)} \tag{2.16}$$

where l is the bridge length, Z_c is the characteristic impedance of the transmission line, and Z is the terminal load impedance. The transmission matrix of the bridge then becomes eqn. (2.17)

$$\Phi_2 = \begin{bmatrix} 1 & 0 \\ \frac{1}{Z_{eq}} & 1 \end{bmatrix} \tag{2.17}$$

The transmission matrix for the last section is given by eqn. (2.18);

$$\Phi_3 = \begin{bmatrix} \cosh(\lambda_2 l_2) & Z_2 \cdot \sinh(\lambda_2 l_2) \\ \frac{1}{Z_2} \cdot \sinh(\lambda_2 l_2) & \cosh(\lambda_2 l_2) \end{bmatrix} \tag{2.18}$$

The ABCD matrix of Figure 2.6 can be computed by substituting eqn. (2.14) and eqn. (2.18) into eqn. (2.13) to get eqn. (2.19) [21]

$$\begin{aligned} A &= \cosh(\lambda_2 l_2)\alpha + \frac{\sinh(\lambda_2 l_2)}{Z_2}\beta \\ B &= Z_2\cosh(\lambda_2 l_2)\alpha + \cosh(\lambda_2 l_2)\beta \\ C &= \cosh(\lambda_2 l_2)\xi + \frac{\sinh(\lambda_2 l_2)}{Z_2}\vartheta \\ D &= Z_1\sinh(\lambda_1 l_1)\xi + \cosh(\lambda_2 l_2)\vartheta \end{aligned} \tag{2.19}$$

where,

$$\begin{aligned} \alpha &= \varrho + \frac{Z_s}{Z_1}\zeta \\ \beta &= Z_1\zeta + Z_s\varrho \\ \xi &= \frac{Z_1\varrho + Z_s\zeta + Z_{eq}\zeta}{Z_1 Z_{eq}} \\ \vartheta &= \frac{Z_1\zeta + Z_s\varrho}{Z_{eq} + \varrho} \end{aligned} \tag{2.20}$$

and,

$$\begin{aligned} \varrho &= \cosh(\lambda_1 l_1) \\ \zeta &= \sinh(\lambda_1 l_1) \end{aligned} \tag{2.21}$$

2.2.3 Statistical Modelling

In the quest to model the PLC channel a priori for system design and performance analysis, there are a good number of works on channel modelling which are not network specific. In [24], the author has adopted the Zimmermann model to develop a PLC channel generator in time domain for each user. The Zimmermann model is stated here for convenience as eqn. (2.22) [1]

$$H(f) = \sum_{i=1}^{N_p} g_i . e^{-(a_0 + a_1 . f^k).d_i} . e^{-j2\pi f \tau_i}. \tag{2.22}$$

The parameters are as defined previously. The difference here is that the parameters are taken as random variables. The points of reflections which generate paths are placed at finite distance interval. The first reflector is fixed at some distance and other reflectors to be allocated according to a Poisson arrival process with some acceptably chosen intensity. The reflection factor g_i are assumed to be real, independent and uniformly distributed in [-1,1]. The parameters a_0, a_1 and k are chosen to adapt to a specific network. The corresponding time domain channel

generator for user u is given by eqn. (2.23) [24]

$$h^{(u)}(t) = 2\text{Re}\{\sum_{p=1}^{N_p}(g_p e^{-\alpha_0 d_p}\frac{\alpha_1 d_p + j2\pi(t-d_p/v)}{(\alpha_1 d_p)^2 + 4\pi^2(t-d_p/v)^2} \times (e^{j2\pi B_1(t-d_p/v)-\alpha_1 B_1 d_p} - e^{j2\pi B_2(t-d_p/v)-\alpha_1 B_2 d_p}))\} \quad (2.23)$$

In [13], the authors modified the above by factoring in the coupling effect considering that it is possible to transmit and receive from two different circuits. The assumption is that in a power network, there can be up to three phases and if the sockets are connected to different phases, then it is possible to transmit and receive from different circuits. In such situations, coupling effect ensure propagation of signals from transmitter to receiver and the channel frequency response shows a concave behaviour. In low frequency, it is strongly attenuated because of lack of connection and at high frequencies the strong attenuation is due to line losses [13]. This frequency loss can be approximated by eqn. (2.24) [13]

$$p_i(f) = g_i + c_i f^{K2} \quad (2.24)$$

Again paths with small gains are neglected and multipaths are approximated by a finite number N_p which is modelled as Poisson random variable. The corresponding channel transfer frequency response is modelled as eqn. (2.25) [13]

$$H(f) = A\sum_{i=1}^{N_p}(g_i + c_i f^{K2})e^{-(a_0+a_1 f^K)l_i}e^{-j2\pi f l_i/v} \quad (2.25)$$

The complex impulse response is computed from the inverse Fourier transform of eqn. (2.25) and assuming $K = 1$ and c_i, the closed-form expression is given by eqn. (2.26)

$$h(t) = A\sum_{i=1}^{N_p}\sum_{k=1}^{2} g_i e^{-a_0 l_i}\frac{(-1)^{k-1}e^{(jt-(a_1/2\pi+j/v)l_i)\omega_k}}{a_1 l_i + j2\pi(\frac{l_i}{v}-t)} \quad (2.26)$$

where $\omega_k = 2\pi B_k$. g_i and c_i can be modelled as a product of a sign flip and a uniformly distributed random variable $u \in [0, 1]$. And since the statistical distribution of the product of large number of uniform random variables approach log-normal, g_i and c_i can be modelled as log-normal variables multiplied by random sign flips. Path lengths as uniformly distributed variable in $[0, L]$ where L is a constant. The authors conclude that N_p can be any distribution depending on the measurements that have to be fitted. The literature pertaining to channel modelling is vast and not of them can be covered in this thesis. Other very interesting works are done by the authors in [25, 26, 27] where they look at frequency based channel models and their properties. The authors in [28, 29] have also proposed channel models employing Mie scattering approach and their results are comparable to Zimmermann

Model.

2.2.4 RMS Delay Spread and Coherence Bandwidth

The previous section has shown that the PLC channel is multipath prone and to characterise this multipath phenomenon, Root Mean Square (RMS) delay spread is a very important metric to consider. Due to multipath, the received signal follow different paths at different time delays as a result of different propagation lengths followed by the signal. Delay spread is the duration difference between the time the first signal arrives at the receiver and the time the last non-negligible echo component arrives.

The RMS delay spread gives an indication of the multipath richness of the channel and it has been found to be log-normally distributed and inversely correlated with channel gain (see, [15],[14]). Orthogonal frequency division multiplexing (OFDM) has been proposed as a promising technique to combat the effects of multipath propagation in PLC networks and understanding of RMS delay spread is key to choosing the guard interval (GI) length which optimises the performance of the OFDM systems [30]. Again, RMS delay spread is inversely related to the coherence bandwidth (CB). CB gives an indication of frequency selectivity of the channel. Hence, the understanding of how the aforementioned factors affect the RMS delay spread is worth understanding for the success of PLC deployment and performance [17],[30].

When the signal symbol duration is big enough in comparison to the delay spread, then there is little smearing of the received signal and one would expect Inter-symbol Interference (ISI) free channel. However, if this delay spread is big enough, then it can result in serious signal distortion [31]. In other words, the RMS delay spread is known to be a good measure of multipath phenomena and provides an indication of the extent of possible distortion of the signal at the receiver due to ISI.

Root mean square delay spread can be estimated from Power Delay Profile (PDP). PDP of a channel gives an estimate of the distribution of transmitted power over propagation paths in a multipath environment and is estimated from the spatial average of channel impulse response [17], i.e., it is the square root of second central moment of the power delay profile. The power delay profile can be determined from inverse Fourier Transform of the frequency channel response either from measurements or from deterministic models given the PLC topology and cable parameters are known. The power delay profile is given by eqn. (2.27)

$$P(\tau) = |h(t,\tau)|^2 \tag{2.27}$$

where $h(t,\tau)$ is the channel impulse response determined from IFFT of the channel frequency response. Average excess delay of transmitted signal due to multipath

is given by eqn. (2.28)

$$\tau_{AVG} = \frac{\sum_i P(\tau_i)\tau_i}{\sum_i P(\tau_i)} \tag{2.28}$$

and the RMS delay can be given by eqn. (2.29) [15],[31]

$$\sigma_{RMS} = \sqrt{(\tau)^2_{AVG} - (\tau_{AVG})^2} \tag{2.29}$$

where,

$$(\tau)^2_{AVG} = \frac{\sum_i P(\tau_i)\tau_i^2}{\sum_i P(\tau_i)} \tag{2.30}$$

Coherence bandwidths are calculated by numerically solving for the frequency separations, where the correlation function's magnitude drops to 0.5 or 0.9 and it is inversely proportional to RMS delay spread. Their values can be computed directly from RMS delay spread values respectively as eqns. (2.31) and (2.32)

$$BW_{0.5} = \frac{1}{5\sigma_{RMS}} \tag{2.31}$$

$$BW_{0.9} = \frac{1}{50\sigma_{RMS}} \tag{2.32}$$

2.3 Power Line Channel Noise

The main focus of this thesis is on PLC noise characteristics and modelling. Power line communication networks' performance can be greatly degraded by noise generated by various noise sources within and/or without the network. Understanding of the noise characteristics is important for the design of their mitigation techniques thereby improving the system performance. Noise in these networks has been found to be non-Gaussian, impulsive and correlated [3, 5, 6]. Specifically, analysis of various noise measurement campaigns in PLC environment has shown that PLC noise is not additive white Gaussian noise but is non-Gaussian. It has two main origins: electrical devices connected to the power network act as noise generators and noise from external wireless sources coupled to the network via radiation [3], [32].

One unique characteristic of PLC noise is that it is very impulsive and the impulses appear in bursts. Impulsive noise (the main source of data errors) is the most challenging one to mitigate and its characteristics are worth investing. Impulsive noise can cause bit or burst errors in high-speed transmission of data in power line communications. This will eventually result in system performance degradation. Therefore understanding and modelling of time behaviour of PLC impulsive noise is a very important challenge that is worth investigating so as to come up with countermeasures to limit their effects on broadband applications in PLC systems. Models developed should be able to capture the details of the noise characteristics as close as possible and again should be easy to simulate in

computers for performance analysis of PLC systems. Recently, the focus has been on models that capture time correlation of bursty impulse noise. Some authors group PLC noise into three types; coloured background noise, narrowband noise and impulsive noise. Impulsive noise can be further classified into periodic impulsive noise synchronous with mains, periodic noise asynchronous with mains and sporadic impulsive noise [3, 32].

Most work on impulsive noise in PLC has concentrated on time domain analysis (impulse amplitude, impulse width and inter-arrival times) without considering its power spectral density distributions [3]. However, it is known that time series intrinsic behaviour is best captured by its spectral analysis (frequency domain). Recently, there has been some work considering frequency domain analysis of PLC noise. In [33], the authors proposed a seven parameter frequency domain model for the power line noise; three parameters to model the coloured background noise and four parameters to represent narrow band interferers. The random processes are defined by their probability density functions and used to build a synthesis filter for noise power spectral density (PSD). No impulsive component was considered in their modelling as the impulsive noise occurrence from measurements was negligible.

In [34], the authors computed PSD of PLC noise by assuming that the model is a linear time invariant filter driven by cyclostationary noise/process. Even though PLC noise is cyclostationary, it is also time variant. The result in [34] is suitable for background noise as it does not vary much with frequency. It is known that PLC noise spectral intensity/power decreases with increasing frequency. The authors in [35] divided the PLC noise into regions in each period and assumed that in each region, the noise is stationary and hence the PSD is flat in each region. In other words, they modelled their system as linear periodically time varying filter driven by a stationary noise. The results here show PLC noise with PSD which is varying both temporally and spectrally. They estimated the PSD of each region using periodogram (nonparametric method), which has low accuracy in comparison to parametric methods of spectral estimation.

More comprehensive analysis of PLC noise in the frequency domain is found in [32]. The authors here were able to estimate power spectral density of various PLC noise components using periodogram averaging. Even though very interesting results are deduced from their work like capturing the cyclostationarity of the PLC noise, periodogram estimation though quite simple and fast to implement suffers from some serious disadvantages. That is, their frequency resolution is poor and normally there is a trade-off between frequency resolution and temporal resolution. Again, peak selection with periodogram is difficult because of side lobes associated with 'leaks' in all frequency coefficients, corrupting the FFT spectrum estimate. This is due to the fact that DFT implicitly assumes periodicity is data and may cause discontinuities at the extremes of the periods [36].

2.4 PLC Noise Classification

Noise in power line communication networks is non-Gaussian and as such can not be modelled as the convenient additive white Gaussian noise. The noise is known to be impulsive and in most cases, occurs in bursts. Therefore, it can be referred as bursty impulsive noise [6]. Due to the unique nature of this noise in power line channels, modulation and decoding schemes optimised for Gaussian channels may not necessarily work well in PLC systems. This has contributed to the increased growth in the interest of PLC noise modelling and analysis. PLC noise from sources both within and without the network and can be classified as follows [3, 32]:

1. Background noise:
    - *Background coloured noise* - It has low power spectral density which varies with frequency. It is caused by multiple sources of unknown origin and it is assumed to be cyclostationary depending on the number and types of devices connected to the power network.
    - *Narrowband noise* - Mainly sinusoidal signals with modulated amplitude due to broadcasting stations operating in the same frequency band. It can also be assumed to be cyclostationary.
2. Impulsive Noise:
    - *Periodic impulsive noise asynchronous to the mains frequency* - Mainly caused by switched power supplies, it is cyclostationary and it is formed by periodic impulses with a repetition rate between 50 and 200 kHz.
    - *Periodic impulsive noise synchronous to the mains frequency* - It has a repetition rate of 50 or 100 Hz and is caused mainly by switching actions of rectifier diodes which are synchronous with the mains cycle.
    - *Asynchronous impulsive noise* - It is the most unpredictable impulse noise caused by switching transients in the power network (i.e., connections and disconnections of devices). The PSD of this type of noise can reach more than 50 dB above background noise values.

For convenience in modelling, these five groups are normally classified into two major groups; background noise and impulsive noise [3, 5, 37].

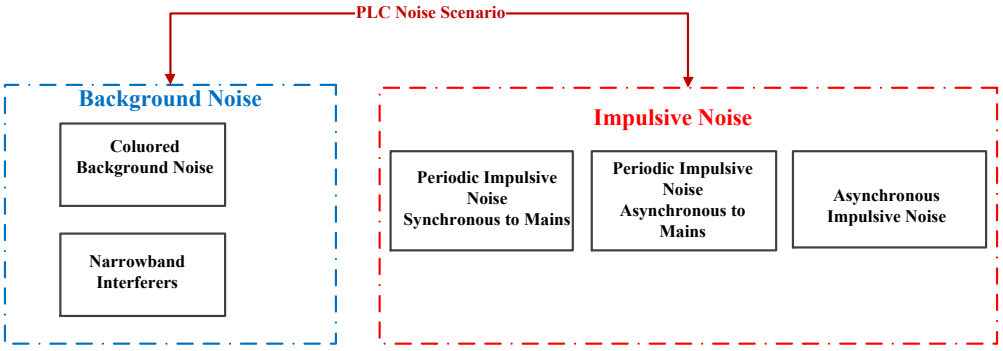

FIGURE 2.8: PLC Noise Classification

2.5 Narrow-band Noise Models

The authors in [34] model narrow-band noise captured in low voltage powerline channels as a cyclostationary Gaussian model (CGM). Here the pdf of the noise sample at instantaneous time $t = iT_s$ is given by eqn. (2.28)

$$p(\nu(iT_s)) = \frac{1}{\sqrt{2\pi\sigma^2(iT_s)}}\exp[-\frac{\nu^2(iT_s)}{2\sigma^2(iT_s)}] \tag{2.33}$$

The unique feature of impulsive noise is captured by a zero-mean Gaussian random variable with a time varying periodic variance with period $T_{AC}/2$, where T_{AC} is the period of AC mains. This implies that the noise pdf is also periodic with the same period. To capture the non-white spectral properties of PLC noise, the authors in [34] multiply the time-varying variance with a decaying function of frequency ($\sigma^2(t, f) = \sigma^2(t)\alpha(f)$). This is like passing a cyclostationary signal through a shape linear time-invariant (LTI) filter.

In [35], CGM is modified to take care of both temporal and spectral properties of PLC noise by replacing the LTI filter in CGM with a linear periodically time-varying (LPTV) filter. Unlike in [34] where input to the LTI filter is a cyclostationary signal, here, the input to the LPTV filter is a stationary signal, i.e.,

$$n[k] = \sum_{\tau} h[k, \tau]s[\tau] \tag{2.34}$$

where $s[\tau]$ is the stationary input to the LPTV filter and $h[k, \tau] = \sum_{i=1}^{M} h_i[\tau]1_{k\in R_i}$ is the LPTV filter. M denotes intervals R_i where the spectral shape is considered flat.

From the findings of the previous authors in this subsection, the authors in [38] did a cyclic spectral analysis of PLC noise in the 3-200 kHz band and proposed adaptive cyclic bit loading scheme in OFDM systems. They ascertain through simulations that the proposed scheme outperforms the available schemes by up to 2 times the throughput of existing schemes and closely approaches optimal adaptive

schemes. From the foregoing discussion, it can be interesting to investigate whether this cyclic behaviour is also inherent in PLC noise in the broadband applications and whether adaptive cyclic bit loading schemes will yield equivalent results as in narrow-band applications.

2.6 Broad-band Noise Models

A recent survey on impulsive noise modelling groups the models into models with memory and those without memory [39]. The popular memoryless models are Middleton Class A, Bernoulli-Gaussian, and symmetric Alpha-Stable models [39, 37]. Even though the memoryless models are able to capture the non-Gaussian and impulsive nature of PLC noise, they fail to capture the temporal correlation that is inherent in PLC noise. To model this temporal correlation, Markov chain based models have been developed. A partitioned Markov chain model was developed in [3] which is able to capture the bursty nature of PLC noise by considering impulsive states and impulsive free states. This model is a generalisation of Gilbert-Eliott model [40]. The main challenge with this model is that it has binary output and is only suitable for binary communication channels. In [5], a Markov-Gaussian model is developed from the same principle as the Bernoulli-Gaussian model, but with an additional parameter which quantifies the channel memory. Even though Markov-Gaussian model is a continuous noise model, its main drawback is that it is restricted to only two states: impulsive free and impulsive sequence states. In each of the states, noise samples follow Gaussian distribution with impulsive states having noise variance which is very high compared to the variance of the impulsive free state.

The authors in [6] extended Middleton Class A model by incorporating an additional parameter that allows for controlling noise impulse memory. The model known as Markov-Middleton introduces noise memory through hidden Markov chain and it is a continuous noise model with finite states and the same probability density function (PDF) as the Middleton Class A model. In each of the finite states, the noise variance is a function of the physical parameters of the noise (number of simultaneous impulsive emissions, impulsive index and strength of the impulsive noise). The noise can be assumed to be a superposition of impulsive source emissions that are Poisson distributed both in space and time and have a temporal correlation. In all the memory models, the additional parameter capturing the noise memory is determined from noise measurements and details can be found in [3],[5] and [6].

There are also other studies on the characteristics of PLC noise which have concentrated on amplitude distributions, impulse width and impulse rate (see [3, 33, 41, 42, 43]) without considering much the frequency and strength of bursts which are prevalent in PLC noise and which impacts heavily on communication system development and performance analysis. Even though our interest is on

indoor low-voltage PLC applications, it should be noted that impulsive noise is a challenge even in other applications (e.g., see [44]). A shift of focus has recently turned into models and analysis considering the cyclostationary nature of PLC noise [45, 34, 32, 38, 46, 35]. This resurgence of interest in PLC noise modelling shows the importance as well as the complexity of noise experienced in power line channels.

2.6.1 Memoryless Models

2.6.1.1 Bernoulli-Gaussian

The assumption here is that the PLC noise has two components: thermal noise and impulsive noise, i.e., $n_{BG} = n_w + \beta n_i$, where n_w is the thermal(background) noise, n_i is the impulsive noise component and β is a Bernoulli random variable with state space $\{0, 1\}$. n_w and n_i are assumed to be independent Gaussian random variables. Defining probability $p = \Pr(\beta = 1)$ and assuming that the noise is real, the Bernoulli-Gaussian noise can be represented as eqn. (2.35) [37, 47]

$$n_{BG} = (1-p)\mathcal{N}(0, \sigma_b^2) + p\mathcal{N}(0, \sigma_i^2) \tag{2.35}$$

where $\mathcal{N}(0, \sigma^2) =: \frac{1}{\sqrt{2\pi\sigma^2}}\exp(\frac{-x^2}{2\sigma^2})$ and $\sigma_i \gg \sigma_b$.

2.6.1.2 Middleton Class A

Middleton [48, 49, 50] proposed a general classification of both natural and/or man-made electromagnetic disturbances and went further to distinguish between three classes of noises: class A, class B and class C, according to the frequency range occupied by the interference in comparison to the receiver bandwidth. Details can be found in the above references (see also [51, 52]). The main advantage of Middleton models is that they are canonical. Of the three, class A model has been proposed for applications in power line networks and in environments prone to impulsive noise because it requires the lowest number of parameters and hence more tractable [50]. The PDF of class A model can be represented as eqn. (2.36)

$$f_X(n_i) = \sum_{m=0}^{\infty} \frac{p_m}{\sigma_m\sqrt{2\pi}}\exp(-\frac{n_i^2}{2\sigma_m^2}) \tag{2.36}$$

where n_i are noise sample at discrete-time index i and p_m is the Poisson arrival process given by eqn. (2.37)

$$p_m = \frac{e^{-A}A^m}{m!} \tag{2.37}$$

with noise variance given by eqn. (2.38)

$$\sigma_m^2 = \sigma^2\frac{m/A + \Gamma}{1+\Gamma} \tag{2.38}$$

where Γ is the ratio of Gaussian to impulsive power ratio, σ^2 is the sum of Gaussian power and impulsive power of noise components. The parameter Γ gives an indication on how strong the impulsive component of the noise compared to the Gaussian component. The smaller the value of the Γ, the more impulsive the noise is. A is the impulsive index and it represents the product of the impulse rate λ, and the impulse mean duration T seen at the receiver ($A = \lambda T$).

Even though class A model requires only three parameters (A, Γ, σ^2), and has been widely used in designing optimal and sub-optimal receivers, it is not able to capture the temporal correlation inherent in environments prone to bursty impulsive noise. Other memoryless models employ alpha-stable distributions and its variants as reported in [53] and the references therein. This has lead to models with memory which is the focus of the proceeding subsection.

2.6.2 Models with Memory

Impulsive noise is caused by appliances connected to the network and their amplitude varies rapidly and is the main cause of system degradation due to bit or burst errors in high-speed data transmission. Background and narrowband noise amplitudes vary slowly over time and can be generally regarded as background noise. Therefore, PLC noise can be reclassified as background and impulsive noise [41]. When investigating the influence of impulsive noise in PLC systems, time domain measurement campaigns are done from which statistics of impulse width, arrival time and inter-arrival time are captured to estimate when impulse events occur. Again, from such data, impulse amplitude, impulse power or power spectral densities are derived, which give a feel of how strong the impulses are [3]. Noise models need to include sufficient details of the physical noise characteristics, and on the hand should be easy to implement in computer simulations. Normally a trade-off has to be balanced.

In [3], partitioned Markov chain-based model with a variable number of states was proposed to capture the transition between impulsive states and impulsive-free states, represented by independent transition probability matrices. Impulsive-free states represent situations when only background noise is observable, while impulsive states represent impulse events. Even though the model in [3] is able to represent the transition between impulsive-free events and impulsive events, it is not able to replicate sufficient samples for wide band communication channel representation. Some of the research work is available in the literature that tries to address this drawback and will be discussed next.

2.6.2.1 Markov-Gaussian

This can be considered as an extension of Bernoulli-Gaussian model and is modelled as a two-state Markov process. The two states correspond to the channel being in a bad state or good state. When in a good state, the additive noise is

only AWGN and when in a bad state, the noise is a superposition of AWGN and impulsive noise. In other words, at each time index k, noise n_k is defined completely by channel state $s_k \in \{G, B\}$ which are binary alphabets for good channel and bad channel respectively [5, 54]. Assuming a complex circularly-symmetric Gaussian random variable with variance depending on channel state s_k, the probability density function of n_k conditioned on s_k is given by eqn. (2.39) [5, 54]

$$p(n_k|s_k) = \frac{1}{2\pi\sigma_s^2}\exp(-\frac{|n_k|^2}{\sigma_s^2}) \tag{2.39}$$

where the noise variance under impulsive state is greater than the good state value. Markov-Gaussian can graphically be represented as shown in Figure 2.9, illustrating the good and bad state. The probabilities of being in a given state is given by eqns. (2.40) and (2.41) respectively

$$P_G = P(s_k = G) = \frac{P_{BG}}{P_{GB} + P_{BG}} \tag{2.40}$$

$$P_B = P(s_k = B) = \frac{P_{GB}}{P_{GB} + P_{BG}} \tag{2.41}$$

and the average number of consecutive samples of persistence in impulsive free and impulsive state is given respectively by eqns. (2.42) and (2.43)

$$T_G = \frac{1}{P_{GB}} \tag{2.42}$$

$$T_B = \frac{1}{P_{BG}} \tag{2.43}$$

In most scenes, the impulsive state is relatively less frequent in comparison to the impulsive free state, that is, $T_G > T_B$. T_G and T_B can be estimated from noise measurements, from which the statistical parameters (P_{GB}, P_{BG}) can be derived. For models with memory, an important parameter that quantifies the channel memory, which can be defined as eqn. (2.44)

$$\gamma = \frac{1}{P_{GB} + P_{BG}} \tag{2.44}$$

When $\gamma = 1$, the channel is memoryless, when $\gamma < 1$, the channel has an oscillatory memory and it has persistent memory when the value of $\gamma > 1$. For bursty channels, $\gamma > 1$ condition will be of interest.

2.6.2.2 Markov-Middleton

The authors in [6] proposed a modification of Middleton class A model based on hidden Markov model (HMM), whose output follow a class A distribution. In addition to class A parameters, this model has an extra parameter for controlling noise memory. Considering a finite state, they truncated the infinite Middleton

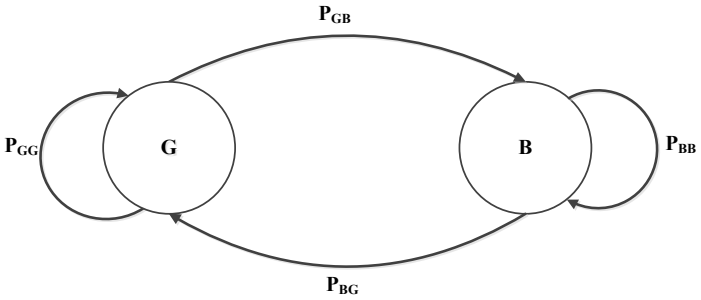

FIGURE 2.9: Two State Gaussian-Markov Model

class A model to the first four terms as eqn. (2.45) [6]

$$\acute{p}(n_k) = \sum_{m=0}^{3} \frac{p_m^{`}}{\sigma_m \sqrt{2\pi}} \exp(-\frac{n_k^2}{2\sigma_m^2}) \tag{2.45}$$

with

$$p_m^{`} = \frac{p_m}{\sum_{m=0}^{3} p_m}$$

Figure 2.10 shows the model with transition state (TS), the duration within the TS being null. The parameter x, which represents correlation between noise samples is independent of class A parameters can be estimated from noise measurements from the following eqn. (2.46)

$$\bar{n_i} = \frac{1}{1 - P_{ii}} = \frac{1}{(1-x)(1-\acute{p_i})} \tag{2.46}$$

where $\bar{n_i}$ is the mean duration is samples spent in state i. The details of how to determine x can be found in [6].

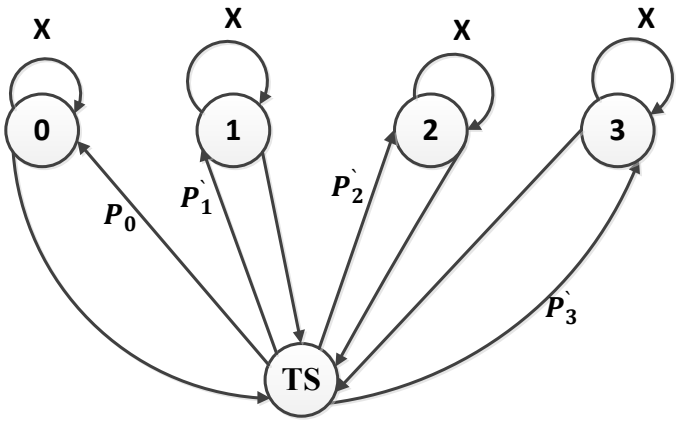

FIGURE 2.10: Markov-Middleton Model

2.7 Conclusion

In this chapter, we have reviewed the challenges of PLC networks, specifically multipath propagation and bursty impulsive noise. Recent PLC noise models incorporate Markov processes in designing models to capture correlation inherent in PLC noise. However, Markov models are only able to capture correlations in small scales since they work on assumption of weak dependence. When there is strong dependence in the signal to be modelled, there more superior models must be explored for a more accurate representation. This thesis will mainly focus on estimating long-range correlation in PLC noise and also perform local scaling analysis so as to come up with noise models that are able to capture this scaling behaviour.

CHAPTER 3

Multipath Propagation Phenomena in Power Line Networks

3.1 Introduction

Power line communication channel is known to be harsh due to multipath phenomena and non-Gaussian noise. Multipath propagation is due to line discontinuities resulting from impedance mismatch at the branches and terminations in the network. For proper design and performance evaluation of a communication system, the channel characteristics need to be understood since the quality of transmission depends on the channel characteristics. The PLC channel is mainly affected by multipath propagation and non-Gaussian noise [1].

According to electromagnetic theory, for maximum power transfer, the transmission medium must be matched to the transceivers, i.e., for the PLC case, the receiver and transmitter impedances must have same impedance as the characteristic impedance of the transmission cable. However, even if this be the case, there are normally branches and terminations in the power networks which bring about impedance mismatch resulting from line discontinuities [1],[23]. The reflections result in the transmitted signal reaching the receiver through different paths with corresponding delays which are attenuated depending on the path lengths followed by the corresponding signals. Electrical loads connected to the power networks have impedances that vary with time during the mains supply cycle and

this causes mismatch that varies with time. Again, there exist impedance mismatch even if there are no loads connected at power terminals, i.e., open circuits and short circuits so long as the termination is not matched with the cable's characteristic impedance [55]. Therefore, an understanding of how these branches and terminations affect the PLC channel contributes a lot in designing the effect's mitigation techniques. The authors in [56] have proposed channel model and taking into consideration of interconnections in power network topology and loadings at terminals with very interesting results.

The network topology parameters (branch length, number of branches, load impedance, etc) has been found to influence the network performance. For instance, the authors in [57] investigated their effects on underground cables PLC systems in Tanzania and found from frequency response of the transfer function that these parameters have effect on the magnitude and position of notches and peaks. Similarly in [58], the same results are seen in medium voltage PLC systems. In [59] their effects on OFDM systems in PLC networks was investigated and the results show that signal attenuation between the transmitter and receiver increases with increase in number of branches and their lengths. For RMS delay spread, authors in [60] found that RMS delay spread tend to fit well by lognormal and Nakagami distributions. The importance of these parameters are important and continue to be studied, and hence their understanding forms the basis of optimal PLC systems.

The main aim of this chapter is to study and analytically explain the effects of branch lengths and termination loadings on the root mean square delay spread of the channel. The root mean square delay spread gives an indication of the multipath richness of the channel and it has been found to be log-normally distributed and inversely correlated with channel gain (see, [15],[14]). A good understanding of how the aforementioned factors affect the RMS delay spread is worth investigating for the success of PLC deployment and performance [17],[30]. A similar study related to the work in this paper has been done by [61] by employing a chain matrix method without looking into the RMS delay spread, which is key in developing mitigation techniques of the effects of multipath propagation in PLC networks.

3.2 Multipath Propagation in PLC Channels

We explain the concept of multipath in PLC with the aid of a simple one tap T-network topology shown in Figure 3.1. This model although simple hence easy to understand, is also popular because all other complex topologies can be decomposed to simple one tap T-network topologies and similar analysis followed. It has been by adopted by [1], [62], [63] among others.

The one tap topology has only one branch and three segments with corresponding lengths and impedances. Assuming signal is injected through terminal **A** and

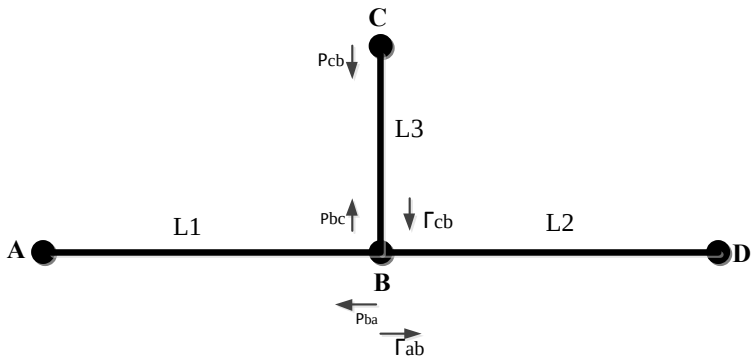

FIGURE 3.1: Simple one branch T-network topology

received at terminal **D**, both matched to the transmission line, the points of reflections will be **B** and **C**. Theoretically, the received signal is a sum of infinite echoes of the transmitted signal and the direct path signal. However, as the signal path increases, its effect diminishes and the received signal can be approximated by a finite number of paths (N) and can be expressed by eqn. (3.1) [1]

$$H(f) = \sum_{i=1}^{N} g_i . e^{-(a_0 + a_1 . f^k) . d_i} . e^{-j2\pi f \tau_i} \tag{3.1}$$

where g_i is the weighting factor which is normally assumed as real-valued but is generally complex and is frequency dependent. This weighting factor is a product of reflection and transmission coefficients discussed later in this paper. The first exponent is the attenuation portion which increases with path distance (d_i) and frequency (f), i.e., it shows a low pass characteristic. The attenuation parameters a_0, a_1 and k, (which represent offset of attenuation,increase of attenuation and exponent of attenuation respectively) can be obtained from magnitude of frequency response. The second exponent is the delay portion. The delay τ_i is given by eqn. (3.2)

$$\tau_i = \frac{d_i \sqrt{\varepsilon_r}}{c_0} = \frac{d_i}{v_p} \tag{3.2}$$

where ε_r is the dielectric constant of the insulating material and c_0 is the speed of light.

Multipath propagation can be represented graphically as in Figure 3.2, where τ_i's represent delays encountered in different paths and G_i's the corresponding gains in each of these paths. Since this work entails investigation of physical operating environment of the PLC system (network topology and loading), the attenuation portion of the channel frequency response can be ignored. This assumption will not affect our conclusions. We also follow a deterministic approach in determining the reflection factors of each path. Deterministic approach, although site specific, accurately provides the analysis required for design and performance of

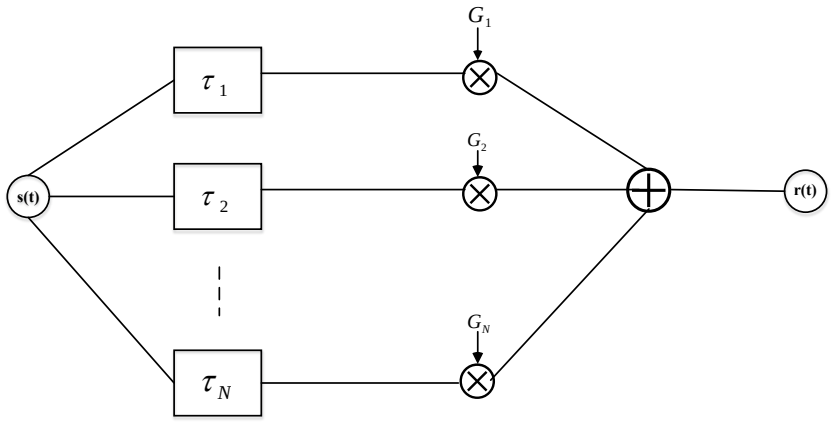

FIGURE 3.2: Multipath Propagation Graphical Model of PLC Channel assuming additive channel noise

PLC systems. The results can be generalized and extended to statistical models which are handy in a priori analysis of systems before deployment.

Taking the previous assumption that the transceivers are matched, the reflection points are B and C with ρ_{ba}, ρ_{bc}, ρ_{cb} as the reflection coefficients and Γ_{ab}, Γ_{cb} as the transmission coefficients. The product of these factors constitutes the weighting factor of each propagation path. Hence, the determination of this factor is very important in PLC channel characterization. From electromagnetic theory, the reflection and transmission coefficients can be computed from eqn. (3.3) [64]

$$\rho = \frac{(Z_L - Z_0)}{(Z_L - Z_0)} \quad \text{and} \quad \Gamma = 1 + \rho \tag{3.3}$$

where Z_L is the impedance seen by the signal at a discontinuity and Z_0 is the characteristic impedance of the transmission cable through which the signal propagates.

Ignoring the attenuation portion in (3.1), the frequency response becomes eqn. (3.4) [65],

$$H(f) = \sum_{i=1}^{N} \left[\prod_{r=1}^{R} \rho_{ir} \prod_{m=1}^{M} \Gamma_{im} \right] e^{-j2\pi f \tau_i} \tag{3.4}$$

where R and M are the number of reflections and transmissions respectively. Taking the inverse fast Fourier transform of the channel frequency response, CIR is obtained as eqn. (3.5)

$$h(t) = \sum_{i=1}^{N} \left[\prod_{r=1}^{R} \rho_{ir} \prod_{m=1}^{M} \Gamma_{im} \right] \delta(t - \tau_i) \tag{3.5}$$

3.2.1 RMS Delay Spread

The previous section has shown that the PLC channel is multipath prone and to characterize this multipath phenomena, RMS delay spread is a very important metric to consider. Due to multipath, the transmitted signal arrives at the receiver via different paths at different time delays as a result of different propagation lengths followed by the signal. Delay spread is the duration difference between the time the first signal arrives at the receiver and the time the last non-negligible echo component arrives.

When the signal symbol duration is big enough in comparison to the delay spread, then there is little time spreading of the received signal and one would expect inter-symbol interference free channel. However, if this delay spread is big enough, then it can result in serious signal distortion [31]. In other words, the RMS delay spread is known to be a good measure of multipath phenomena and provides an indication of the extent of possible distortion of signal at the receiver due to ISI.

Root mean square delay spread can be estimated from power delay profile. PDP of a channel provides an indication of the distribution of transmitted power over various paths in a multipath environment and is estimated from the spatial average of channel impulse response [17], i.e., it is the square root of second central moment of the power delay profile. The RMS delay can be given by eqn. (3.6) [15],[31]

$$\tau_{rms} = \sqrt{\frac{\sum_{i=0}^{N} \tau_i^2 |h_i|^2}{\sum_{i=0}^{N} |h_i|^2} - \left(\frac{\sum_{i=0}^{N} \tau_i |h_i|^2}{\sum_{i=0}^{N} |h_i|^2} \right)^2} \tag{3.6}$$

3.3 Determination of Reflection Factors and Signal Propagation Lengths

It has been shown in the previous section that power networks are branched networks with terminations that are connected to loads with time varying impedance. The meaning of this is that for PLC applications, impedance mismatch is inevitable leading to multipath propagation. The effect of impedance mismatch leading to impedance discontinuities in PLC channels can accurately be estimated if network topology and cable characteristics are known a priori. For this to be realized, reflection factors within a given path followed by a signal need to be determined in addition to propagation length followed by the signal. It is worth noting that propagation length followed by the first arriving signal (i.e, the most significant path in terms of signal strength) is not necessarily equal to the transmitter-receiver physical distance. But, for simplicity, we will assume that the first arriving signal followed a direct path without reflections and hence the path length is assumed to be equal with the physical transmitter-receiver length.

TABLE 3.1: Reflection factors and propagation lengths for 4 path one tap T-network topology

N	**Signal Path**	**Reflection Factors**	**Propagation Length** (m)
1	A→B→D	0.6667	200
2	A→B→C→B→D	0.4444	220
3	A→B(→ C → B)^2 →D	-0.1481	240
4	A→B(→ C → B)^3 →D	0.0494	260

Considering Fig. 3.1, the direct path (A→B→D) will have a reflection factor only consisting of transmission coefficient as it has no reflection component. The propagation length will be $L1+L2$. The second possible path' (A→B→C→B→D) reflection factor is given by $\Gamma_{ab} \times \rho_{cb} \times \Gamma_{cb}$ and the corresponding propagation length is $L1 + 2.L3 + L2$. The reflection factors for $N \geq 3$ can be computed from eqn. (3.7)

$$g_i = \Gamma_{ab} \times \rho_{cb}(\times\rho_{bc} \times \rho_{cb})^{N-2} \times \Gamma_{cb} \tag{3.7}$$

and the propagation length from eqn. (3.8)

$$l_N = L1 + 2(N-1) \times L3 + L2. \tag{3.8}$$

For Figure 3.3, the same principle applied above is used appropriately. For one branch, the above procedure for one tap network is used as it is in calculating both reflection factors and propagation lengths. Any of the three taps can be chosen randomly for one tap application as this will not affect the analysis. However, for two tap and three tap, same method is used but considering the various reflection and transmission coefficients at each of the impedance discontinuities.

One tap T-network configuration of Figure 3.1 is employed for this analysis with the branch length being varied as 10 m, 15 m, 20 m and 25 m. Section lengths $L1$ and $L2$ being 120 m and 80 m respectively. Again, we assume open circuit (representing the worst case scenario) at the load terminal for easy analysis.

Using the above procedure for one tap topology with branch length of 10 m, the reflection factors and propagation lengths followed by a signal from transmitter to receiver is given in Table 3.1. The assumption is that there are only 4 paths with non-negligible contribution at the receiver. The first arriving path (shortest path) has the highest contribution since it has less reflections hence less attenuation. The determination of this first arriving path and its distribution is important as it provides the reference point of other significant paths but is beyond the scope of this study. Interested readers can refer to [66], [19]. In [66], it is reported that the first arriving path can be approximated by log-normal probability density distribution with decreasing mean and increasing variance as number of branches between transmitter and receiver increases. In [19], the authors classify PLC channels into clusters using the magnitude of first arriving path.

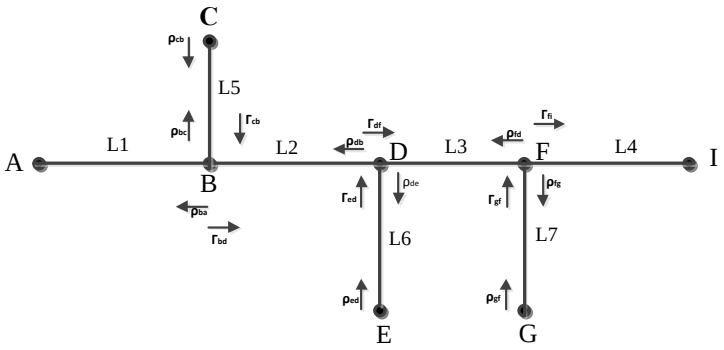

FIGURE 3.3: A Three-tap branched network topology

3.4 Simulation Results

We assume that the transmission cables in the power network are of the same type, hence they also have the same characteristic impedance. Transceiver is also assumed to be matched to the cable characteristic impedance leaving impedance discontinuities only at branches and load terminals for both single tap and three tap network. Cables' characteristic impedance is assumed to be approximately equal to 70 Ω each. The open-circuit and short-circuit impedances used in these simulations are 100 $M\Omega$ and 0 Ω respectively. The results in this paper are simulations performed in MATLAB software.

3.4.1 Impact of Branch Length

Figure 3.5 shows the frequency response of the channel configuration under study. The number of notches increases with corresponding increase in branch length. However, the amplitude remains the same even with increasing frequency. Table 3.2 is the corresponding values of RMS delay spread. It is evident that the delay spread increases with increasing branch length. This can be attributed to the fact that as the propagation length increases, more reflections occur within the propagation path. This increases the propagation duration a signal takes from transmitter to the receiver increasing delay in relation to the first arriving path signal.

TABLE 3.2: RMS Delay Spread Variation with Branch Length

Branch length (m)	**RMS Delay Spread** μsec	**Mean Delay** μsec
10	0.1973	0.1633
15	0.2992	0.2449
20	0.3975	0.3266
25	0.4226	0.4082

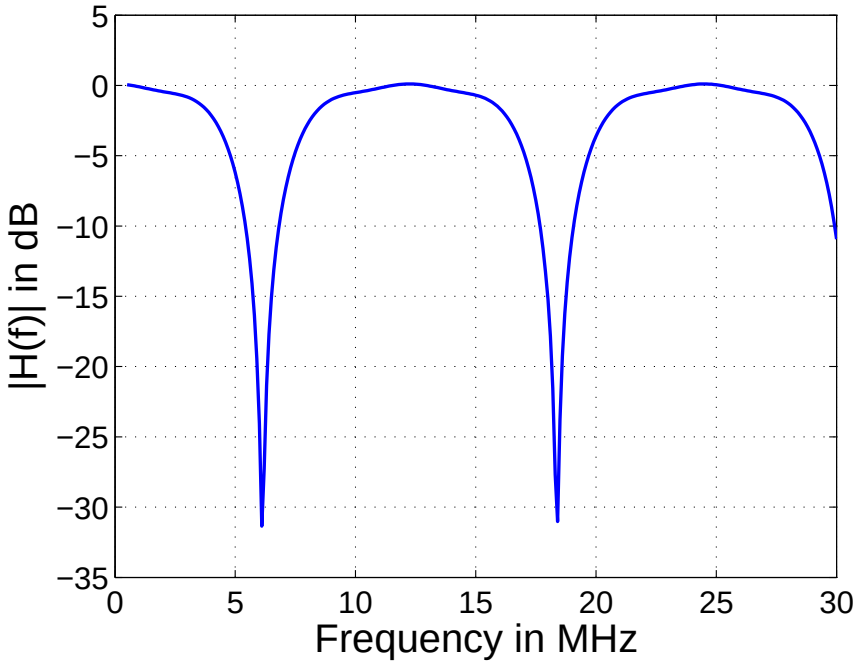

(a) 10 m

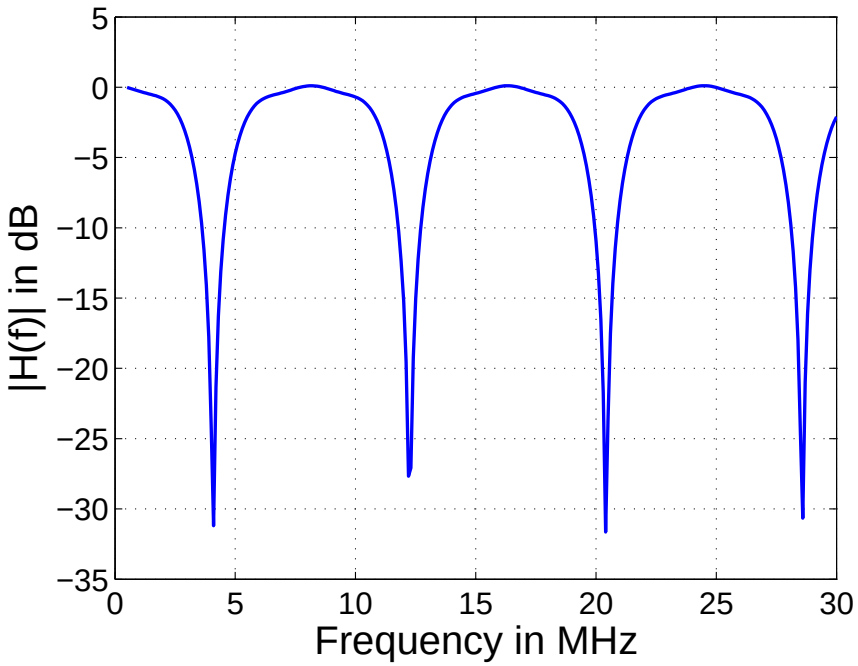

(b) 15 m

FIGURE 3.4: Frequency response for one tap topology with various branch lengths

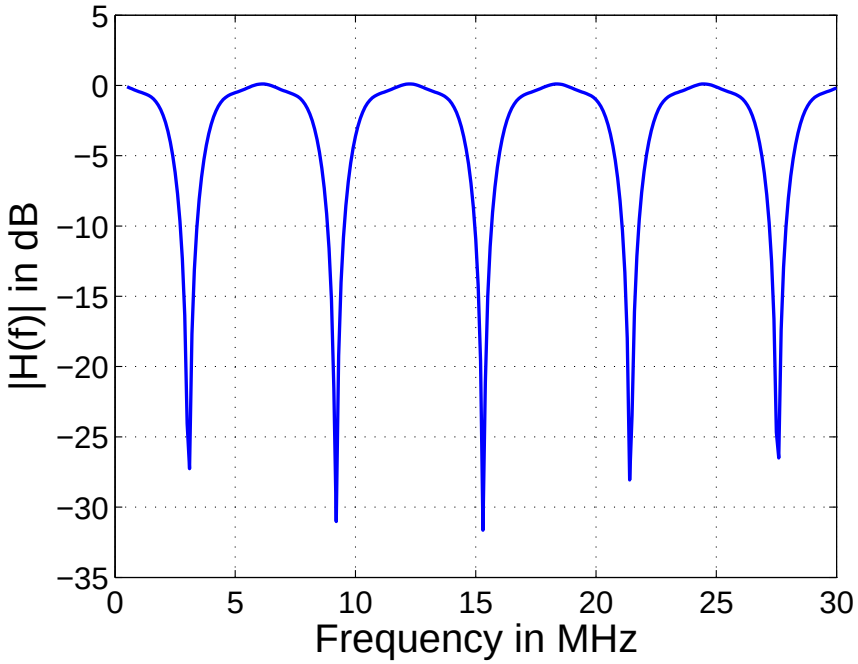

(a) 20 m

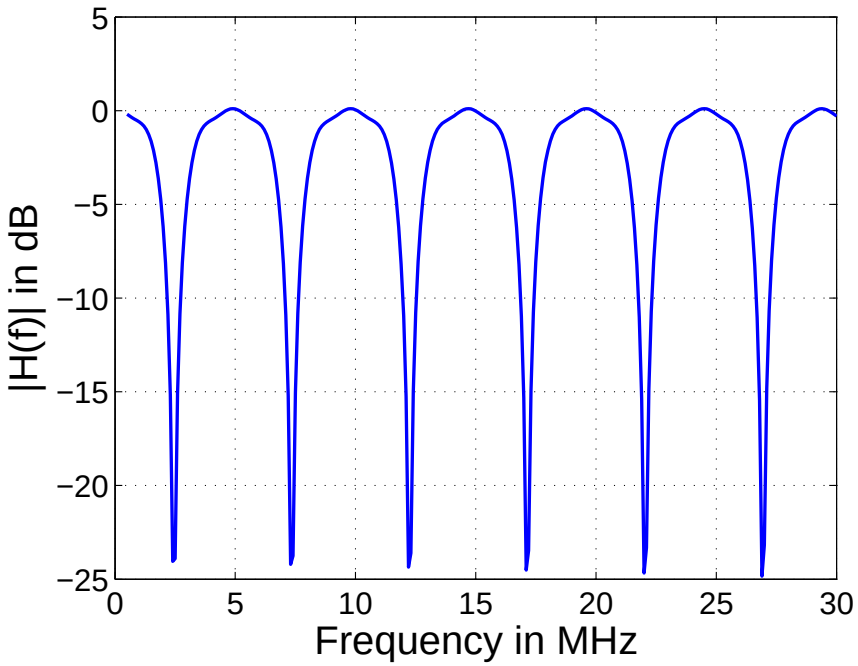

(b) 25 m

FIGURE 3.5: Frequency response for one tap topology with various branch lengths

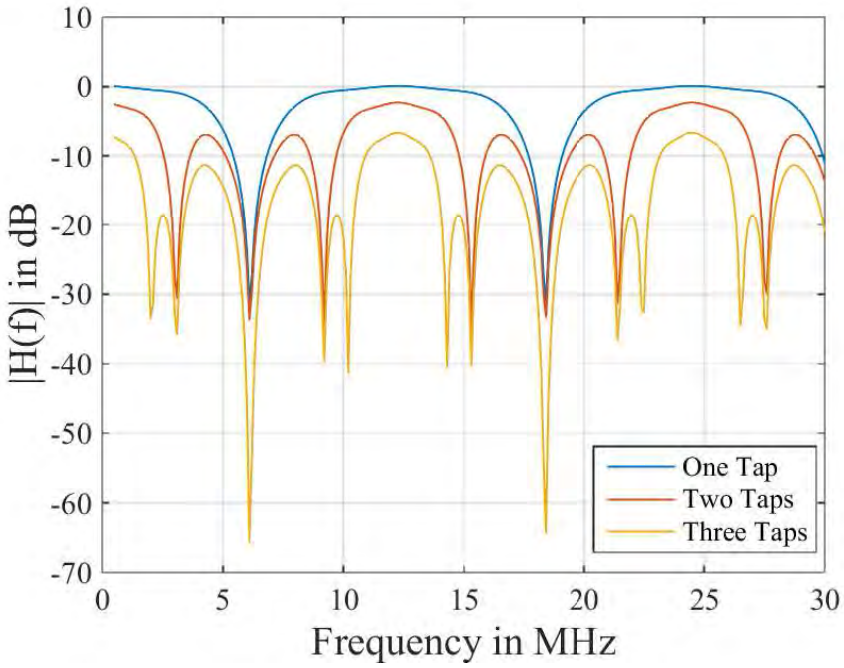

FIGURE 3.6: Frequency response for three tap topology with same branch length

3.4.2 Impact of Number of Branches

With increase in number of branches, the probable propagation paths and lengths increases. Figure 3.6 shows the results for a three tap network topology. The notch depth increases as the number of branches increases but it can be seen that the position for the deep notches appear at the same position for all the cases (i.e., for one tap, two tap and three tap). As expected, the number of notches increased with increase of branches due to increased propagation length. Otherwise, the trend is not the same for RMS delay spread values. RMS delay spread values are found to be 0.1973μs, 0.2177μs and 0.1853μs respectively for one tap, two tap and three tap respectively. The three tap value shows a discrepancy which require further research. However, as the number of branches increases, some paths cancel each other and may result in the three tap having a lower RMS delay spread value.

3.4.3 Impact on Terminal Loading

Here we take two extremes of the loading: open circuit and short circuits. It is seen that the effect of open circuit and short circuit are the same but shifted 180 degrees apart. The results are shown in Figure 3.7. Figure 3.7 (a) is a mirror image of Figure 3.7 (b). For the RMS delay spread for the two scenarios, there is no much difference, i.e., 0.1973μs and 0.2219μs for open circuit and short circuit respectively.

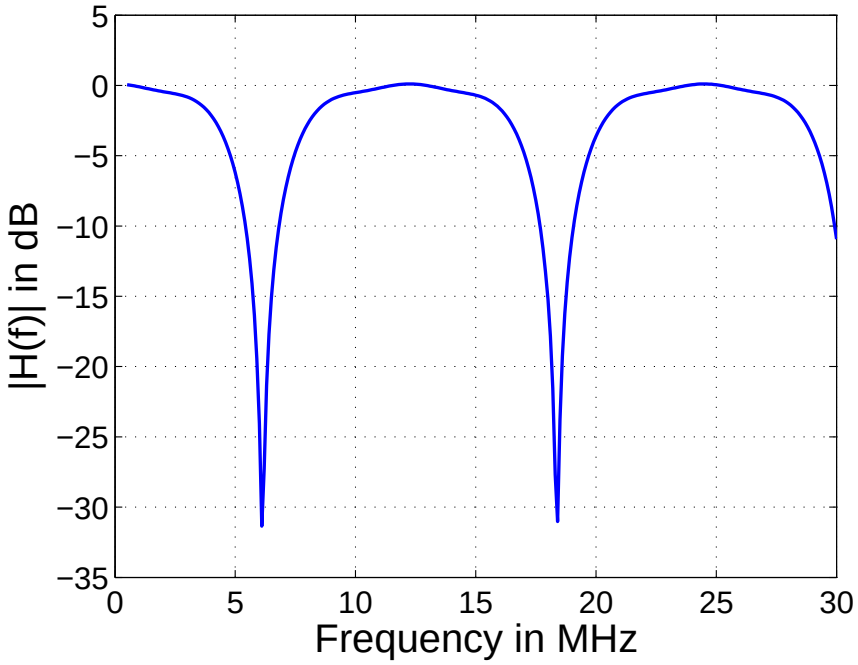

(a)

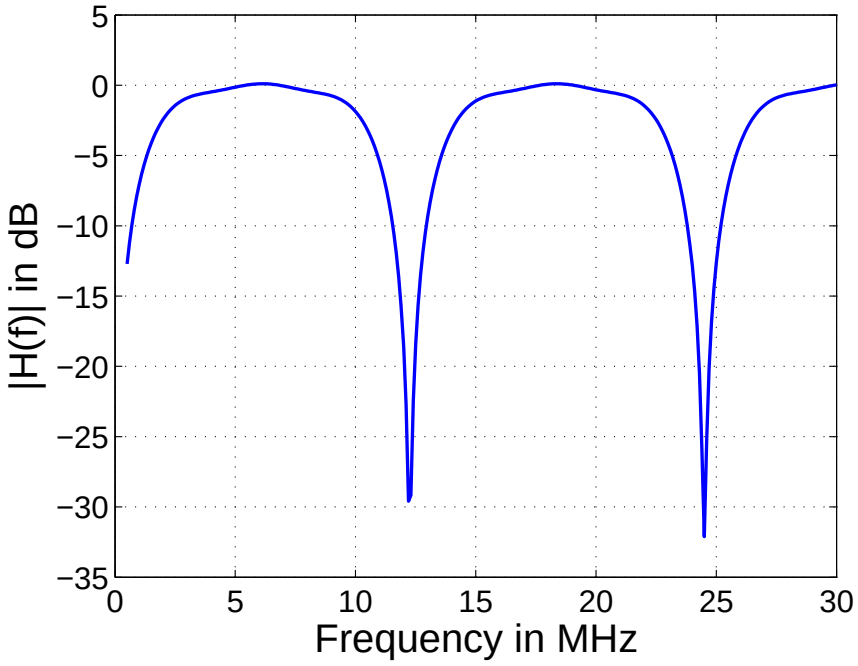

(b)

FIGURE 3.7: Frequency Response for one tap topology with termination (a) Open circuited (b) Short circuited

For one-tap branched network, when the load terminals are matched with transmission cable characteristics impedance, the cable behaves like an infinitely long cable and no reflections are encountered in the channel. Otherwise when there are many branches, then there will be many signal generated within the neighbouring branches. This means that the frequency response of the channel remains flat without any notches and there is no RMS delay spread since only the shortest path is seen by the signal. The values for RMS delay spread for the channel are below 0.6 μs which is comparable to the values obtained from measurements in [17] and [67].

3.5 Conclusion

A typical Power line communication channel is a branched network. An analytical study of a simple T-network has been presented in this chapter. Simulation results show that the number and/or position of notches are not affected by the position of the branching node between the transmitter and receiver but by its length, as long as the length between the transmitter and receiver remains unchanged. Otherwise by varying the length of branch, the number of notches increases proportionally. The RMS delay spread increases as the propagation paths with non-negligible effects increases. This is because a number of echoes arrive at the receiver via different paths from the transmitter. As the number of branches increases, the depth of notches increases and even reach the noise floor values. Extreme cases of loading at the terminals has also been reported, but assuming static loads. Further research is to study the behaviour of the hybrid (T-topology and ring topology) PLC channel when the load impedance varies, which is a more practical case and the findings will go a long way in establishing the best multipath mitigation techniques for the PLC channel.

CHAPTER 4

Estimation of Long-Range Dependence in Power Line Channel Noise

4.1 Introduction

In this chapter, the study is concerned with understanding of the correlation structure of power line channel noise. Correlation can be defined as a measure of self-similarity of a signal with its delayed version. It reveals the periodicity or randomness of the signal. The more correlated a signal is, the more concentrated its power spectral density. Conversely, the more random or unpredictable a signal is, the wider the spread of its power spectrum. Correlation structure of a signal is crucial in estimation problems, decision-making and detection, and in system analysis. Noise in power line communication networks is a serious impairment to the success of high speed data transmission in PLC networks. Therefore, studies on its characteristics continue to be of interest to the research and design community so as to come up with more accurate methods of modelling it, and efficient ways of mitigating its effects in PLC systems. The question that we intend to answer in this chapter is whether noise encountered in power line networks is self-similar and the significance of this information in noise modelling.

Several studies have shown that PLC noise is highly correlated, that is, it has persistence in memory and modelling this noise should be able to take that into consideration [6, 68, 5]. This is important because codes for error correction

in communication systems assuming memoryless channels may not necessarily be optimal in channels with memory. The effect of persistence in memory is that what happens now will affect the future, that is to say, the results are sensitive to initial conditions. In probabilistic terms, the probability of a channel remaining in a certain state is higher than the steady-state probability of being in that state [40]. The interest of this study is to investigate whether we can conclude that PLC noise shows long-range dependence by estimating the Hurst parameter (H), which measures the intensity of long-range dependence. When this parameter ranges between 0.5 and 1, (i.e., $1/2 < H < 1$), then the data is said to show long range dependence. This will play a key role in noise modelling and PLC system error performance analysis.

Preliminary results show that PLC noise exhibits statistical long range dependence [4]. However, the authors in [4] applied one method only for estimating Hurst parameter. Even though the method used in the said study is one of the oldest and most popular method of estimating Hurst parameter, studies show that Hurst parameter estimation is not a straight forward procedure and no single estimator can be trusted to give accurate results [69]. It is normally recommended that a number of methods be used for estimation of the parameter before conclusive conclusions can be made. In this study, we employ three methods for Hurst parameter estimation and compare the values obtained by these methods.

In addition, preliminary research shows that PLC noise exhibits self-similarity and can be predicted by fractal theory. In modelling noise employing fractal theory, the Hausdorff dimension (D) needs to be approximated. D is related to Hurst parameter (H), which is a measure of self-similarity. Hence, it is important to estimate H for accurate noise prediction using fractal theory. H parameter estimators assume stationarity in time series data, but studies have shown that PLC noise is not stationary [32, 35]. Non-stationarity, trends and periodicity affects the estimators [70, 69]. Therefore, preprocessing is required for the case of PLC noise before estimating H to make it stationary as periodicity and nonstationarity affect the H estimators.

In this study, we remove the periodicity hidden in the PLC noise obtained from measurement campaign within several university offices, workshops and laboratories. Then long-range dependence is estimated from this pre-processed noise data by employing three estimation algorithms: R/S (rescaled adjusted range) method, aggregated variance method and absolute values of aggregated series method. Results from the said estimation methods though not the same, show that the Hurst parameters obtained from various noise measurements are greater than 0.5, implying the presence of self-similarity with long-term memory. Results from this study will find valuable applications in PLC noise modelling using fractal and chaos theory and in error performance analysis in both narrowband and broadband PLC systems.

4.2 Noise Measurement Set up

Characterization and modelling of noise present in power line communication system requires rigorous noise measurement campaign. For this study, PLC noise measurements were recorded using the set-up shown in Figure 4.1. The set up comprises a coupling unit used for protecting Digital Storage Oscilloscope (DSO) from high power network currents. The coupling unit also acts as a high pass filter, allowing only signals of interest to pass through. The DSO employed here as a receiver is capable of recording 14 million data point samples and was set to sample noise at a rate of 50 Mega-samples per second. This implies that we are able to capture noise from the lower cut-off frequency of the coupling unit (100 kHz) to 25 MHz frequency range.

Three scenarios are used in this study. First, noise measurements were done in one of the postgraduate study offices with electrical loads being fluorescent lights, desktop computers and air conditioners. The sample is shown in Figure 4.2. It should be noted that these electric loads are the PLC noise generators and the adjacent offices connected to the same bus-bars have similar loads. Secondly, noise from Electronic Laboratory (Figure 4.3) was measured when students were undertaking their practicals. In addition to fluorescent lights and air conditioners, electronic loads with components like silicon controlled rectifiers (SCRs) and measurement equipment were connected to the power network. Lastly, PLC noise was measured in a stand-alone five bedroomed apartment (Figure 4.4). The electrical loads here include lights, television set, washing machine, two fridges and a vacuum cleaner. The first two scenarios are situated within the University of KwaZulu-Natal and the third one is located away from the University. These scenarios are just representatives of actual PLC channels and there is nothing so special about their location apart from the different loads in these locations which also act as noise generation sources.

Noise measurements were done when all of these loads were running/switched on, and from Figures 4.2, 4.3 and 4.4 it can be seen that each of the different environments generate unique noise samples due to different noise sources. Moreover, the switching times (ON and OFF) of these loads are also random and the noise is expected to show this randomness without correlation. However, previous studies have established that PLC noise though generated from different sources randomly, is correlated. It is also known that some extra noise from without the power grid is coupled to the indoor network via conduction or radiation [3].

4.2.1 Deseasonalization of PLC Noise

Deseasonalization of PLC Noise is to remove periodicity in the noise so that the noise sequence is stationary. The noise sequence is first passed through a finite impulse response (FIR) passband filter to select the spectral components of interest (0.1-25 MHz). The cyclic autocorrelation function of the filtered sequence ($w(n)$)

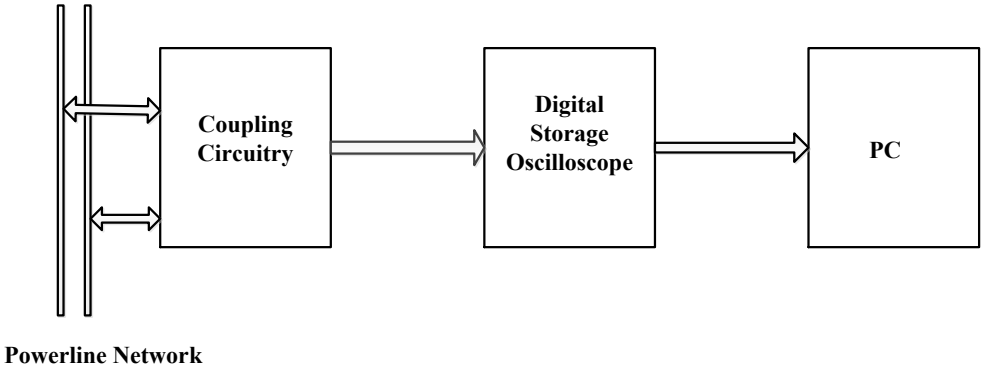

FIGURE 4.1: Power line noise measurement set-up

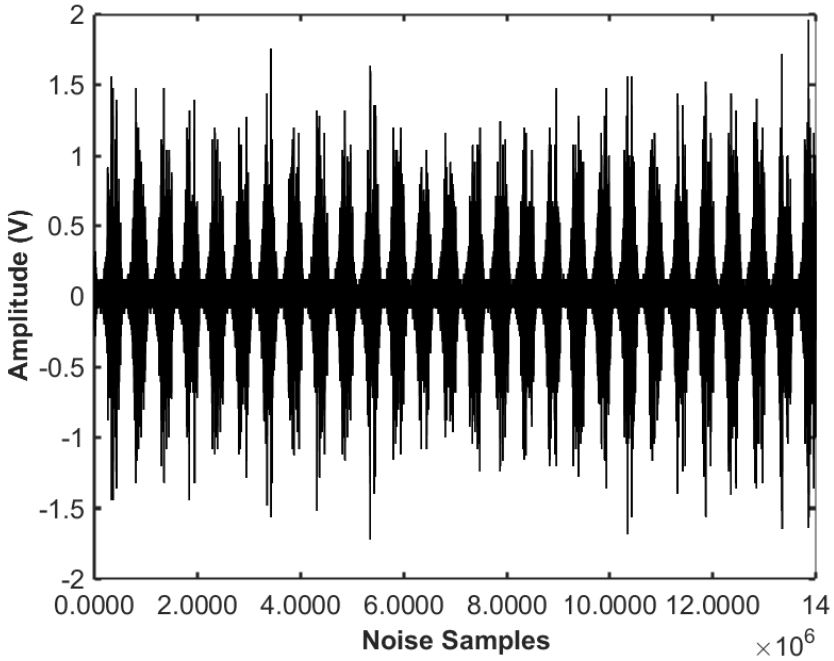

FIGURE 4.2: Office Noise measurement samples

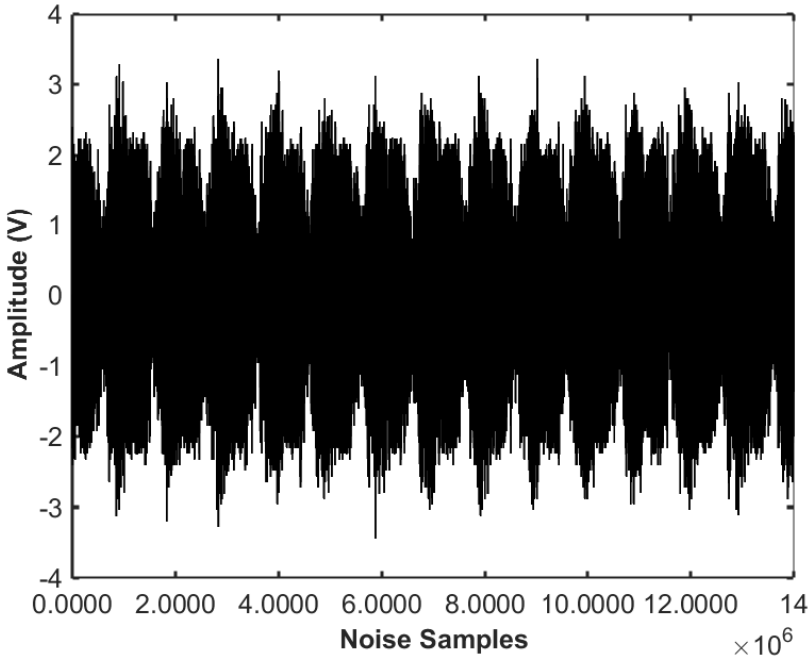

FIGURE 4.3: Laboratory Noise measurement samples

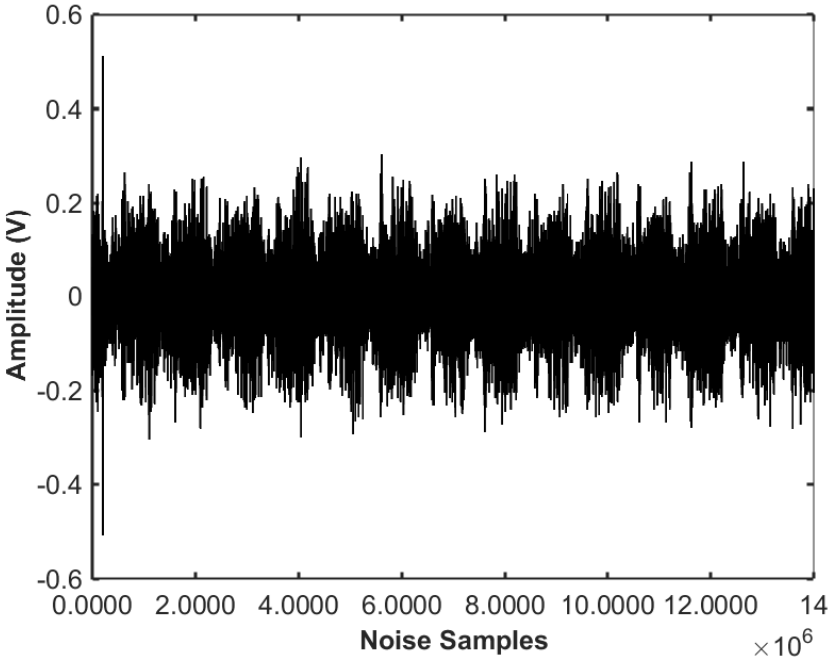

FIGURE 4.4: Apartment Noise measurement samples

is then computed as eqn. (4.1)

$$R_w(\alpha_k, \tau) = \frac{1}{N} \sum_{n=0}^{N-1} w(n)w(n+\tau)e^{-j2\pi\alpha_k n} \tag{4.1}$$

where α_k denotes the kth cyclic frequency and τ is the lag. Periodicity of the sequence can then be identified by peaks in $R_w(\alpha_k, \tau)$. After evaluating the cyclostationary period, measured in samples, the deseasonalization procedure of the noise can be summarized as follows [31]. For a given season s, determine the mean value μ_s and the standard deviation σ_s respectively as eqn. (4.2) and (4.3)

$$\mu_s = \frac{1}{\lfloor N/P \rfloor} \sum_{p=0}^{\lfloor N/P \rfloor - 1} w_{p,s} \tag{4.2}$$

and

$$\sigma_s = \sqrt{\frac{1}{\lfloor N/P \rfloor} \sum_{p=0}^{\lfloor N/P \rfloor - 1} (w_{p,s} - \mu_s)^2} \tag{4.3}$$

where $\lfloor \cdot \rfloor$ denotes floor function, P is the period in samples and s is the season. Then the cyclostationarity can be removed by employing one-to-one transformation as eqn. (4.4)

$$z_{p,s} = \frac{w_{p,s} - \mu_s}{\sigma_s} \tag{4.4}$$

4.2.2 Long-Range Dependence Estimation

In this section, procedures for three methods used for estimating H parameters is briefly discussed and the results are tabulated in the next section.

4.2.2.1 R/S Analysis (Rescaled adjusted range)

R/S is considered as one of the oldest and best known method for estimating H parameter [71, 72, 73]. The time series data of length N is divided into d sub-series of length n. Next for each sub series $m = 1, \cdots, d$, we compute the mean (E_m) and standard deviation (S_m). Then we normalize the data by subtracting the sample mean from it, i.e.,$X_{i,m} = Z_{i,m} - E_m$ for $i = 1, \cdots, n$, from which we create a cumulative time series $Y_{i,m} = \sum_j^i X_{j,m}$ for $i = 1, \cdots, n$. From the cumulative series, we then find the range, $R_m = \max\{Y_{1,m}, \cdots, Y_{n,m}\} - \min\{Y_{1,m}, \cdots, Y_{n,m}\}$. Then we rescale the range with standard deviation R_m/S_m. Finally, the mean value of the rescaled range for all the sub series of length n is calculated from eqn. (4.5),

$$(R/S)_n = \frac{1}{d} \sum_{m=1}^{d} R_m/S_m. \tag{4.5}$$

The value of H can be estimated by calculating the value of slope of a plot of logarithm of $(R/S)_n$ against the logarithm of n.

4.2.2.2 Aggregated Variance Method

In this method, the original time series is divided into blocks of size m, $X = \{X_i, i \geq 1\}$ and the average within each block is calculated [73]. This is considered the aggregated series from eqn. (4.6)

$$X^{(m)}(k) = \frac{1}{m} \sum_{i=(k-1)m+1}^{km} X(i) \qquad k = 1, 2, \cdots \tag{4.6}$$

for successive values of m. Then the sample variance of $X^{(m)}(k), k = 1, 2, \cdots,$ within each block is calculated from eqn. (4.7)

$$\hat{\text{V}}\text{ar}X^{(m)} = \frac{1}{N/M} \sum_{k=1}^{N/m} (X^{(m)}(k))^2 - (\frac{1}{N/m} \sum_{k=1}^{N/m} X^{(m)}(k))^2 \tag{4.7}$$

This procedure is repeated for different values of m and a plot of the logarithm of the sample variance versus log m is done. m is chosen such that it is equidistant on a log scale, so that $m_{i+1}/m_1 = C$, where C is a constant which depends on the length of the series and the desired number of points. The resulting points form a straight line with a slope $\beta = 2H - 2, \quad -1 \leq \beta < 0$.

4.2.2.3 Absolute Values of Aggregated Series Method

This method is quite similar to the aggregated variance method and that data sequence is split in the same way. That is, calculate the aggregated series as in eqn. (4.6). Then find the sum of absolute values of the aggregated series for different values of m from eqn. (4.8) [73]

$$\frac{1}{N/m} \sum_{k=1}^{N/m} |X^{(m)}(k)| \tag{4.8}$$

Then the logarithm of the absolute values of the aggregated series is plotted versus the logarithm of m. The result should be a line with a slope of $H - 1$.

4.3 Results and Discussion

The first task as discussed in the previous sections was to identify the cyclic frequencies present in PLC noise by examining peaks in cyclic autocorrelation function of the noise. Principally, interference generated by various loads in the power network can be characterised by multiple cyclostationary periods. However, for simplicity, we only considered the lower cyclic frequencies which were found to be double the mains frequency. This was done after the raw measured noise had been passed through a FIR filter to analyse only the noise with occupying frequencies of

TABLE 4.1: Hurst Parameters for PLC Noise Measurements at various Locations

Location	R/S Method	Absolute Values of Aggregated Series Method	Aggregated Variance Method
Electronic Lab	0.6657	0.6486	0.6551
Offices	0.5264	0.5187	0.5091
Apartment	0.6767	0.7297	0.7224

interest in the broadband application range. The results in this chapter has been published in [8].

Hurst parameter estimation is problematic though it is mathematically well defined. The chosen methods are well-known techniques which have been used for a long time and hence can be trusted. However, from the results presented both in Figures 4.5, 4.6, 4.7, and Table 4.1 show that the values obtained by these methods vary and it is difficult to say categorically which of them performs better than the others more so for raw data with unknown Hurst parameter. However, what is certain and important for our study is that the values obtained by all the methods though different, ranges above 0.5, implying that PLC noise exhibits long-range dependence. The values estimated by aggregated variance and absolute values of aggregated series methods are very close to each other. This can be attributed to the fact that their algorithms are also very similar. R/S method though well established tends to converge very slowly compared to the rest of the methods as the data length increases.

The values for different locations are not very implicit, more noise measurement campaigns are ongoing for a more comprehensive study and conclusion. A more realistic noise modelling is a first step in combating noise which is a serious challenge in powerline communications systems. Error correction methods designed for memoryless channels are not necessarily optimal for channels showing long memory. This is because in long memory environment, what happens now will have effect on channel states in the future.

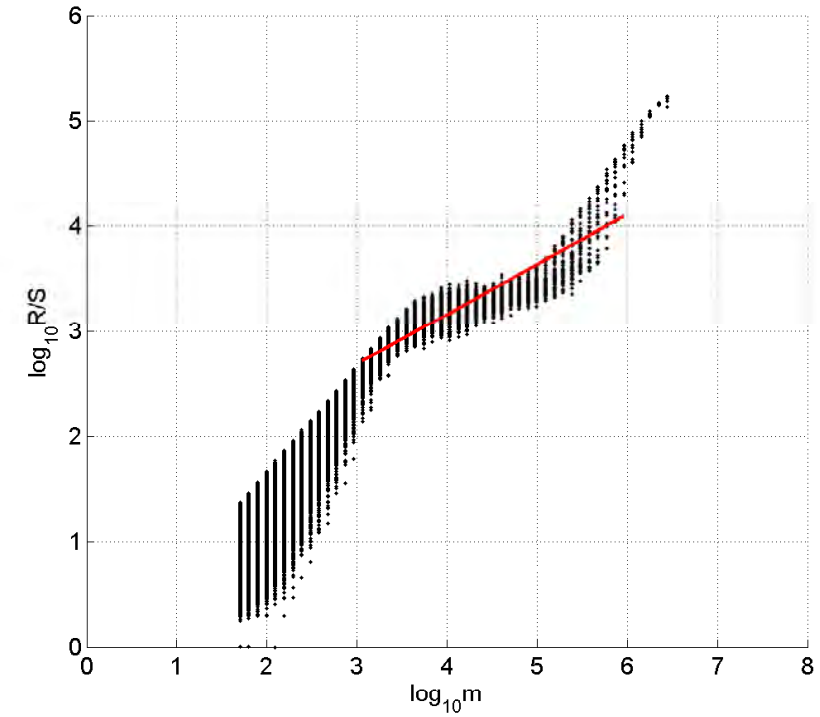

FIGURE 4.5: R/S Method Hurst Parameter Estimation for an Apartment

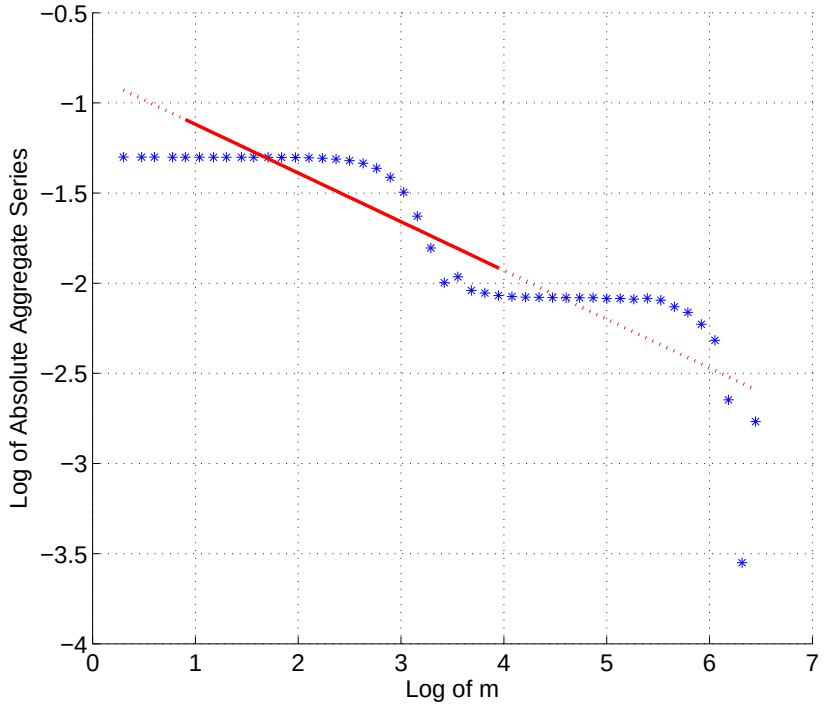

FIGURE 4.6: Absolute Aggregated Series Hurst Parameter Estimation for an Apartment

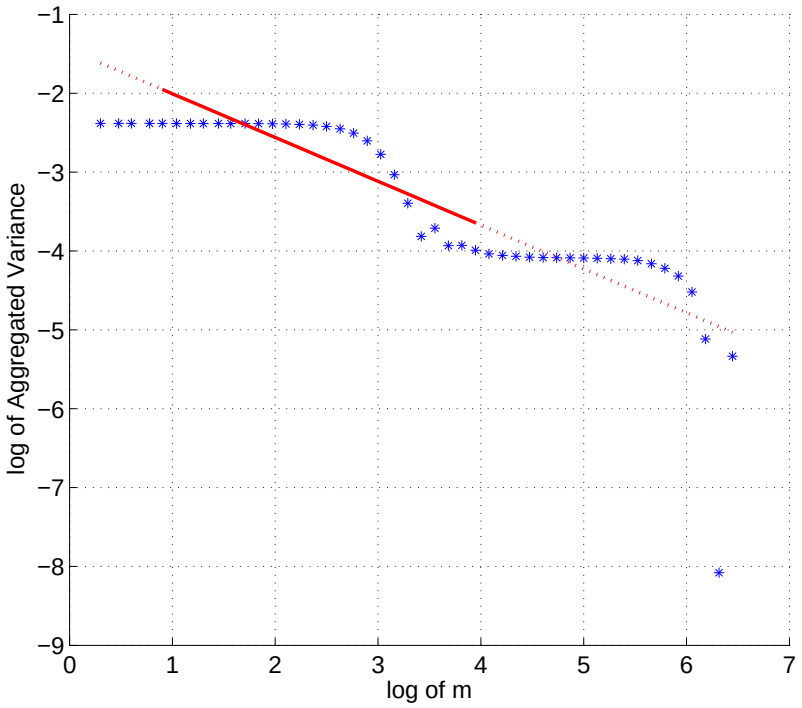

FIGURE 4.7: Aggregated Variance Method Hurst Parameter Estimation for an Apartment

4.4 Conclusion

Three methods of estimating Hurst parameter, which is a measure of long-range dependence have been employed for powerline noise measured for four different locations. All the methods show that PLC noise exhibits long-range dependence and therefore any PLC noise modelling should take this into consideration. In our analysis, we removed cyclostationarity of the PLC noise before estimating Hurst parameter. Periodicity and non-stationarity are known to affect the outcome of Hurst estimators and can result in unrealistic/confusing conclusions. Moreover, Hurst parameter estimated can be employed in determining Hausdorff dimension for accurate channel modelling using fractal/chaos theory. The next chapter investigates and reports results on multifractal analysis of PLC noise as to ascertain whether Hurst parameter alone is good enough to characterize the correlation in PLC noise.

CHAPTER 5

Multifractal Analysis of Bursty Impulsive Noise Power Line Communication Channels

5.1 Introduction

Fractal structure of power line communication channel noise and its impacts on PLC systems is not yet well published in the literature. The authors in [4] have done studies on self-similarity and fractal analysis of PLC noise and they observe that PLC noise exhibits long-range dependence . Empirical results from the previous chapter of this thesis also confirmed that PLC noise exhibits long-range dependence. Long-range dependence can be determined by estimating the Hurst parameter H, which is a measure of the intensity of LRD. LRD measures high variability in flow or arrival in time series data/signal. There is a relationship between channel memory and H parameter. The questions that this study is trying to answer is whether the Hurst parameter (derived from second order moment) alone is good enough to characterise the correlation structure of PLC noise. Specifically, in this study, we perform multifractal analysis to PLC noise measured from three different locations (University Electronic Laboratory, Postgraduate Office, and stand-alone Apartment). Multifractal analysis is superior to LRD analysis. It is a statistical tool that is able to measure the frequency with which bursts of different strengths occur in a signal [74].

The multifractal theory is a well-developed technique and has been used in

various fields in analysis and modelling of scaling behaviour of measures/functions in time series processes. Some of the signal and processing analysis based on multifractal include bit error rate process analysis of 11 Mbps wireless MAC-to-MAC channels [75], internet traffic and network traffic measurement estimations [74, 76], image feature extraction [77], stock market analysis [78, 79], biomedical analysis [80, 81] and so on. We stress that in this chapter, noise model is not being developed, but the study is concerned with investigating multifractal nature of PLC noise and the origins of these multifractals in PLC noise. Noise model that captures the multifractal nature of PLC noise is the theme of the next chapter in this thesis.

This chapter presents a multifractal analysis of bursty impulsive noise measured from power line networks from three different environments. We employ multifractal detrended fluctuation analysis and detrending moving average algorithm, which are well-developed multifractal analysis techniques for non-stationary time series data and can easily be implemented to analyse measured noise data. Results show that power line noise exhibits both long-range dependence and multifractal scaling behaviour with different strengths depending on the environments where they were captured. The multiscaling behaviour is due to long-range correlation inherent in the power line noise. The source of this local multiscaling behaviour is determined by the analysis of a shuffled series of the original data captured from the power network.

Multifractal analysis is able to show clearly both the strengths and frequency of occurrence of bursts occurring in PLC noise which can then be applied for accurate modelling of the noise. The significance of these results is that new power line noise models should be developed that capture both LRD and multifractal scaling for more accurate performance evaluation of power line communication systems. The existing noise models though able to replicate temporal dependence of PLC noise, are not able to capture this local scaling behaviour which results show is inherent in PLC noise. Preliminary findings of the work in this chapter has been published in [9] and the complete work has been submitted for journal publication [10] and is under review.

5.2 Multifractal Analysis

Multifractal spectrum provides a good measure of characterising non-stationary time series signals. Methods for estimating multifractal spectrum are well developed and continue to excite much research. Selection of methods to be used for analysis depend on the required accuracy, computational speed and type of data [77]. Moreover, the methods are not equivalent and quite often produce different results. The interest is normally to extract fractal/multifractal properties of a given signal rather than seeking for exact fractal dimension. Among the well developed and most accurate is the wavelet transform modulus maxima (WTMM)

[82, 83, 84, 85]. However, its computational cost is the major hindrance to its application.

Here we apply two methods: multifractal detrended fluctuation analysis [86] and multifractal detrending moving average analysis [79]. Their choice is due to ease of implementation and fast computational applicability. Again, their accuracy has been seen to be comparable to WTMM [86, 87]. Both have been developed for non-stationary time series signals and there are MATLAB codes available on-line that can be modified by the intended users for their implementation [88, 79].

5.2.1 Autocorrelation Function

Autocorrelation function (ACF) can be a good starting point for correlation analysis of time series data. It provides correlation of ith measurement with that of $(i+l)$th one for different time lags l. It can be used as a preliminary indicator of existence of long-range dependence in a time series data. Considering a time series data $\{x_i\}_{i=1}^{N}$ with $i = 1, \cdots, N$, N representing the length of the series, the auto-covariance function is given by eqn. (5.1)

$$R^{'}(l) = \langle \bar{x}_i \bar{x}_{i+l} \rangle = \frac{1}{N-l} \sum_{i=1}^{N-l} \bar{x}_i \bar{x}_{i+l} \tag{5.1}$$

where $\bar{x}_i = x_i - \langle x \rangle$ and $\langle x \rangle$ is the mean of the series. The ACF $R_{xx}(l)$ is then given by $R^{'}(l)$ normalized by the variance of the series $\langle \bar{x}_i^2 \rangle$. The time series is short range dependent when its ACF declines exponentially ($R_{xx}(l) \propto \exp(-l/l_o)$) for $l \to \infty$. When ACF declines as power-law ($R_{xx}(l) \propto l^{-\gamma}$) for $l \to \infty$ and $0 < \gamma < 1$, then the series is said to have long-range dependence.

Due to unknown trends and noise in time series data, direct calculations of $R_{xx}(l)$ is usually not advisable. Moreover, autocorrelation analysis and power spectrum analysis fail to capture the correlation behaviour in most non-stationary time series due to unknown trends that might be in the time series. However, there are methods available for determining the local scaling behaviour of time series data. These methods differ in the way fluctuation measure are defined, and the type of polynomial trends eliminated in each window size [89].

5.2.2 Multifractal Detrended Fluctuation Analysis

Multifractal Detrended Fluctuation Analysis is a generalisation of detrended fluaction analysis (DFA) to cater for non-stationary time series data and the procedure consist of five steps [86]. Let us consider a series x_i of length n and is of compact support, the procedure for MDFA involves the following steps:

I. The first step involves the construction of time series 'profile' (this step converts the noise time series to random walk-like series) from the original data

as eqn. (5.2)

$$y(k) \equiv \sum_{i=1}^{k}(x_i - \bar{x}) \quad k = 1, \cdots, n \tag{5.2}$$

where $\bar{x}$ is the mean of the time series.

II. In the second step, the profile $y(k)$ is then divided into non-overlapping segments of equal length s, that is, n_s =int(n/s). If the length n of the series is not a multiple of s, then a small portion of it may remain. To utilise this portion also, the procedure is repeated from the opposite end, making $2n_s$ segments altogether.

III. In the third step, local trend for each of the $2n_s$ segments is determined by least-square fit of the series. Then the variance is determined as eqn. (5.3)

$$F^2(s,l) = \frac{1}{s}\sum_{k=1}^{s}\{y[(l-1)s+1] - y_l(k)\}^2 \tag{5.3}$$

for each segments, $l = 1, \cdots, n_s$ and eqn. (5.4),

$$F^2(s,l) = \frac{1}{s}\sum_{k=1}^{s}\{y[n-(l-n_s)s+1] - y_l(k)\}^2 \tag{5.4}$$

for each segments $l = n_s + 1, \cdots, n_s$, where $y_l(k)$ is the polynomial fit in segment l.

IV. The qth order fluctuation function can then be obtained by averaging of all the segments in the fourth step as eqn. (5.5)

$$F_q(s) = \{\frac{1}{2n_s}\sum_{v=1}^{2n_s}[F^2(s,v)]^{q/2}\}^{1/q} \tag{5.5}$$

where q is a variable that can take any value apart from zero. Steps (2) to (4) are repeated for several different time scales s.

V. The last step is to estimate the scaling behaviour of the fluctuation functions by plotting on log-log scale $F_q(s)$ versus scale s for each value of q. If the time series exhibits long-range correlation, then $F_q(s)$ increases with increase in scale s as a power-law from eqn. (5.6)

$$F_q(s) \sim s^{h(q)}. \tag{5.6}$$

The multifractal scaling exponent $h(q)$ in (5.6) is known as generalized H exponent and is the well-known H parameter for $q = 2$ for stationary time series. For monofractal series, the exponent $h(q)$ is independent of q and it is dependent on q for multifractal time series data. Multifractal scaling exponent $h(q)$ is related

to standard multifractal formalism scaling exponent $\tau(q)$ as eqn. (5.7)

$$\tau(q) = qh(q) - D_f \tag{5.7}$$

where D_f is the fractal dimension of the geometrical support of the multifractal measure and for time series data, $D_f = 1$ [86][79]. For multifractal time series, $\tau(q)$ is a non linear function of q. An alternative way of characterizing multifractal series is by the singularity strength function $\alpha(q)$ and the multifractal spectrum function $f(\alpha)$ [79, 86] via Legendre transform as eqn. (5.8)

$$\alpha(q) = \frac{d\tau(q)}{dq} \quad \text{and} \quad f(\alpha) = q\alpha - \tau(q) \tag{5.8}$$

5.2.3 Multifractal Detrending Moving Average Algorithm

Multifractal detrending moving average algorithm [79] is a generalization of the detrending moving average (DMA) algorithm [90] initially designed for fractal analysis for non-stationary time series data. MDMA was developed to analyse both multifractal time series and multifractal surfaces. Its algorithm can be summarized as follows [79].

I. The first step is to construct a sequence of cumulative sums $y(t)$, eqn. (5.9) assuming a time series $x(t)_1^N$, where N is the length of the time series, i.e.,

$$y(t) = \sum_{i=1}^{t} x(i) \quad t = 1, 2, \cdots, N \tag{5.9}$$

II. The second step is to determine the residual sequence, eqn. (5.10) by detrending the signal series by subtracting the moving average function from the cumulative sums series computed in step one.

$$r(i) = y(i) - \tilde{y}(i) \tag{5.10}$$

where $n - \lfloor (n-1)\theta \rfloor \leq i \leq \lfloor N - (n-1)\theta \rfloor$ and $\tilde{y}(t)$, eqn. (5.11) is the moving average function in a moving window,

$$\tilde{y}(t) = \frac{1}{n} \sum_{k=-\lfloor (n-1)\theta \rfloor}^{\lceil (n-1)(1-\theta) \rceil} y(t-k) \tag{5.11}$$

where n is the window size and θ is a parameter determining the position of the window. θ takes values in the range $[0, 1]$. Mostly, three special cases are normally considered, namely, $\theta = 0$ (backward moving average), in which the moving average function is calculated over the past $n - 1$ data points of the signal. The second case is for $\theta = 0.5$ (centred moving average) for which moving average function is calculated over half past and half future data

points of the signal. The last case is when $\theta = 1$ (forward moving average) on which the moving average function is calculated on $n-1$ data points of the signal in the future.

III. In the third step, the residual sequence $r(i)$ is divided into N non overlapping segments of the same size n, where $N = \lfloor N/n - 1 \rfloor$. Denoting each segment by r_v, the root-mean-square function $F_v(n)$ can be calculated by eqn. (5.12)

$$F_v^2(n) = \frac{1}{n}\sum_{i=1}^{n} r_v^2(i) \tag{5.12}$$

IV. The fourth step involves determining the qth order overall fluctuation function $F_q(n)$ as eqn. (5.13)

$$F_q(n) = \{\frac{1}{N_n}\sum_{v=1}^{N_n} F_v^q(n)\}^{\frac{1}{q}} \tag{5.13}$$

V. Finally, in the last step, the values of segment size n can be varied to determine the power-law relation between the function $F_q(n)$ and scale n as eqn. (5.14)

$$F_q(n) \sim n^{h(q)}. \tag{5.14}$$

When $h(q)$ has been estimated, then scaling exponent dependent on q can be determined from (5.7). Similarly, singularity strength and multifractal spectrum can be estimated from (5.8).

5.3 Results & Discussion

5.3.1 Unfiltered PLC Noise Analysis

Multifractal spectrum and their corresponding $q-$order dependent scaling exponent estimated from two methods (MDFA and MDMA) for PLC noise data measured from various environments are shown in Figures 5.1, 5.2, and 5.3 for Office, Laboratory and Apartment respectively analysed by MDFA. Similarly, Figures 5.4, 5.5 and 5.6 respectively show results from MDMA technique. From these figures, it is evidenced that the PLC noise has a scaling behaviour that is sensitive to small fluctuations within its segments. This is characterised by the left truncated multifractal spectrum shown in each of the locations by both the methods. Again, the multifractal spectrum diagrams show that original data series has wider spectrum than the shuffled data series. The wider the spectrum the more multifractal the data is. From this we can conclude that the multifractal behaviour of impulsive is destroyed by shuffling. This in turn means that the source of this multifractal nature is due to long-range correlations present in the time series. The $q-$order dependent scaling exponent graphs give an indication that PLC noise is multifractal as the scaling exponent of the original time series data is dependent on $q-$order

of the fluctuations, that is, the scaling exponent is non-linear. When the time series data is shuffled, the scaling exponent is more or less linear, which implies monofractal behaviour.

Table 5.1 and Table 5.2 respectively provide values of singularity spectrum parameters estimated by multifractal detrended fluctuation analysis and multifractal detrended moving average algorithm. The most important parameter is the spectrum span ($\Delta\alpha = \alpha_{max} - \alpha_{min}$) which is a measure of irregularity of the signal/time series. From Table 5.1, the values of the span for noise from various locations show that PLC noise from office has a spectrum distribution which is more non-uniform than both noises from laboratory and apartment which seem very close. When the data is shuffled, the span is negligible except for one of office data. In the office data, the span of original data is 0.93 and that of the shuffled data is 0.41. The implication for these values is that the shuffled data shows weaker multifractal behaviour than the original data. Similar results are seen for noise captured in an apartment, however, for laboratory data, the shuffled series show no evidence of multifractality.

Results from second method (MDMA) gives an indication that it is the laboratory data that show weak multifractal behaviour in the shuffled series (Table 5.2). Since the multifractal behaviour of PLC noise is not yet known, we can not conclude from the results which of the methods gives a better analysis than the other. However, it is evident from the two methods used in the analysis that PLC noise exhibits multifractal behaviour but the nature and source of this behaviour require further investigation.

Another important parameter of measure is α_0. Viewing the singularity spectrum as frequency distribution of singularity strength, α_0 provides the value of the singularity strength which is most frequent in the distribution. The value of α_0 provides the measure of correlation characteristics of the signal/time series. Both the methods show that PLC noise exhibits long-range correlation since the most frequent singularity strength ranges between 0.5 and 1.

TABLE 5.1: Singularity Spectrum Parameters estimated by multifractal detrended fluctuation analysis

Location	Data	Measure Indices			
		α_0	α_{min}	α_{max}	$\Delta\alpha$
Office	Original	0.77	0.45	1.38	0.93
	Shuffled	0.88	0.73	1.14	0.41
Laboratory	Original	0.46	0.37	1.10	0.73
	Shuffled	0.50	0.48	0.56	0.08
Apartment	Original	0.79	0.64	1.35	0.71
	Shuffled	0.76	0.64	0.90	0.26

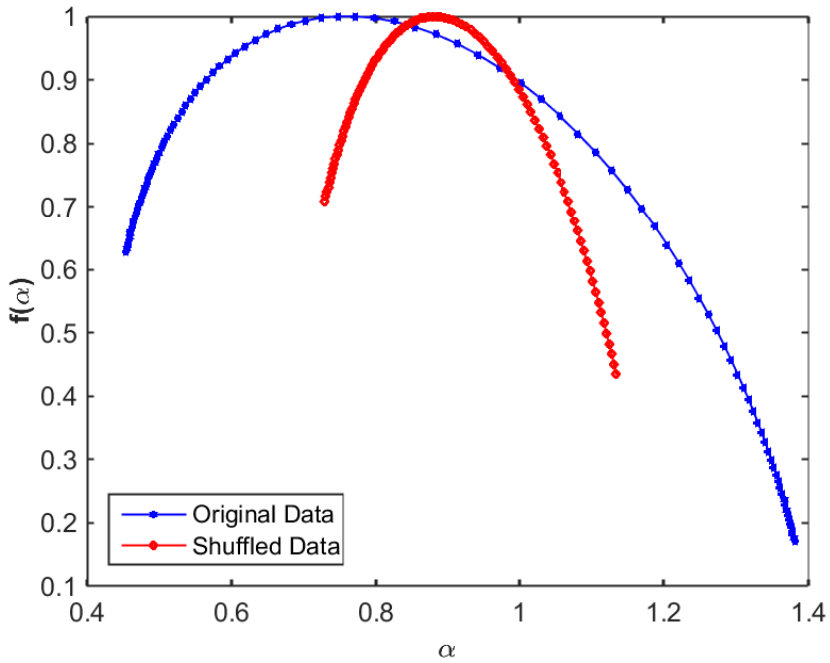

(a) Multifractal Spectrum

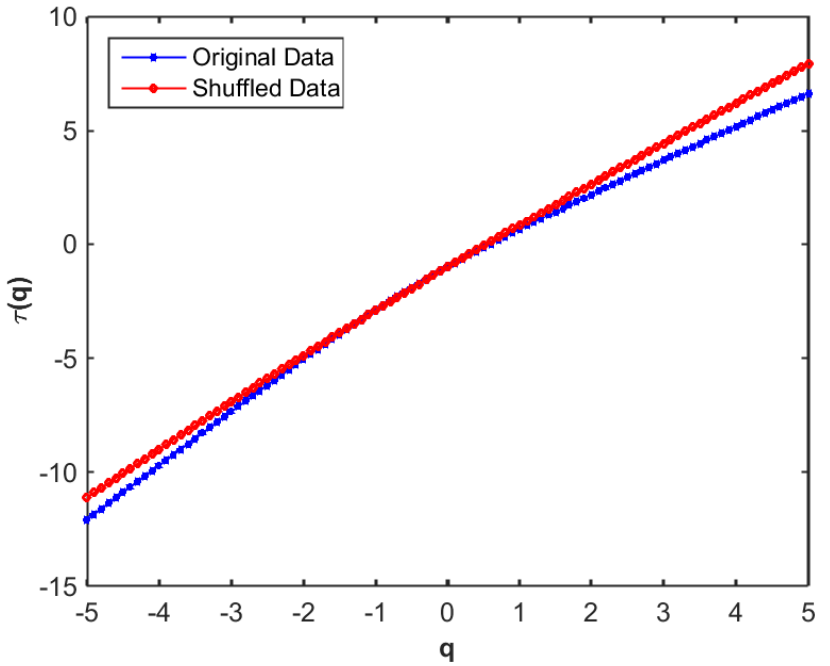

(b) Scaling Exponent

FIGURE 5.1: Multifractal Spectrum and Scaling Exponent of Data from postgraduate Office estimated by multifractal detrended fluctuation analysis

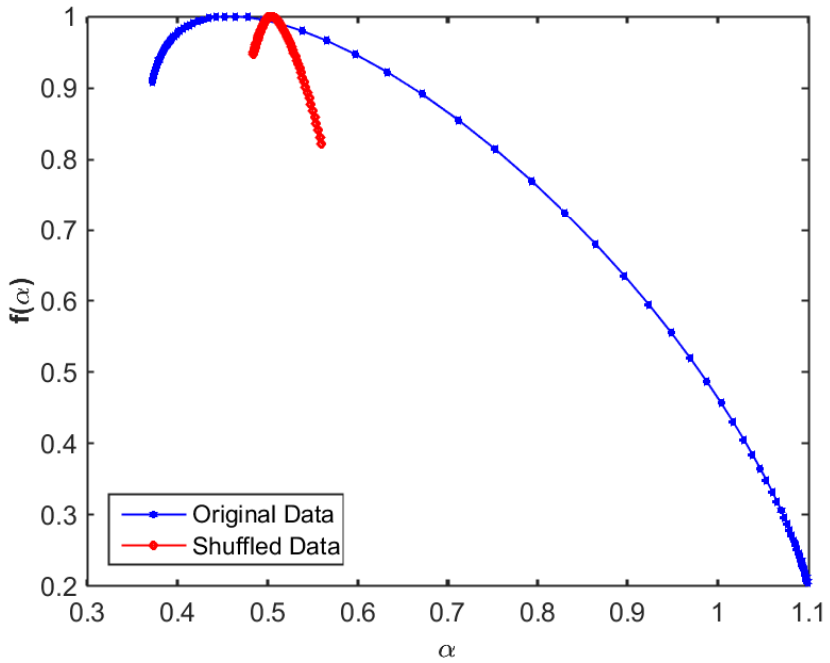

(a) Multifractal Spectrum

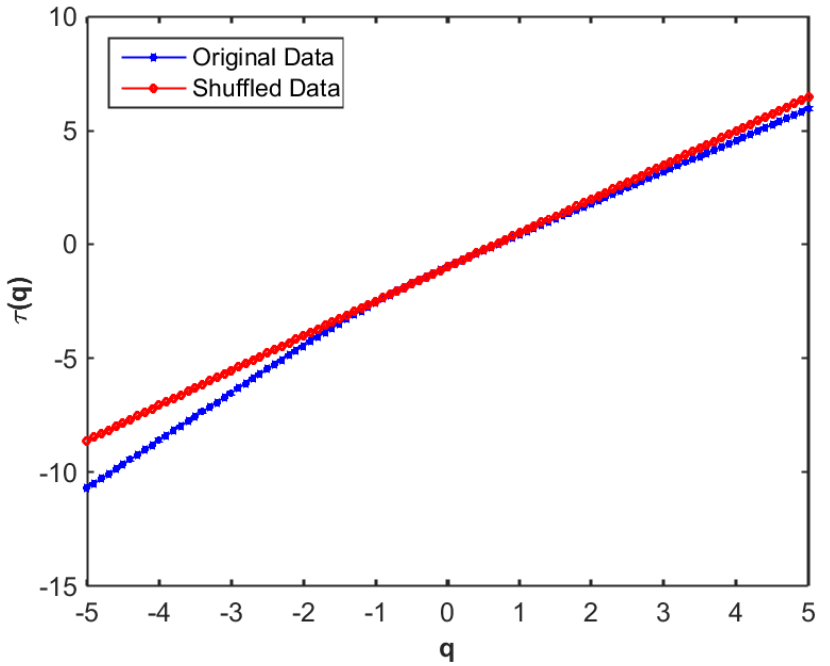

(b) Laboratory Scaling Exponent

FIGURE 5.2: Multifractal Spectrum and Scaling Exponent of Data from stand-alone Apartment estimated by multifractal detrended fluctuation analysis

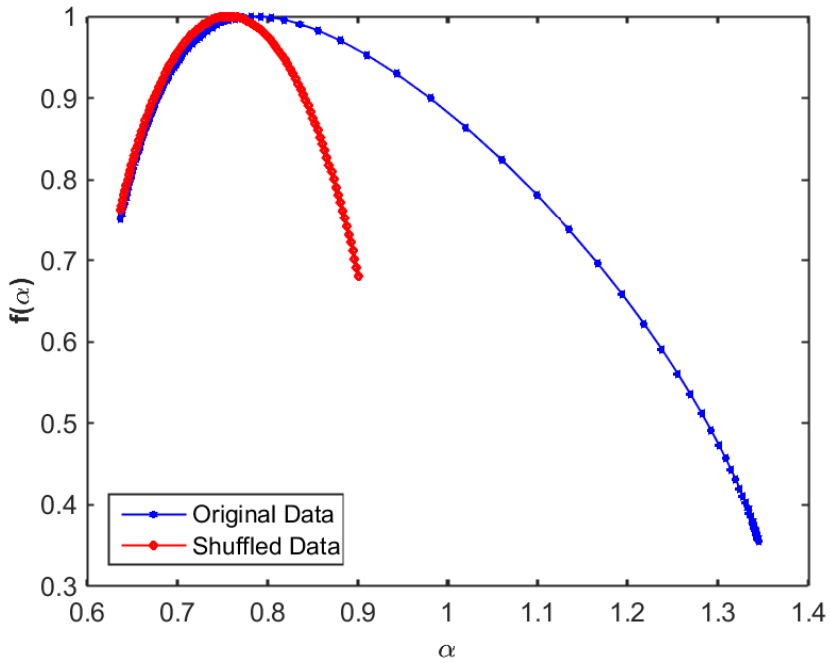

(a) Multifractal Spectrum

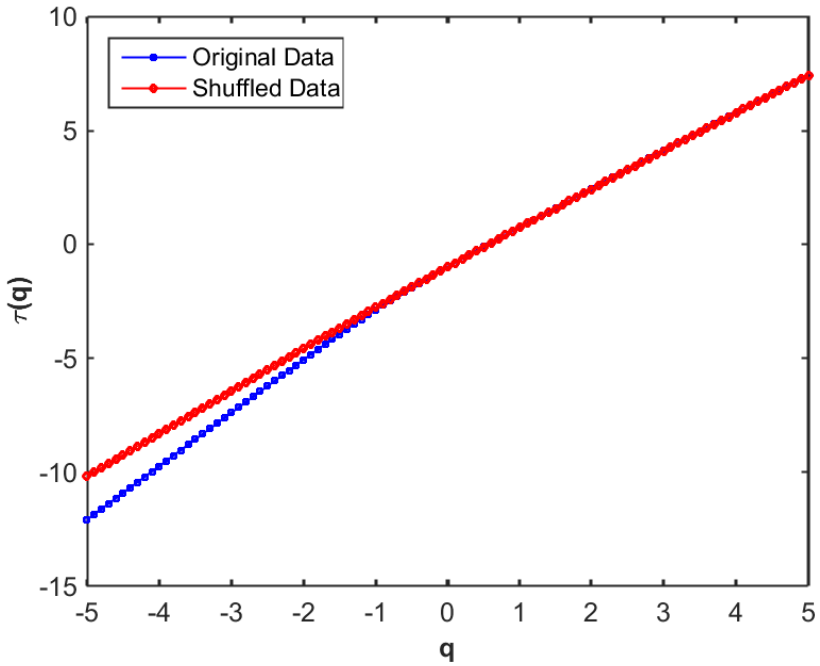

(b) Scaling Exponent

FIGURE 5.3: Multifractal Spectrum and Scaling Exponent of Data from stand-alone Apartment estimated by multifractal detrended fluctuation analysis

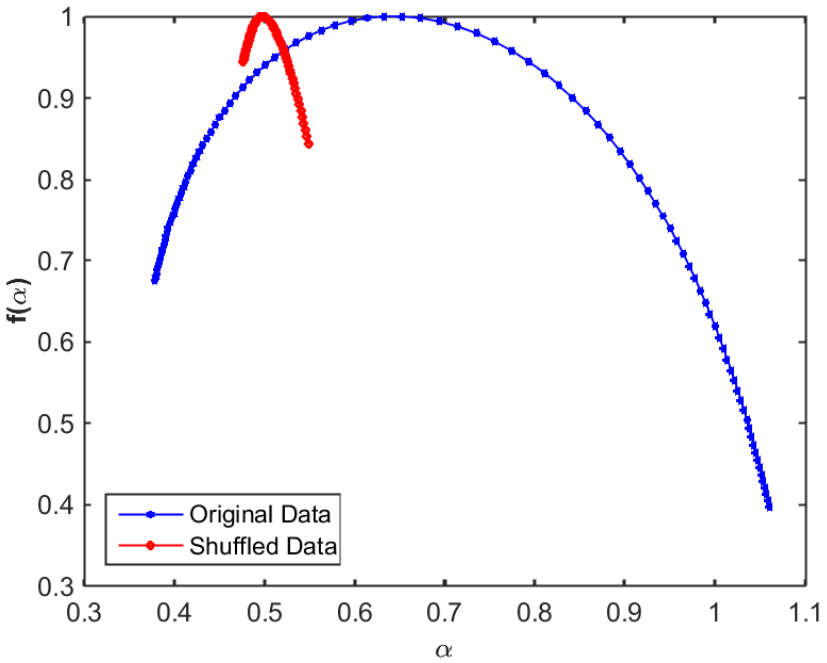

(a) Multifractal Spectrum

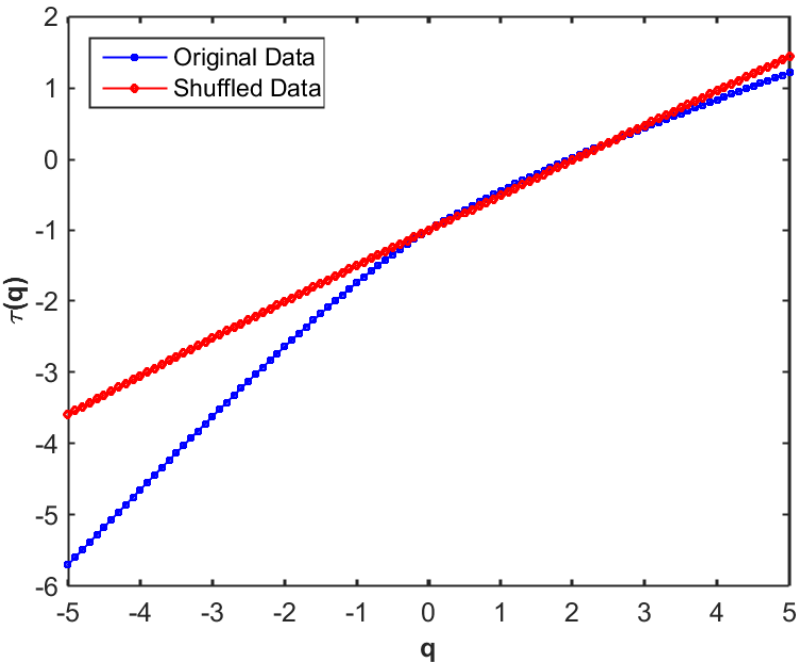

(b) Scaling Exponent

FIGURE 5.4: Multifractal Spectrum and Scaling Exponent of Data from postgraduate Office estimated by multifractal detrended moving average algorithm

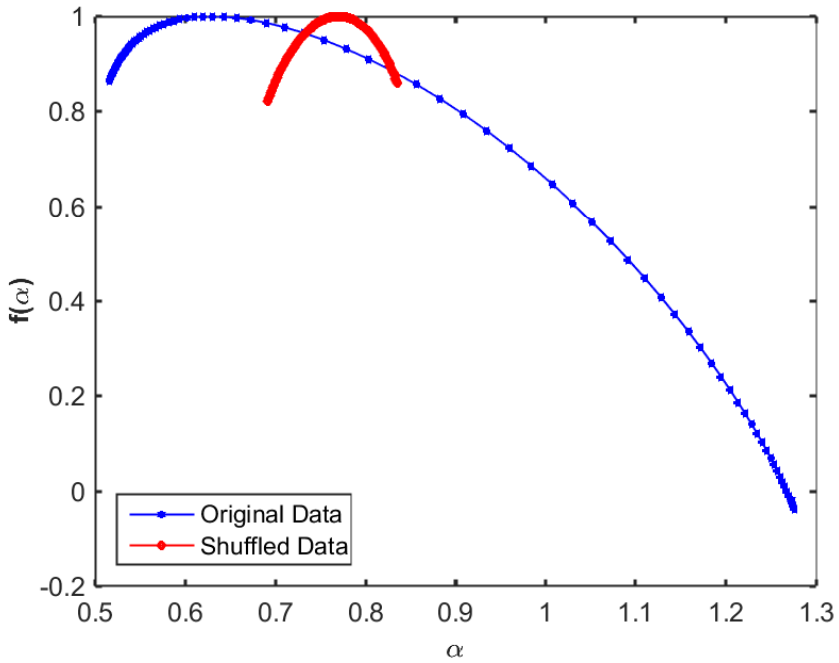

(a) Multifractal Spectrum

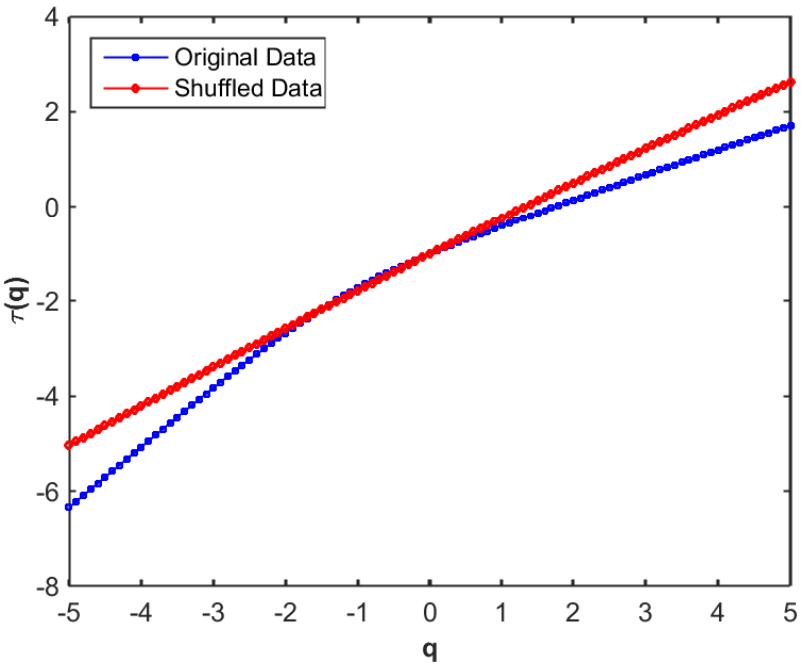

(b) Scaling Exponent

FIGURE 5.5: Multifractal Spectrum and Scaling Exponent of Data from University Electronic Laboratory estimated by multifractal detrended moving average algorithm

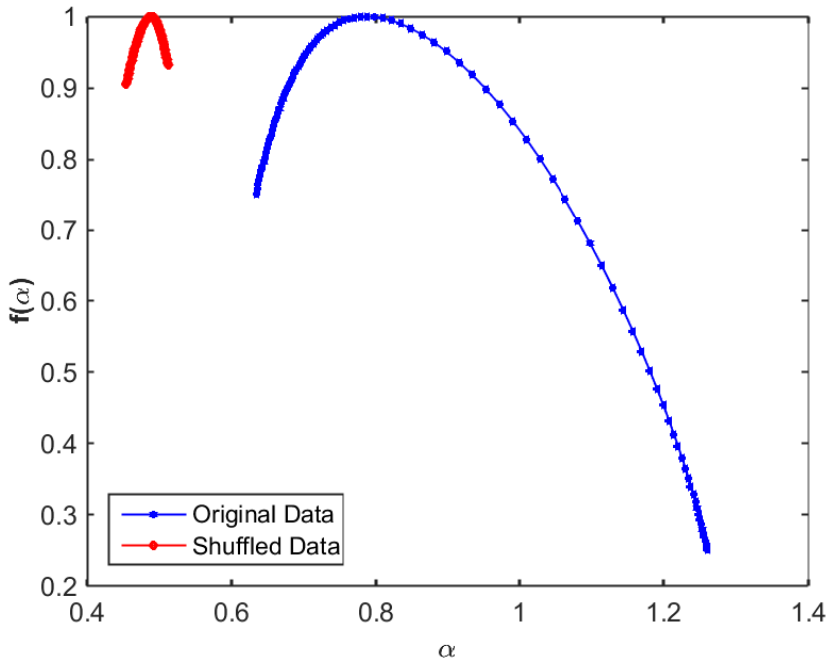

(a) Apartment Multifractal Spectrum

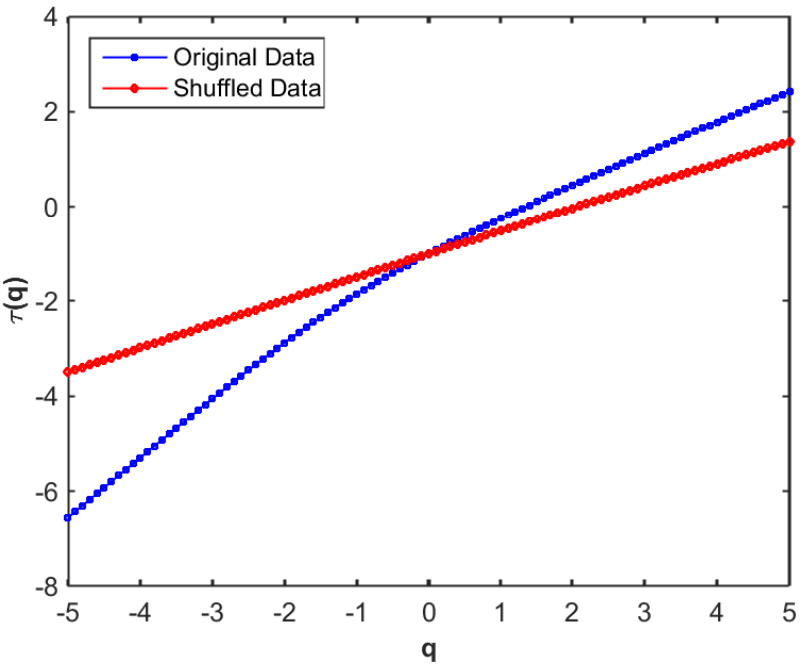

(b) Apartment Scaling Exponent

FIGURE 5.6: Multifractal Spectrum and Scaling Exponent of Data from stand-alone Apartment estimated by multifractal detrended moving average algorithm

TABLE 5.2: Singularity Spectrum Parameters estimated by multifractal detrended moving average algorithm

Location	Data	Measure Indices			
		α_0	α_{min}	α_{max}	$\Delta\alpha$
Office	Original	0.64	0.38	1.06	0.68
	Shuffled	0.50	0.48	0.55	0.07
Laboratory	Original	0.63	0.52	1.28	0.76
	Shuffled	0.77	0.69	0.84	0.15
Apartment	Original	0.79	0.63	1.26	0.63
	Shuffled	0.49	0.45	0.51	0.06

5.3.2 Filtered PLC Noise Analysis

Power line communication channel Noise that was captured in the frequency band of 0.1 MHz to 25 MHz was decomposed into low frequency ($0.1-10$ MHz) and high frequency ($10-25$ MHz) components. Measured time series data is FIR filtered to perform analysis on both low-frequency and high-frequency components of the noise. The decomposed components were then analysed by the MDFA technique with a view to investigating multifractal characteristics of these noise components. Interesting results can be seen in Figures 5.7, 5.8, and 5.9 where empirical analysis show that the multifractal characteristics of PLC noise, in general, is mainly being contributed by the low-frequency components. In [41], it was reported that noise spectrum has relatively high values at low frequency than at high frequencies. This was attributed to many sources of low-frequency noise in the power network and short-wave radios in the low-frequency band. We can also conclude from the findings in this study that these low-frequency sources are the main contributors of the scaling behaviour inherent in PLC noise. Again, it is known that man-made impulsive noise is mainly in the low frequencies [42] and at these low frequencies, the noise PSD is high [47].

Since the multifractal behaviour of PLC noise is due to bursty impulsive noise, the results showing that low-frequency components of PLC noise are more multifractal than the high-frequency component (which is monofractal or very weak multifractal for the cases of office and apartment scenarios) is valid. Low-frequency components of PLC in from office and laboratory data retain the same shape (left truncated concave shape) of multifractal spectrum as the unfiltered time series data. However, the low-frequency component of apartment data has a full concave multifractal spectrum. These results continue to confirm that different locations have sources which contribute to the noise characteristics uniquely. We intend to isolate the individual noise sources and characterise their behaviour according to the frequency and strengths of impulsive noise they generate. Investigating the characteristic of individual noise sources is a common practice in PLC communications and will be an interesting future work.

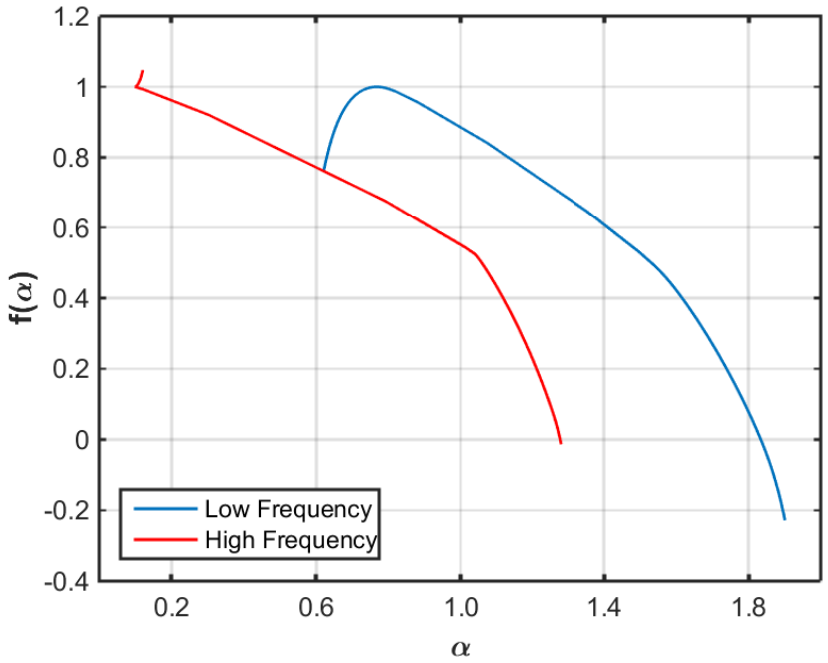

FIGURE 5.7: Office Multifractal Spectrum for Filtered PLC Noise Time Series from various locations derived from multifractal detrended fluctuation analysis

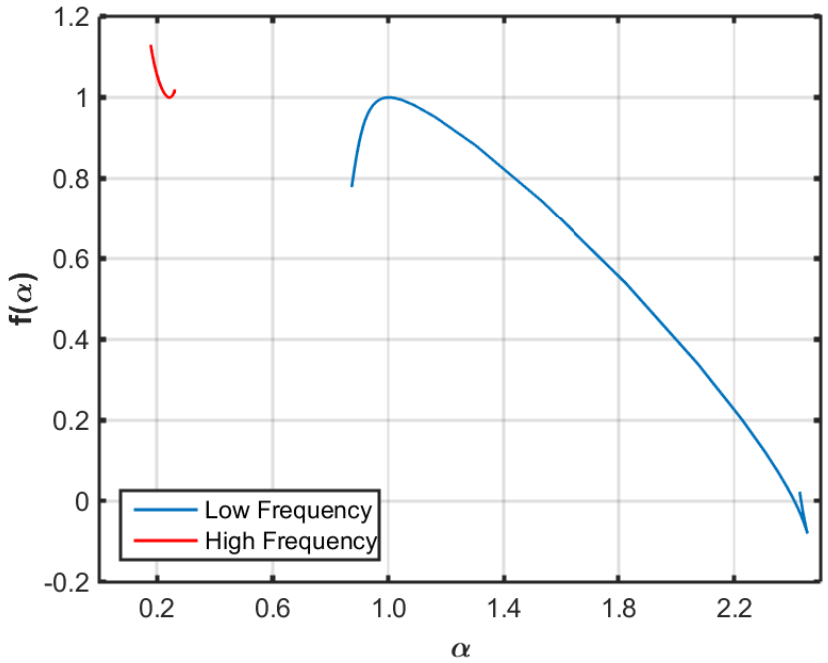

FIGURE 5.8: Laboratory Multifractal Spectrum for Filtered PLC Noise Time Series from various locations derived from multifractal detrended fluctuation analysis

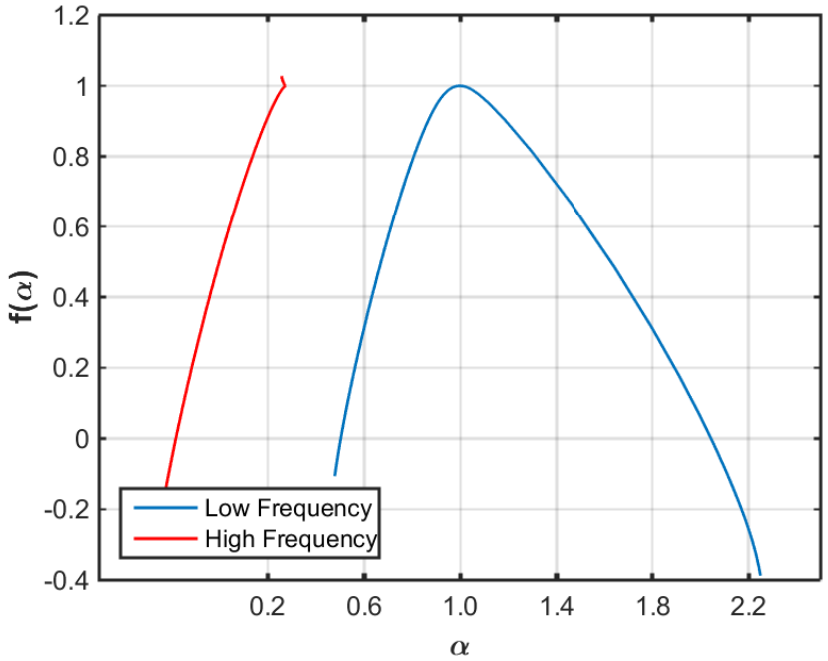

FIGURE 5.9: Apartment Multifractal Spectrum for Filtered PLC Noise Time Series from various locations derived from multifractal detrended fluctuation analysis

5.4 Conclusion

Multifractal analysis of PLC noise measured from an office environment, University electronic laboratory and a stand-alone apartment, reveal that PLC noise exhibits multifractal behaviour, meaning that it can not be accurately characterised by a single power-law scaling exponent. This multifractal characteristic is mainly encountered in the low-frequency band (< 10 MHz) where there are many sources of bursty impulsive noise. Results from the findings also show that PLC noise has long-range dependence behaviour. It will also be interesting to capture noise from individual noise generators and investigate their scaling behaviour. Furthermore, the findings of this study point to the fact that there is need for new models to be developed for PLC noise that will be able to capture more accurately its LRD and multifractality nature. The impact of these noise characteristics on performance analysis of power line communication systems also needs to be investigated and forms our future research.

CHAPTER 6

Binomial Multiplicative Cascade Model for Bursty Impulsive PLC Noise

6.1 Introduction

In the last two chapters, it has been empirically shown that noise in the power line communication networks has a temporal correlation (long-range persistence) and the impulses appear in bursts. Specifically, in Chapter 5, strengths and frequency of occurrence of these bursts were analysed with multifractal analysis tools. The next important challenge is whether PLC noise can be modelled in away that replicates the findings in the previous chapters and the effects of these new findings on receiver design. In this chapter, we try to investigate the former challenge while the latter is left for future work.

Even though Gaussian-Markov and Middleton-Markov models [5, 6] have become popular for PLC noise modelling, it is known that Markov and Poisson models cannot adequately describe self-similar properties of bursty noise. Therefore, there is a need to come up with a model that can faithfully describe the multifractal properties exhibited in PLC noise as evidenced in the previous chapters through empirical analysis of noise captured in various scenarios.

In modelling, the expectation is to come up with a model simple enough and able to be used in simulations with ease and at the same time be able to replicate

accurately as possible the properties of interest. Therefore, there is always a trade-off between complexity (i.e., tractability with as few parameters a possible) of the model and its accuracy. Multifractal spectrum distributions from empirical studies in the previous chapter were asymmetrical in shape, specifically left truncated. Theories of multiplicative cascade processes is well documented in the literature and is already a mature technology that has been applied in different fields involving intermittent turbulence: solar wind turbulence [91, 92, 93], rain and clouds [94], geophysical fields [95, 96], financial series and asset returns [97, 98], minerals and minings [99], network traffic modelling [74, 76, 75, 100, 101] among others.

Apart from multiplicative cascade processes, other authors have proposed Markov Switching multifractal processes to model volatilities [102] and the reference therein. Some recent works have also attempted to generalise multifractal processes using infinitely divisible distributions [103, 104, 105, 106, 107, 108, 109, 110]. The results from these models look interesting, however, the technique is still in developing stages and may not be appropriate for modelling asymmetrical distributions. This can be a good study for future work on how to adapt these infinitely divisible cascades to model asymmetrical multifractal spectrum. For our study, we will limit ourselves to models which have been shown to be able to model asymmetrical multifractal spectrum [91, 99, 100, 111]. The motivation for restricting ourselves to these models is because, from our analysis we were able to ascertain that PLC noise has a multifractal distribution which is asymmetrical, specifically left truncated. The model is described in the next section with a brief review of the basic binomial multiplicative cascade model which forms the foundation of the asymmetrical generalised binomial cascade process.

6.2 Multiplicative Cascade Processes

Models of multiplicative cascade have been around for a long time and can be seen as mathematical constructs that can appropriately capture the intermittent and highly irregular behaviour. It can be defined as a process that iteratively fragments a given set into smaller and smaller segments according to some geometric rule and also distributes the total measure of the given set depending on some other rule [100],[111]. Different methods/techniques of generating multifractal processes then depend on these two rules (how to divide a given set into smaller segments, and how to distribute the total mass/measure of the given set) depending on the application of interest.

If we assume a measure μ defined in a small segment within a finite 1-D set T and its value with a linear measuring size ϵ satisfies eqn. (6.1)

$$\mu(\epsilon) \propto \epsilon^{\alpha(q)} \tag{6.1}$$

where $\propto$ and $\alpha(q)$ represents 'proportional to' and singularity index respectively.

The measure μ is a function of scale ϵ which has scale invariance property such that

$$\alpha \propto \frac{\log[\mu(\epsilon)]}{\log\epsilon} \quad \text{as} \quad \epsilon \longrightarrow 0 \tag{6.2}$$

The distribution of singularity index (α) within the entire set T determines whether the measure possesses multifractality or not. The $q-$th order moment of the measure can be represented with partition function as eqn. (6.3)

$$\mathbb{X}_q(\epsilon) = \sum_{t=1}^{N_\alpha(\epsilon)} \mu_t^q(\epsilon) \tag{6.3}$$

where $N_\alpha(\epsilon)$ is the number of segments of size ϵ covering the entire given set. If the entire set can be classified into subsets with different singularity index α_i and, hence, different fractal dimensions ($f(\alpha_i) \leq 1$), then the field/measure μ is described as multifractal with the following relations eqn. (6.4)

$$\begin{aligned} \sum[\mu(\epsilon)]^q &= \epsilon^{\tau(q)}, \\ \alpha(q) &= \tau'(q), \\ f(\alpha) &= \alpha(q)q - \tau(q) \end{aligned} \tag{6.4}$$

where $\tau(q)$ is the scaling function, the rest are as defined earlier. $\tau(q)$ is a non-linear function of q for multifractal measure and linear for monofractal measure. $\alpha(q)$ is a decreasing function of q and $f(\alpha)$ is a convex function for multifractal measures, otherwise for monofractal, $\alpha(q)$ is a constant function of q and $f(\alpha)$ becomes a single spike or a shrink like convex spectrum. The degree of multifractality is being determined by the ranges and curvatures of these functions.

6.2.1 Binomial Multiplicative Cascade Model

The simplest of all multiplicative cascade processes is the binomial multiplicative cascade, consisting of an interactive process in the compact interval $[0, 1]$ [100]. Without loss of generality, the initial measure is assumed to be unity and is to be preserved in all stages. Let us assume that m_1 and m_2 are two multipliers for cascade generation such that $m_1 = r$ and $m_2 = 1 - r$ with r being a random variable between 0 and 1. At the initial stage (level one) of iteration $n = 0$, unit measure μ_0 is uniformly distributed on the interval $[0, 1]$. At the second cascade iteration (level one), the unit measure is divided into two parts with measures m_1 and m_2 and assigned to sub-intervals $L_{00} = [0, 1/2]$ and $L_{01} = [1/2, 1]$ respectively. At the next levels, each sub-interval in the previous level is again divided into two parts and each part assigned corresponding measures such that at iteration k, there are 2^k disjoint dyadic sub-intervals of type $[t, t + 2^k]$ with measure μ in the dyadic interval $[t, t + 2^k]$ given by eqn. (6.5) [100]

$$\mu[t, t + 2^k] = \mu[\delta_k] = m_1^{kf_1} m_2^{kf_2} \tag{6.5}$$

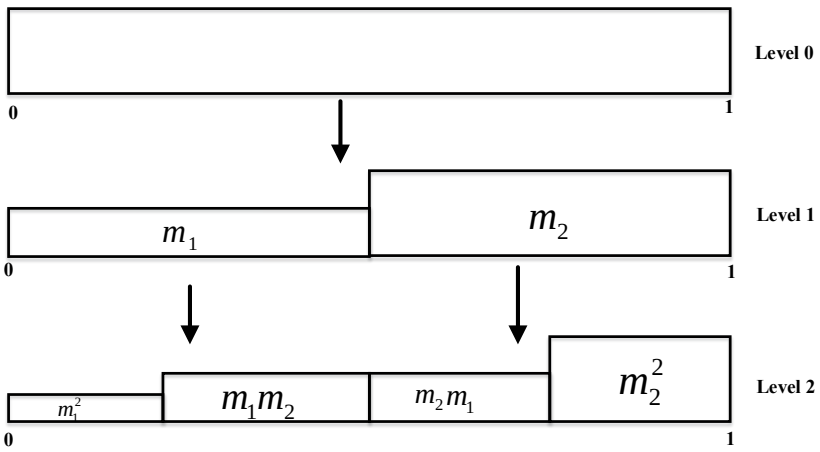

FIGURE 6.1: Basic Binomial Cascade Process

where f_1 and f_2 denote respectively the relative frequencies of 0's and 1's in the cascade development. At each level/stage of iteration, the total mass of each dyadic interval is preserved, that is unity in the case described here. Figure 6.1 shows a construction of a conservative binomial cascade, that is, at each level of iteration, the sum of the multipliers equal unity.

6.2.2 Generalized Asymmetrical Binomial Cascade Model

Since from our multifractal analysis, it was established that the multifractal spectrum of PLC noise show asymmetrical behaviour, specifically left truncated, we propose to adopt the asymmetrical generalised binomial model introduced by [111]. This is a five parameter model, which is simple enough for tractability and has physical meaning to the processes that generate the multiplicative cascade nature. Moreover, estimation of the model parameters is quite straight forward, being derived from the multifractal spectrum, unlike other asymmetrical models with more tedious parameter estimation (e.g., [100]).

In this model, each unit length is divided into s equal segments. s_1 of the segments receive $m_1 > 0$ portion of the total mass of the measure, while s_2 of the segments receive $m_2 > 0$ portion of the total measure. $s_1 + s_2 \leq s$ and $m_1 + m_2 = 1$ for conservative multiplicative cascades. The segment length at nth partition is given by $\epsilon_n = (1/s)^n$, and the segments are subject to k times the segments with measure (m_1/s_1) and $n-k$ times those with measure (m_2/s_2). Hence, the measures of these segments are given by eqn. (6.6) [111]

$$\mu_k = (m_1/s_1)^k (m_2/s_2)^{n-k}. \tag{6.6}$$

The number of segments with measure μ_k will be given by $N_k = s_1^k s_2^{n-k}\binom{n}{k}$ and the partition function is given by eqn. (6.7)

$$\begin{aligned}\mathbb{X}_q(\epsilon_n) &= \sum_{k=0}^{n} \mu_k(\epsilon_n)^q s_1^k s_2^{n-k}\binom{n}{k} \\ &= \sum_{k=0}^{n} \left[(m_1/s_1)^k (m_2/s_2)^{n-k}\right]^q s_1^k s_2^{n-k}\binom{n}{k} \\ &= \left[s_1^{1-q}m_1^q + s_2^{1-q}m_2^q\right]^n \end{aligned} \tag{6.7}$$

The exponent function $\tau(q)$ can then be derived from eqn. (6.7) as eqn. (6.8)

$$\tau(q) = -\frac{\log[s_1^{1-q}m_1^q + s_2^{1-q}m_2^q]}{\log s} \tag{6.8}$$

and singularity index function $\alpha(q)$ as eqn. (6.9)

$$\alpha(q) = -\frac{\xi\log(m_1/s_1) + (1-\xi)\log(m_2/s_2)}{\log s} \tag{6.9}$$

where

$$\xi = \frac{s_1^{1-q}m_1^q}{s_1^{1-q}m_1^q + s_2^{1-q}m_2^q}$$

Given eqns. (6.7) and (6.8), one can derive $f(\alpha)$ as eqn. (6.10)

$$f(\alpha) = \alpha(q)q - \tau(q) \tag{6.10}$$

From the singularity function (6.9) it can easily be shown that

$$\begin{aligned}\alpha_{max} = \alpha(-\infty) &= -\frac{\log(m_1/s_1)}{\log s} \\ \alpha_{min} = \alpha(\infty) &= -\frac{\log(m_2/s_2)}{\log s} \\ \alpha(0) &= -\frac{1}{\log s}\left[\frac{s_1\log(m_1/s_1) + s_2\log(m_2/s_2)}{s_1+s_2}\right]\end{aligned} \tag{6.11}$$

similarly, from multifractal spectrum function (6.10), it can be shown that

$$\begin{aligned}f(\alpha_{max}) &= \frac{\log s_1}{\log s} \\ f(\alpha_{min}) &= \frac{\log s_2}{\log s} \\ f(\alpha(0)) &= \frac{\log(s_1+s_2)}{\log s}\end{aligned} \tag{6.12}$$

The other multifractal indices $(\Delta\tau, \Delta\alpha)$ are proportional to logarithmic transformation of $(m_1/s_1)/(m-2/s_2)$. The larger the values of these indices, the more complex the distribution, meaning stronger multifractality. A part from modelling

the asymmetrical distribution, the model also explicitly gives the relationship between the parameters involved in the binomial multiplicative cascade process and the multifractal indices [111].

6.3 Parameters Estimation

The five parameter model can provide both multifractality and asymmetry and can thus be used to characterize fields/measure which exhibit such phenomenon. In any modelling, parameter estimation is an important part of the process. For this model, we need to derive the five parameters from the multifractal analysis s explained in a three step procedure below [111].

Step.1 In the first step, the values of $f(\alpha_{max})$, $f(\alpha_{min})$ and $f(\alpha(0))$ as well as those of α_{max} and α_{min} are to be estimated from multifractal analysis as outlined in Chapter 5. Either of the multifractal analysis techniques can be used to estimate the above parameters, of which all are read from multifractal spectrum.

Step.2 From the values estimated from fractal dimension spectra in step one above, the values of s_1, s_2 and s can iteratively be estimated from the following eqn. (6.13)

$$\begin{aligned} s_1 &= e^{f(\alpha_{max})\log s} \\ s_2 &= e^{f(\alpha_{min})\log s} \\ s &= e^{\frac{\log(s_1+s_2)}{f(\alpha(0))}} \end{aligned} \tag{6.13}$$

The iterations can be implemented in MATLAB or Microsoft Excel with s as the object function, and the values of s_1 and s_2 calculated accordingly. In our case, we implemented them in MATLAB using *while* function such that iterations are run until the values of each side of equal sign are very close to each other to acceptable accuracy.

Step.3 The values of measures m_1 and m_2 can then be calculated from the estimated values of parameters in step two above using the following eqn. (6.14) and eqn. (6.15) respectively

$$m_1 = \exp(-s_1\alpha_{max}\log s) \tag{6.14}$$

$$m_2 = \exp(-s_2\alpha_{min}\log s) \tag{6.15}$$

TABLE 6.1: Estimates of the proposed generalized binomial cascade multiplicative model parameters

Parameter	Value
s_1	2.6785
s_2	0.8823
s	3.5609
m_1	0.578
m_2	0.419

6.4 Results & Discussion

6.4.1 Multifractal Spectrum

We have done a multifractal analysis of noise data measured in one of the University workshops using detrending moving average algorithm. The multifractal spectrum is as shown in Figure 6.2 illustrated as 'experimental' in the figure. From the spectrum we were able to get the values of α_{max}, α_{min}, $f(\alpha_{max})$, $f(\alpha_{min})$ and $f(\alpha(0))$ which we use to estimate the parameters of the proposed model in an attempt to model the multifractal spectrum. This is also shown in the same graph for comparison purposes, labelled as 'proposed model'. The parameter estimates were computed as detailed in the previous section and the values are shown in Table 6.1.

From Figure 6.2, it can be seen that the proposed model shares the same shape as that gotten from the multifractal analysis. Both are right truncated, meaning that noise measured from this location is sensitive to large magnitudes of local fluctuations. However, their estimate of $\alpha(0)$, which is shown by the peak of the multifractal spectrum show different values. The peak value represents the Holder's exponent that appears most in the spectrum, that is, the impulsive noise burst strength that appears most frequently in the data. Since this peak value is very important, we further decided to optimize the coefficient of dispersion (m_1, m_2) so that the proposed model could fit the experimental 'close' enough. The result is as shown in Figure 6.3. Even though the optimized model seem not to estimate accurately the range of α $(\Delta\alpha)$, which is the multifractal signature, it is within the acceptable range. $\Delta\alpha$ indicates the irregularity of the multifractal behaviour of the signal/data. We stress here that, still some more optimization needs to be done for more accurate multifractal spectrum estimate, and is left for future work.

6.4.2 Model Validation

To validate our proposed model, we applied two statistical techniques: the Chi-square statistic and the Kullback-Leibler (KL) divergence to compare how 'close' the proposed model is to the actual spectrum from the multifractal analysis. The

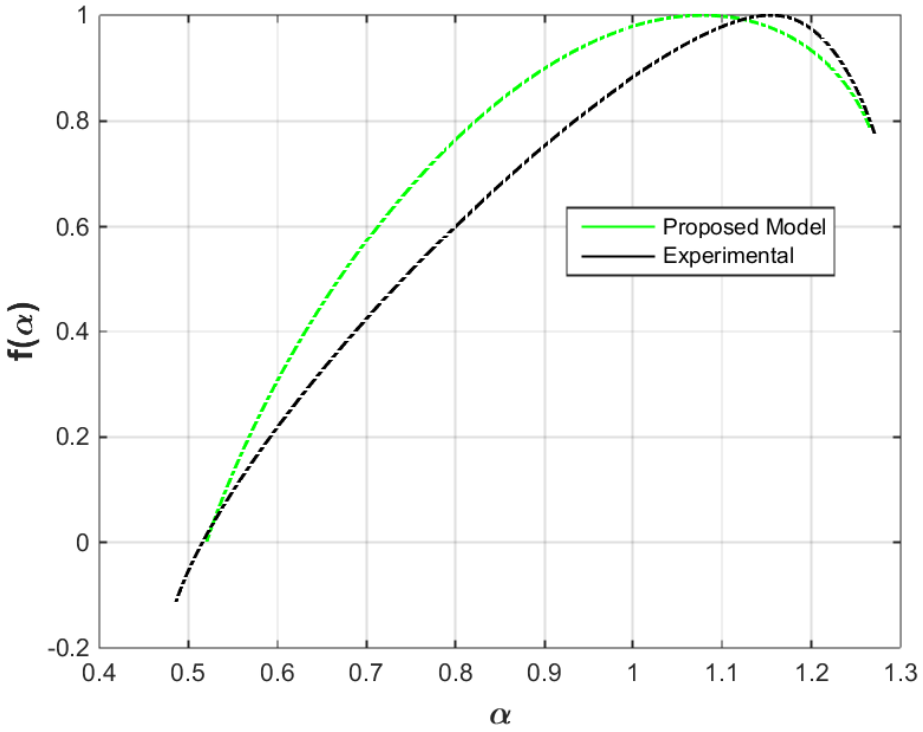

FIGURE 6.2: Simulated Multifractal Spectrum of Generalised Binomial Multiplicative Cascade Model

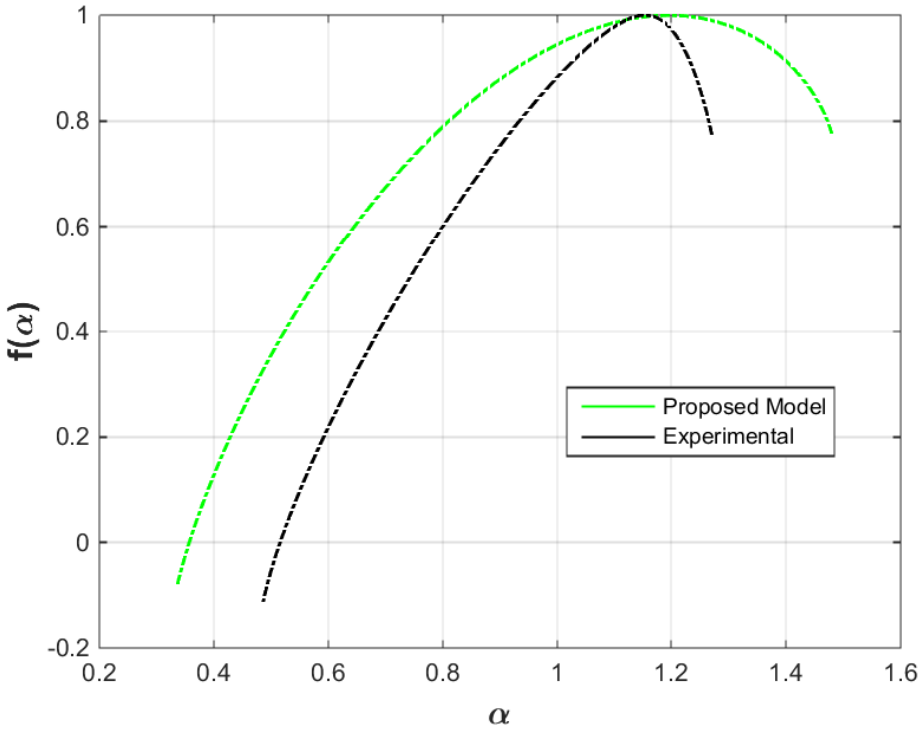

FIGURE 6.3: Simulated Multifractal Spectrum of Generalised Binomial Multiplicative Cascade Model with Coefficient of Dispersion Optimized

chi-square statistic is given by eqn. (6.16)

$$\chi^2 = \sum_i \frac{(O_i - E_i)^2}{E_i} \tag{6.16}$$

where O_i and E_i, respectively, are the observed and expected frequencies of α's of the multifractal spectrum. Similarly, the Kullback-Leibler divergence employed as a measure of closeness between two distributions is given by eqn. (6.17)

$$KL(P||Q) = \sum_{i=1}^{KL} P_i \log \frac{P_i}{Q_i} \tag{6.17}$$

where P and Q are the observed and expected distributions (proposed model estimates and experimental) respectively. The χ^2 value for 95% confidence level calculated is 21.40, which is lower than p-value read from chi-square tables (124.342 for 100 degrees of freedom), hence the null is accepted. Similarly, the KL value calculated is positive (0.0048), hence, we have the confidence the optimised proposed model (as shown in Figure 6.3) is a good attempt in modelling the bursty impulsive noise found in PLC channels. However, for Figure 6.2, the chi-square statistic value show that it has to be rejected as the calculated p-value is 158.97 against the accepted value of 124.342 for 100 degrees of freedom. The KL value is 0.21 which is high, since, for close enough distributions, the KL should as close as possible to zero.

6.5 Conclusion

In this chapter, we have introduced a new model in an attempt to model the bursty impulsive noise found in power line communication networks. The proposed model shows good prospect of simulating the multiscaling behaviour inherent in PLC noise and therefore it forms a good foundation for designing multifractal filters that can be employed to simulate PLC noise more accurately. However, the model parameters still need some optimisation of its coefficient of dispersion. An optimisation algorithm for this task will be addressed in our future work so as to come up with a good trade-off between how accurate the model estimates the peak value of $f(\alpha)$ and the range of α ($\Delta\alpha$).

CHAPTER 7

Conclusion and Recommendations for Future Work

This chapter gives a summary of the thesis and recommendations for further work.

7.1 Concluding Remarks

In chapter 1, an introduction to the thesis was provided stressing the need for multiscaling analysis in the motivation section. Knowing scaling behaviour in signals/data traces provides information necessary to pick the right tools for analysis and modelling so as to improve the accuracy of the findings. The chapter ended by highlighting the contributions of the thesis and proving the structure of the thesis.

Chapter 2 gave a detailed review of the impairments found in power line communication channels, giving more emphasis on channel noise which was the focus of the study. Strengths and shortcomings of the models available in the literature for simulating PLC noise were highlighted with the aim to show the gap that this thesis was trying to fill.

In chapter 3, we followed a deterministic approach to show the relationship between branch lengths and loadings at the terminations and their effect on RMS delay spread. RMS delay spread addresses the multipath richness of the channel and it is inversely related to the coherence bandwidth which provides frequency selectivity of a given channel. Simulation results showed that a number of notches in frequency response and RMS delay spread increases with increase in branch

length. However, when the number of branches was increased between transceivers, but keeping the branch lengths the same, the notch depth increases but appear at the same position for the deep notches. When extreme load conditions are utilised (i.e., from open-circuit to short-circuit conditions), the effect on notches was the same but shifted by 180 degrees and variation in delay spread is not significant.

Chapter 4 and 5 reported findings of long-range dependence and multiscaling behaviour inherent in PLC noise respectively. In chapter 4, three estimators for Hurst parameter showed that PLC noise in all the scenarios where measurements were taken is long-range correlated, that is, PLC noise is strongly dependent even in large scales. In chapter 5, we were able to quantify the strengths of bursts and their frequency of occurrence using multifractal spectrum.

In chapter 7, a generalised binomial cascade multiplicative model has been proposed and validated by both chi-square and Kullback-Leibler divergence statistics to represent the multiscaling behaviour of PLC noise. PLC noise is inherently impulsive and the impulses appear in bursts. It is important to have a model that will be able to model the strengths and frequency of these bursts. The proposed model has shown good prospect of the same.

7.2 Recommendations for Future Work

A good number of research work in PLC noise characterisation normally isolate individual noise generators (electric loads) and analyse their characteristics. In our future work we also intend to isolate individual electric loads known to generate impulsive noise then characterise and model their multifractal behaviour. This can be a very interesting research worth pursuing further as most research in the past has also pursued the contribution of each load to the general characteristic of PLC noise.

Secondly, the various impulsive noise components (periodic impulsive noise asynchronous to the mains frequency, periodic impulsive noise synchronous to the mains frequency and asynchronous impulsive noise) need to be decomposed and each component characteristics analysed as to ascertain which of the impulsive noise components is more bursty and similarly what are the strengths and frequency of occurrence of these bursts. In other words, how is the multiscaling behaviour of these different components and consequently, what are the sources of these multiscaling behaviour if present in these individual components.

Thirdly, multifractal shaping filter that synthesises the multiscaling behaviour of the PLC noise which can be used in simulations is also worth pursuing. How these multifractal shaping filter parameters can be tuned such that the properties of interest are understood for ultimate accurate transceiver design and noise mitigation techniques can be quite challenging but is still worth investigating.

Lastly, it is known that linear and non-linear filters have effects on signals and the measuring equipment normally act either as linear or non-linear filters and at

times as non-linear transforms. These can have serious effects on multifractal analysis of signals from experimental measurements. Moreover, pre-processing signals can also lead to logarithmic transforms and need to be taken into consideration during analysis. These factors were not considered during our study and may be interesting for future work.

References

[1] M. Zimmermann and K. Dostert. "A multipath model for the powerline channel". In: *IEEE Trans. Commun.* 50.4 (2002), pp. 553–559.

[2] L. T. Berger, A. Schwager, and J. J. Escudero-Garzás. "Power Line Communications for Smart Grid Applications". In: *Journal of Electrical and Computer Engineering* 2013 (2013). DOI: 10.1155/2013/712376.

[3] M. Zimmermann and K. Dostert. "Analysis and modeling of impulsive noise in broad-band powerline communications". In: *IEEE Trans. Electromagn. Compat.* 44.1 (2002), pp. 249–258.

[4] Z. Wang, Y. Zhao, and C. Zhao. "Fractal Prediction Algorithm of L-PLC Channel Noise Based on Phase Space Reconstruction". In: *Proc. IEEE International Conference on Intelligent Computation Technology and Automation*. Changsha, China, 2010, pp. 343 –346.

[5] D. Fertonani and G. Colavolpe. "On reliable communications over channels impaired by bursty impulse noise". In: *IEEE Trans. Commun.* 57.7 (2009), pp. 2024–2030.

[6] G. Ndo, F. Labeau, and M. Kassouf. "A Markov-Middleton model for bursty impulsive noise: Modeling and receiver design". In: *IEEE Trans. Power Del.* 28.4 (2013), pp. 2317–2325.

[7] M. O. Asiyo and T. J. Afullo. "Power Line Communications Channel Multipath Phenomena and RMS Delay Spread". In: *Proc. Southern Africa Telecommunication Networks and Applications Conference (SATNAC)*. Arabella, Hermanus, Western Cape, South Africa, 2015, pp. 93–97.

[8] M. O. Asiyo and T. J. Afullo. "Prediction of Long-Range Dependence in Cyclostationary Noise in Low-Voltage PLC Networks". In: *Progress of Electromagnetics Research Symposium*. Shanghai, China, 2016, pp. 4954–4958.

[9] M. O. Asiyo and T. J. Afullo. "Multifractal Analysis of Bursty Impulsive Noise in Low-Voltage Indoor Power Line Channels". In: *Proc. Southern Africa Telecommunication Networks and Applications Conference (SATNAC).* George, Western Cape, South Africa, 2016, pp. 86–90.

[10] M. O. Asiyo and T. J. Afullo. "Analysis of Bursty Impulsive Noise in Low-Voltage Indoor Power Line Channels: Local Scaling Behaviour". In: *SAIEE Africa Research Journal-(under review: 2016-618)* ().

[11] W. Zhu et al. "State-of-art Power Line Communications Channel Modelling". In: *Procedia Computer Science* 17 (2013), pp. 563–570.

[12] M. Gotz, M. Rapp, and K. Dostert. "Power line channel characteristics and their effect on communication system design". In: *IEEE Commun. Mag.* (2004), pp. 78–86.

[13] A. M. Tonello et al. "A fitting algorithm for random modeling the PLC channel". In: *IEEE Trans. Power Del.* 27.3 (2012), pp. 1477–1484.

[14] A. M. Tonello, F. Versolatto, and A. Pittolo. "In-Home power line communication channel: Statistical characterization". In: *IEEE Trans. Commun.* 62.6 (2014), pp. 2096–2106.

[15] S. Galli. "A novel approach to the statistical modeling of wireline channels". In: *IEEE Trans. Commun.* 59.5 (2011), pp. 1332–1345.

[16] M. Tlich et al. "Indoor Power-line communications channel characterization up to 100 MHz-Part I: One-Parameter deterministic model". In: *IEEE Trans. Power Del.* 23.3 (2008), pp. 1392–1401.

[17] M. Tlich et al. "Indoor Power-line communications channel characterization up to 100 MHz-Part II: Time-Frequency Analysis". In: *IEEE Trans. Power Del.* 23.3 (2008), pp. 1402–1409.

[18] H. Meng et al. "Modeling of transfer characteristics for the broadband power line communication channel". In: *IEEE Trans. Power Del.* 19.3 (2004), pp. 1057–1064.

[19] B. Tan and J. Thompson. "Powerline Communications Channel Modelling Methodology Based on Statistical Features". In: *CoRR* (2012). URL: `http://arxiv.org/abs/1203.3879`.

[20] H. Philipps. "Modeling of powerline communication channels". In: *3rd IEEE ISPLC.* 1999.

[21] T. Esmailian, F. R. Kschischang, and P. G. Gulak. "An In-building power line channel simulator". In: *IEEE Int. Symp. Powerline Commun. Applications.* Athens, Greece, 2002.

[22] I. C. Papaleonidopouluos et al. "Statistical analysis and simulation of indoor single phase low voltage power-line communication channels on the basis of multipath propagation". In: *IEEE Trans. Consum. Electron.* 49.1 (2003), pp. 89–99.

[23] D. Anastasiadou and T. Antonakopoulos. "Multipath characterization of indoor power-line networks". In: *IEEE Trans. Power Del.* 20.1 (2005), pp. 90–99.

[24] A. M. Tonello. "Wideband impulse modulation and receiver algorithms for multiuser power line communications". In: *EURASIP J. Adv. Signal Process.* 2007 (2007), pp. 1–14.

[25] S. Galli and T. C. Banwell. "A deterministic frequency-domain model for the indoor power line transfer function". In: *IEEE J. Selected Areas Commun.* 24.7 (2006), pp. 1304–1316.

[26] S. Galli and T. C. Banwell. "A novel approach to the modelling of the indoor power line channel - Part II: Transfer function and its properties". In: *IEEE Trans. Power Del.* 20.3 (2005), pp. 1869–1878.

[27] T. C. Banwell and S. Galli. "A novel approach to the modelling of the indoor power line channel Part I: Circuit analysis and companion model". In: *IEEE Trans. Power Del.* 20.2 (2005), pp. 655–663.

[28] C. T. Mulangu, T. J. Afullo, and N. Ijumba. "Estimation of Specific Attenuation Due to Scattering Points for Broadband PLC Channels". In: *Progress In Electromagnetics Research Symposium,* Kuala Lumpur, MALAYSIA, 2012.

[29] C. T. Mulangu, T. J. Afullo, and N. Ijumba. "Scattering points size distribution for indoor broadband PLC channels". In: *Progress In Electromagnetics Research Symposium,* Kuala Lumpur, MALAYSIA, 2012.

[30] A. M. Tonello et al. "Cyclic Prefix Design and Allocation in Bit-Loaded OFDM over Power Line Communication Channels". In: *IEEE Trans. Commun.* 58.11 (2010), pp. 3265–3276.

[31] K. W. Hipel and A. I. McLeod. *Time Series Modelling of Water Resources and Environmental Systems.* New York: Elsevier, 1994.

[32] J. A. Cortes et al. "Analysis of the indoor broadband power-line noise scenario". In: *IEEE Trans. Electromag. Compat.* 52.4 (2010), pp. 849–858.

[33] D. Benyoucef. "A new statistical model of the noise power density spectrum for powerline communication". In: *Proc. 7th IEEE Int. Symp. Powerline Commun. Applications.* Vol. 136-141. Kyoto,Japan, 2003.

[34] M. Katayama, T. Yamazato, and H. Okada. "A mathematical model of noise in narrowband power line communication systems". In: *IEEE J. Selected Areas Commun.* 24.8 (2006), pp. 1267–1276.

[35] M. Nassar et al. “Cyclostaionary noise modelling in narrowband power-line communication for smart grid applications”. In: *Proc. IEEE Int. Conf. Acoust. Speech Signal Process.* Kyoto, Japan, 2012, pp. 3089–3092.

[36] F. S. Schlindwein and D. H. Evans. “Autoregressive spectral analysis as an alternative to fast Fourier transform analysis of Doppler ultrasound signals”. In: *Diagnostic Vascular Ultrasound*. Ed. by E. Arnold. 1992. Chap. 8, pp. 74–84.

[37] S. P. Herath, N. H. Tran, and T. Le-Ngoc. “On optimal input distribution and capacity limit of Bernoulli-Gaussian impulsive noise channels”. In: *Proc. IEEE Int. Conference Commun.* 2012.

[38] K. F. Nieman et al. “Cyclic spectral analysis of power line noise in the 3-200 kHz Band”. In: *Proc. 17th IEEE Int. Symp. Powerline Commun. Applications*. Johannesburg, South Africa, 2013, pp. 315–320.

[39] T. Shongwe, A. J. H. Vinck, and H. C. Ferreira. “A study on impulse noise and its models”. In: *J. SAIEE* 106.3 (2015), pp. 119–131.

[40] M. Mushkin and I. Bar-David. “Capacity and coding for the Gilbert-Elliot channels”. In: *IEEE Trans. Infor. Theory* 35.6 (1989), pp. 1277–1290.

[41] H. Meng, Y. L. Guan, and S. Chen. “Modeling and analysis of noise effects on broadband power-line communications”. In: *IEEE Trans. Power Del.* 20.2 (2005), pp. 630–637.

[42] T. Guzel et al. “Noise Modeling and OFDM receiver design in Power-line communication”. In: *IEEE Trans. Power Del.* 26.4 (2011), pp. 2735–2742.

[43] J. Yin, X. Zhu, and Y. Huang. “Modeling of amplitude-correlated and occurrence-dependent impulsive noise for power line communication”. In: *Proc. IEEE Int. Conference Commun.* 2014.

[44] G. Acciani et al. “SOM-Based Approach for the Analysis and Classification of Synchronous Impulsive Noise of an In-Ship PLC System”. In: *ISRN Artificial Intelligence* 2012 (2012). DOI: 10.5402/2012/105694.

[45] Y. Hirayama et al. “Noise analysis on wide-band PLC with high sampling rate and long observation time”. In: *Proc. 7th IEEE Int. Symp. Powerline Commun. Applications*. Kyoto, Japan, 2003, pp. 142–147.

[46] F. Gianaroli et al. “Statistical modeling of periodic impulsive noise in indoor power-line channels”. In: *IEEE Trans. Power Del.* 27.3 (2012), pp. 1276–1283.

[47] L. B. Bert et al. “On noise modeling for Power Line Communications”. In: *Proc. IEEE Int. Sym. Power line Commun, Appl.* 2011.

[48] D. Middleton. “Statistical-physical models of electromagnetic interference”. In: *IEEE Tran. Electromagnetic Compat.* 19.3 (1977), pp. 106–127.

[49] D. Middleton. "Non-Gaussian noise models in signal processing for telecommunications: New methods and results for class A and class B noise models". In: *IEEE Trans. Inf. Theory* 45.4 (1999), pp. 1129–1149.

[50] D. Middleton. "Procedures for determining the parameters of the first order canonical models of class A and class B electromagnetic interference". In: *IEEE Tran. Electromagnetic Compat.* EMC-21.3 (1979), pp. 190–208.

[51] A. D. Spaulding and D. Middleton. "Optimum reception in an impulsive interference environment - Part I: Coherent detection". In: *IEEE Tran. Commun.* COM-25.9 (1977), pp. 910–923.

[52] S. M. Zabin and H. V. Poor. "Efficient Estimation of Class A noise parameters via EM algorithm". In: *IEEE Tran. Inform. Theory* 37.1 (1991), pp. 60–72.

[53] A. M. Nyete, T. Afullo, and I. Davidson. "Statistical analysis and characterization of low voltage power line noise for telecommunication applications". In: *IEEE AFRICON 2015*. Addis Ababa, Ethopia, 2015.

[54] J. Mitra and L. Lampe. "Convolutionally coded transmission over markov-Gaussian channels: Analysis and decoding metrics". In: *IEEE Tran. Commun.* 58.7 (2010), pp. 1939–1949.

[55] D. K. Misra. *Radio-Frequency and Microwave Communication Circuits: Analysis and Design*. 2nd ed. New York: John Wiley Sons, 2001.

[56] J. Anatory, M. M. Kissaka, and N. H. Mvungi. "Channel model for broadband power-line communication". In: *IEEE Trans. Power Del.* 22.1 (2007), pp. 135–141.

[57] J. Anatory et al. "The Influence of Load Impedance, Line Length, and Branches on Underground Cable Power-Line Communications (PLC) Systems". In: *IEEE Trans. Power Delivery* 23.1 (2008), pp. 180–187.

[58] J. Anatory et al. "Broadband Power Line Communications: The factors Influencing Wave Propagations in the Medium Voltage Lines". In: *IEEE Int. Symp. Powerline Commun. Applications*. 2007, pp. 127–132.

[59] J. Anatory et al. "The Effects of Multipath on OFDM Systems for Broadband Power-Line Communications a Case of Medium Voltage Channel". In: *World Academy of Science, Engineering and Technology* 54 (2009), pp. 367–370.

[60] T. R. Oliveira, C. B. Z. andSergio L. Netto, and M. V. Ribeiro. "Statistical Modeling of the Average Channel Gain and Delay Spread in In-Home PLC Channels". In: *IEEE Int. Symp. Powerline Commun. Applications*. 2015, pp. 184–188.

[61] A. Rennane, C. Konate, and M. Machmoum. "A simplified deterministic approach for accurate modelling of the indoor power line channel". In: *Proc. 3rd ICSNC*. 2008.

[62] F. Zwane and T. J. O. Afullo. "An Alternative Approach in Power Line Communication Channel Modelling". In: *Prog. Electromag. Research* 47 (2014), pp. 85–93.

[63] H. He et al. "Analysis of reflection of signal transmitted in low-voltage powerline with complex wavelet". In: *IEEE Trans. Power Del.* 19.1 (2004), pp. 86–91.

[64] D. M. Pozar. *Microwave engineering*. 4th ed. USA: John Wiley & Sons, 1998.

[65] S. Guzelgoz, H. B. Celebi, and H. Arslan. "Articulating factors defining RMS delay spread in LV PLC networks". In: *J. Comput. Sys. Networks Commun.* 2010 (2010), pp. 1–9.

[66] S. Guzelgoz, H. B. Celebi, and H. Arslan. "Statistical characterization of the paths in multipath PLC channels". In: *IEEE Trans. Power Del.* 26.1 (2011), pp. 181–187.

[67] M. Mosalaosi and T. J. O. Afullo. "Dispersive Characteristics for broadband indoor power-line communication channels". In: *Proc. SATNAC*. 2014.

[68] K. S. Al-Mawali and Z. M. Hussain. "Performance of Bit-Interleaved Coded OFDM in Power Line Communications with Impulsive Noise". In: *Proc. IEEE International Conference on Advanced Technologies for Communications*. Hai Phong, Vietnam, 2009, pp. 2162–1020.

[69] T. Karagiannis, M. Faloutsos, and R. H. Riedi. "Long-Range Dependence: Now you see it, now you don't!" In: *Proc. IEEE Global Telecommunications Conference*. Taipei, Taiwan, 2002, pp. 2165–2169.

[70] Z. Yu, L. Yee, and Y. Zu-Guo. "Relationships of exponents in multifractal detrended fluctuation analysis and conventional multifractal analysis". In: *Chin. Phys. B* 20.9 (2011), pp. 1–9.

[71] R. Weron. "Estimating Long Range Dependence: Finite Sample Properties and Confidence Intervals". In: *Physica A* 312 (2002), pp. 285–299.

[72] A. A. Anis and E. H. Lloyd. "The Expected Value of the Adjusted Rescaled Hurst Range of Independent Normal Summands". In: *Biometrica* 63.1 (1976), pp. 111–116.

[73] M. S. Taqqu, V. Teverovsky, and W. Willinger. "Estimators for long-range dependence: an empirical study". In: *Fractals* 3.4 (1995), pp. 785–799.

[74] I. W. Lee and A. O. Fapojuwo. "Analysis and modeling of a campus wireless network TCP/IP traffic". In: *Computer Networks* 53 (2009), pp. 2674–2687.

[75] S. A. Khayam et al. "Markov and multifractal wavelet models for wireless MAC-to-MAC channels". In: *Performance Evaluation* 64 (2007), pp. 298–314.

[76] L. Atzori, N. Aste, and M. Isola. "Estimation of multifractal parameters in traffic measurement: An accuracy-based real-time approach". In: *Computer Communications* 29 (2006), pp. 1879–1888.

[77] T. Parrinello and R. A. Vaughan. "Multifractal analysis and feature extraction in satellite imagery". In: *Int. J. Remote Sensing* 23.9 (2002), pp. 1799–1825.

[78] M. Dai et al. "Mixed multifractal analysis of China and US stock index series". In: *Chaos, Solitons and Fractals* 87 (2016), pp. 268–275.

[79] G.-F. Gu and W.-X. Zhou. "Detrending moving average algorithm for multifractals". In: *Physical Review E* 82.1 (2010). DOI: 10.1103/PhysRevE.82.011136.

[80] O. Dick and I. Svyatogor. "Potentialities of the wavelet and multifractal techniques to evaluate changes in the functional state of the human brain". In: *Neurocomputing* 82 (2012), pp. 207–215.

[81] A. N. Parlon et al. "Multifractal characterization of cerebrovascular dynamics in newborn rats". In: *Chaos, Solitons and Fractals* 77 (2015), pp. 6–10.

[82] A. Arneodo, E. Bacry, and J. Muzy. "The thermodynamics of fractals revisited with wavelets". In: *Physica A* 213.1 (1995), pp. 232–275.

[83] A. Arneodo et al. "Wavelet based fractal analysis of DNA sequences". In: *Physica D* 96 (1996), pp. 291–320.

[84] J. F. Muzy, E. Bacry, and A. Arneodo. "Wavelets and multifractal formalism for singular signals: Application to turbulence data". In: *Phy. Rev. Letters* 67.3515 (1991).

[85] J. F. Muzy, E. Bacry, and A. Arneodo. "Multifractal formalism for fractal signals: The structure-function approach versus the wavelet-transform modulus-maxima method". In: *Phys. Rev. E* 47.875 (1993).

[86] J. W. Kantelhardt et al. "Multifractal detrended fluctuation analysis of nonstationary time series". In: *Physica A* 316.87 (2002), pp. 1–14.

[87] K. Xu, P. Shang, and G. Feng. "Multifractal time series analysis using the improved 0-1 test model". In: *Chaos, Solitons and Fractals* 70 (2015), pp. 134–143.

[88] E. A. F. Ihlen. "Introduction to multifractal detrended fluctuation analysis in Matlab". In: *Frontiers in Physiology* 3.141 (2012), pp. 1–18.

[89] E. Koscielny-Bunde et al. "Long-term persistence and multifractality of ricer runoff records: Detrended fluctuation studies". In: *J. Hydrology* 322 (2006), pp. 120–137.

[90] E. Alessio et al. "Second-order moving average and scaling of stochastic time series". In: *Eur. Phys. J. B* 27 (2002), pp. 197–200.

[91] W. M. Macek and A. Wawrzaszek. "Evolution of asymmetric multifractal scaling of solar wind turbulence in the outer heliosphere". In: *Journal of Geophysical Research* 114 (2009), pp. 1–11.

[92] W. M. Macek. "Multifractality and intermittency in the solar wind". In: *Nonlin. Processes Geophys.* 14 (2007), pp. 695–700.

[93] A. Szczepaniak and W. M. Macek. "Asymmetric multifractal model for solar wind intermittent turbulence". In: *Nonlin. Processes Geophys.* 15 (2008), 615–620.

[94] D. Schertzer and S. Lovejo. "Physical Modeling and Analysis of Rain and Clouds by Anisotropic Scaling Multiplicative Processe". In: *Journal of Geophysical Research* 92.D8 (1987), pp. 9693–9714.

[95] S. Lovejoy and D. Schertzer. "On the simulation of continuous in scale universal multifractals, part I: Spatially continuous processes". In: *Computers & Geosciences* 36 (2010), pp. 1393–1403.

[96] Z. Voros. "On multifractality of high-latitude geomagnetic fluctuations". In: *Annals Geophys.* 18.10 (2000), pp. 1273–1282.

[97] E. Bacry, A. Kozhemyak, and J. Muzy. "Log-normal continuous cascade model of asset returns: aggregation properties and estimation". In: *Quantitative Finance* 13.5 (2013), pp. 795–818.

[98] J. F. Muzy, J. Delour, and E. Bacry. "Modelling fluctuations of financial time series: from cascade process to stochastic volatility model". In: *European Physical Journal B* 17 (2000), pp. 537–548.

[99] Q. Cheng. "Multifractal interpolation method for spatial data with singularities". In: *The Southern African Institute of Mining and Metallurgy* 115 (2015), pp. 235–240.

[100] J. W. de Godoy Stenico and L. L. Ling. "A new binomial conservative multiplicative cascade approach for network traffic modelling". In: *Advanced Information Networking and Applications*. Barcelona, Spain, 2013.

[101] P. Abry et al. "Multiscale nature of network traffic". In: *IEEE Signal Processing Magazine* 19.3 (2002), pp. 28–46.

[102] L. E. Calvet and A. J. Fisher. "How to forecast long-run volatility regime switching and the estimation of multifractal processes". In: *Journal of Financial Econometrics* 2.1 (2004), pp. 49–83.

[103] P. Chainais, R. Riedi, and P. Abry. "Compound Poisson Cascades". In: *Annales de l'Université Blaise Pascal Colloque Auto-Similarité et Applications, Clermont-Ferrand*. 2002.

[104] P. Chainais. "Multidimensional infinitely divisible cascades: Application to modelling of intermittency in turbulence". In: *European Physical Journal B* 51 (2006), pp. 229–243.

[105] P. Chainais, R. Riedi, and P. Abry. "Scale invariant infinitely divisible". In: *Proc. Int. Symp. Physics in Signal and Image Processing*. 2003.

[106] P. Chainais. "Infinitely Divisible Cascades to Model the Statistics of Natural Images". In: *IEEE Tran. Pattern Analysis Machine Intelligence* 29.12 (2007), pp. 2105–2119.

[107] P. Chainais, R. Riedi, and P. Abry. "On Non-Scale-Invariant Infinitely Divisible Cascades". In: *IEEE Tran. Commun.* 51.3 (2005), pp. 1063–1083.

[108] J. Barral and X. Jin. "On exact scaling log-Infinitely divisible cascades". In: *ArXiv e-prints* (Aug. 2012). arXiv: 1208.2221 [math.PR].

[109] E. Bacry and J. Muzy. "Log-Infinitely Divisible Multifractal Processes". In: *Communications in Mathematical Physics* 236.3 (2003), pp. 449–475. DOI: 10.1007/s00220-003-0827-3. URL: http://dx.doi.org/10.1007/s00220-003-0827-3.

[110] A. Arneodo, S. Manneville, and J. Muzy. "Towards log-normal statistics in high Reynolds number turbulence". In: *The European Physical Journal B - Condensed Matter and Complex Systems* 1.1 (1998), pp. 129–140. DOI: 10.1007/s100510050162. URL: http://dx.doi.org/10.1007/s100510050162.

[111] Q. Cheng. "Generalized binomial multiplicative cascade processes and asymmetrical multifractal distributions". In: *Nonlinear Processes in Geophysics* 21 (2014), pp. 477–487.